Department of Chemistry

Hot electron-induced electrochemiluminescence studies with different cathode materials and electrode geometries

Tiina Ylinen-Hinkka

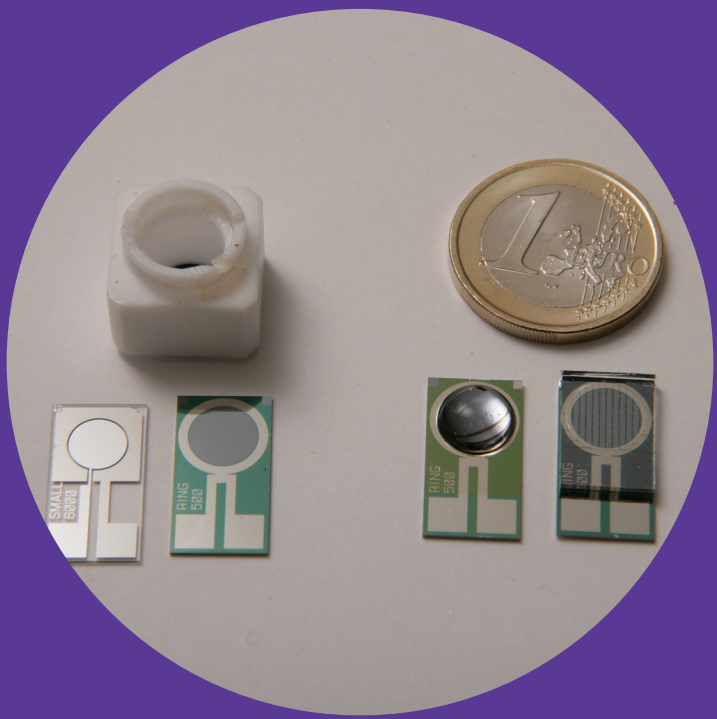

Aalto University

DOCTORAL DISSERTATIONS

Aalto University publication series
DOCTORAL DISSERTATIONS 150/2012

Hot electron-induced electrochemiluminescence studies with different cathode materials and electrode geometries

Tiina Ylinen-Hinkka

Doctoral dissertation for the degree of Doctor of Science in Technology to be presented with due permission of the School of Chemical Technology for public examination and debate in Auditorium KE2 (Komppa Auditorium) at the Aalto University School of Chemical Technology (Espoo, Finland) on the 18th of January 2013 at 12 o'clock.

Aalto University
School of Chemical Technology
Department of Chemistry
Laboratory of Analytical Chemistry

Supervising professor
prof. Sakari Kulmala

Thesis advisor
prof. Sakari Kulmala

Preliminary examiners
prof. Keijo Haapakka, University of Turku, Finland
prof. Ari Ivaska, Åbo Akademi University, Finland

Opponent
prof. Larry J. Kricka, University of Pennsylvania, Philadelphia, USA

Aalto University publication series
DOCTORAL DISSERTATIONS 150/2012

ISBN 978-952-60-4866-6 (printed)
ISBN 978-952-60-4867-3 (pdf)
ISSN-L 1799-4934
ISSN 1799-4934 (printed)
ISSN 1799-4942 (pdf)
http://urn.fi/URN:ISBN:978-952-60-4867-3

Unigrafia Oy
Helsinki 2012

Finland

441 697
Printed matter

Aalto University

Abstract

Aalto University, P.O. Box 11000, FI-00076 Aalto www.aalto.fi

Author
Tiina Ylinen-Hinkka

Name of the doctoral dissertation
Hot electron-induced electrochemiluminescence studies with different cathode materials and electrode geometries

Publisher School of Chemical Technology

Unit Department of Chemistry

Series Aalto University publication series DOCTORAL DISSERTATIONS 150/2012

Field of research Analytical Chemistry

Manuscript submitted 11 June 2012 **Date of the defence** 18 January 2013

Permission to publish granted (date) 29 August 2012 **Language** English

☐ **Monograph** ☒ **Article dissertation (summary + original articles)**

Abstract

In this research, different cathode materials and electrode geometries were tested for hot electron induced electrochemiluminescence (HECL). The cathode has to be a conductor and it has to be covered by a thin insulator layer. During the pulse polarisation, electrons can be tunnel emitted through the thin insulator film. The tunnel emitted electrons having high energy are called hot electrons. If the energy of these electrons is above the conduction band edge of water, they may enter the conduction band of water and are likely to become hydrated electrons. Hot and hydrated electrons can induce redox reactions that are not achieved at active metal electrodes in aqueous solution using traditional electrochemistry.

The research revealed that the substrate material of the electrode can be quite freely chosen. The substrate material does not necessarily have to be a conductor, if a thin conductive layer is deposited on it. According to the tests, Al_2O_3, SiO_2 and Si_3N_4 made by different deposition methods are suitable insulating layers. From the tested electrodes, the highest HECL-intensities were measured by thermally oxidised Si, Al/Al_2O_3 and Si/Al_2O_3 made by atomic layer deposition (ALD), and Si/SiO_2 and Al/SiO_2 made by plasma enhanced chemical vapour deposition (PECVD).

An important difference between the research in this thesis and the earlier HECL research is the usage of integrated electrodes. In these devices, both anode and cathode are integrated on the same microfabricated silicon or glass chip. Also the sample confinement can be integrated on the same chip. In case of integrated sample confinement, the sample area is either defined by a hydrophobic ring or it is a PDMS chamber. The integrated sample confinement with a hydrophobic ring can be filled by dispensing straight to the electrode surface and the PDMS chamber by dipping the chip's edge in sample solution. Because the chips are disposable, the usage of integrated sample confinements prevents cross-contamination between samples.

The applicability of the chip containing the hydrophobically defined sample confinement in the immunoassay of C-reactive protein (CRP) was also tested. The immunoassay of CRP with the chips was compared to another immunoassay method exploiting HECL. Both methods are suitable for determination of low CRP concentration and they are potential point-of-care measurement methods. However, the usage of the chips quickens the analysis, makes it easier to the user, and decreases the volume of the reagents needed.

Keywords HECL, thin film deposition, integrated electrodes, immunoassay

ISBN (printed) 978-952-60-4866-6 **ISBN (pdf)** 978-952-60-4867-3

ISSN-L 1799-4934 **ISSN (printed)** 1799-4934 **ISSN (pdf)** 1799-4942

Location of publisher Espoo **Location of printing** Helsinki **Year** 2012

Pages 158 **urn** http://urn.fi/URN:ISBN:978-952-60-4867-3

Tekijä
Tiina Ylinen-Hinkka

Väitöskirjan nimi
Erilaisten katodimateriaalien ja eristekerrosten käyttö kuumia elektroneja hyödyntävissä elektrokemiluminesenssimittauksissa

Julkaisija Kemian tekniikan korkeakoulu

Yksikkö Kemian laitos

Sarja Aalto University publication series DOCTORAL DISSERTATIONS 150/2012

Tutkimusala Analyyttinen kemia

Käsikirjoituksen pvm 11.06.2012 **Väitöspäivä** 18.01.2013

Julkaisuluvan myöntämispäivä 29.08.2012 **Kieli** Englanti

☐ **Monografia** ☒ **Yhdistelmäväitöskirja (yhteenveto-osa + erillisartikkelit)**

Tiivistelmä

Tutkimuksessa testattiin erilaisten katodimateriaalien ja eristekerrosten käyttöä kuumien elektronien aikaansaamassa elektrokemiluminesenssissa (HECL). Johtavaa materiaalia olevan katodin päällä on oltava ohut eristekerros, jonka läpi elektronit voivat tunneloitua pulssipolarisaation vaikutuksesta. Tunneloituneita elektroneja, joilla on korkea energia, kutsutaan kuumiksi elektroneiksi. Jos elektronin energia on korkeampi kuin veden johtavuusvyön reunaenergia, voi kuuma elektroni siirtyä veden johtavuusvyölle ja muuttua hydratoituneeksi elektroniksi. Kuumat ja hydratoituneet elektronit voivat aikaansaada sellaisia hapetus–pelkistys-reaktioita, jotka eivät normaalisti toteudu aktiivisten metallien pinnalla vesiliuoksissa.

Tutkimuksessa havaittiin, että elektrodin substraattimateriaali on melko vapaasti valittavissa, eikä sen tarvitse välttämättä olla johde, jos sen päälle kasvatetaan ohut johtava kerros. Eristemateriaaliksi todettiin soveltuvan eri tekniikoilla tehdyt Al_2O_3, SiO_2 ja Si_3N_4. Testatuista elektrodeista suurimman HECL-intensiteetin tuottivat termisesti oksidoitu Si, atomikerroskasvatuksella (ALD) valmistetut Al/Al_2O_3 ja Si/Al_2O_3 sekä plasma-avusteisella kemiallisella kaasufaasikasvatuksella (PECVD) valmistetut Si/SiO_2 ja Al/SiO_2.

Merkittävin ero aikaisempiin HECL-tutkimuksiin on pii- tai lasisirulla olevien integroitujen elektrodien käyttö. Joissain siruissa oli myös hydrofobisen renkaan tai PDMS-kammion määrittämä näytealue, jolloin erillistä näytekennoa ei tarvittu. Hydrofobista rengasta käytettäessä näyte voitiin pipetoida suoraan sirulle, ja PDMS-kammiota käytettäessä näyte voitiin imeä näytekammioon pienestä näytepisarasta kapillaarivoimien avulla. Koska sirut ovat kertakäyttöisiä, estää integroitujen näytekammioiden käyttö kontaminaatiota näytteiden välillä.

Tutkimuksessa testattiin myös hydrofobisen renkaan sisältävän sirun soveltuvuutta C-reaktiivisen proteiinin (CRP) alhaisten pitoisuuksien määrittämiseen. CRP-immunomääristystä integroiduilla elektrodeilla verrattiin toiseen HECL:ää hyödyntävään määritysmenetelmään. Molemmat menetelmät soveltuvat alhaisten CRP-pitoisuuksien määrittämiseen, ja ne ovat potentiaalisia point-of-care -määritysmenetelmiä. Sirujen käyttö kuitenkin nopeuttaa ja helpottaa analyysiä sekä vähentää reagenssien kulutusta.

Avainsanat HECL, ohutkerroskasvatus, integroidut elektrodit, immunomääritys

ISBN (painettu) 978-952-60-4866-6 **ISBN (pdf)** 978-952-60-4867-3

ISSN-L 1799-4934 **ISSN (painettu)** 1799-4934 **ISSN (pdf)** 1799-4942

Julkaisupaikka Espoo **Painopaikka** Helsinki **Vuosi** 2012

Sivumäärä 158 **urn** http://urn.fi/URN:ISBN:978-952-60-4867-3

Preface

First of all, I would like to thank my supervisor prof. Sakari Kulmala for giving me an opportunity to do my doctoral studies in his laboratory. I also appreciate his work in CHEMSEM graduate school when he was arranging interesting summer schools and seminars for doctoral students. I give my great gratitude to Dr. Antti J. Niskanen whose strong knowledge both in theory and practice of microfabrication was essential for this research. I am also grateful to prof. Sami Franssila who gave valuable comments both on the articles and on the thesis.

I express my gratitude to Dr. Timo Ala-Kleme who familiarised me with hot electron-induced electrochemiluminescence for the first time during my M.Sci. studies at the University of Turku. I offer my thanks to Ms. Piia Mäkinen and Mr. Jarkko Eskola from Labmaster Oy whose advices have been beneficial for the immunoassay studies. I also want to thank my pre-examiners, prof. Ari Ivaska and prof. Keijo Haapakka, for their encouraging remarks on my thesis manuscript.

I give my thanks to the personnel working in the laboratory of Analytical chemistry during my doctoral studies. I want to thank especially Ms. Sirje Liukko, Mr. Markus Håkansson, Dr. Jiang Qinghong, Ms. Outi Rajamäki, Ms. Päivi Kuosmanen, Mr. Arttu Leinonen, Mr. Matti Pusa and Mr. Kalle Salminen for interesting discussions concerning scientific issues as well as life in general. I give my special thanks to Dr. Johanna Suomi, in addition to being a colleague and friend, for the language check of my thesis.

I want to thank my friends and chemist colleagues Marika, Anu and Kaisa for being my peer group in working as a chemist, being a mother and combining these two. I am also grateful of the support from my friends Heli, Katriina, Helena, Taija and Maija.

I give my great gratitude to my parents Airi and Eero for their continuous support and encouragement throughout my whole life and especially during my doctoral studies. I also want to thank my sister Liisa with whom I have been able to share the best and the worst moments of my life.

Last but not least I want to thank my husband Ville and my son Elias for their endless love and patience and for their ability to keep my focus in the most important things in the life.

Espoo, 1.9.2012
Tiina Ylinen-Hinkka

Contents

List of Publications

This thesis consists of an overview and of the following publications which are referred to in the text by their Roman numerals.

I Ylinen, T., Suomi, J., Helin, M., Ala-Kleme, T., Kulmala, S., Time-resolved detection of hot electron-induced electrochemiluminescence of fluorescein in aqueous solution, *Journal of Fluorescence* **16** (2006) 27–33.

II Jiang, Q., Sun, S., Håkansson, M., Langel, K., Ylinen, T., Suomi, J., Kulmala, S., Electrochemiluminescence and chemiluminescence of a carboxylic acid derivative of ruthenium(II)tris-(2,2'-bipyridine) chelate synthesized for labeling purposes, *Journal of Luminescence* **118** (2006) 265–271.

III Niskanen, A.J., Ylinen-Hinkka, T., Kulmala, S., Franssila, S., Ultrathin tunnel insulator films on silicon for electrochemiluminescence studies, *Thin Solid Films* **517** (2009) 5779–5782.

IV Niskanen, A.J., Ylinen-Hinkka, T., Pusa, M., Kulmala, S., Franssila, S., Deposited dielectrics on metal thin films using silicon and glass substrates for hot electron-induced electrochemiluminescence, *Thin Solid Films* **519** (2010) 430–433.

V Niskanen, A.J., Ylinen-Hinkka, T., Kulmala, S., Franssila, S., Integrated microelectrode hot electron electrochemiluminescent sensor for microfluidic applications, *Sensors and Actuators B: Chemical* **152** (2011) 56–62.

VI Ala-Kleme, T., Mäkinen, P., Ylinen, T., Väre, L., Kulmala, S., Ihalainen, P., Peltonen, J., Rapid electrochemiluminoimmunoassay of human C-reactive protein at planar disposable oxide-coated silicon electrodes, *Analytical Chemistry* **78** (2006) 82–88.

VII Ylinen-Hinkka, T., Niskanen, A.J., Franssila, S., Kulmala, S., Immunoassay of C-reactive protein by hot electron induced electrochemiluminescence using integrated electrodes with hydrophobic sample confinement, *Analytica Chimica Acta* **702** (2011) 45–49.

Author's contribution

Publication I

Major role in the research part. Writing of the article.

Publication II

Participation in the research part. Contribution to writing the article.

Publication III

Planning the sample series, carrying out all the HECL measurements, and analysing the HECL results. Significant role in writing the article.

Publication IV

Planning the sample series, carrying out all the HECL measurements, and analysing the HECL results. Significant role in writing the article.

Publication V

Participation in the designing and development of the devices, carrying out all the HECL measurements, and analysing the HECL results. Significant role in writing the article.

Publication VI

Participation in the research part. Contribution to writing the article.

Publication VII

Innovating the subject of the article, planning the immunoassay procedure, carrying out all the experiments, and analysing the results. Writing of the article.

List of Abbreviations

Abbreviation	Meaning
AFM	Atomic force microscopy
ALD	Atomic layer deposition
anti-hCRP	Anti-human C-reactive protein, an antibody of CRP produced by human body
C/I/E	Conductor/Insulator/Electrolyte
CCD	Charge-coupled device
CDC	Centers for Disease Control and Prevention
CL	Chemiluminescence
CRP	C-reactive protein
CVD	Chemical vapour deposition
DNA	Deoxyribonucleic acid
ECL	Electrochemiluminescence
FMOC-OH	(9-fluorenyl)methanol
hCRP	C-reactive protein produced by human body
HV	High vacuum
ITO	Indium tin oxide, an optically transparent electrical conductor
LPCVD	Low pressure chemical vapour deposition
LPD	Liquid phase deposition
MOS	Metal-oxide-semiconductor
NCS	Isothiocyanate

PDMS	Polydimethyl siloxane, a silicone polymer
PECVD	Plasma enhanced chemical vapour deposition
PL	Photoluminescence
PMT	Photomultiplier tube
PTFE	Polytetrafluoroethylene
PVD	Physical vapour deposition
RCA-cleaning	A standard wafer cleaning process, originally developed at the Radio Corporation of America (RCA)
RCL	Radioluminescence
SAM	Self-assembled monolayer
SC	Standard cleaning
sccm	Standard cubic centimetres per minute, a unit of flow rate
SHE	Standard hydrogen electrode
SU-8	An epoxy-based negative photoresist
TMA	Trimethylaluminium
TMAH	Tetramethyl ammonium hydroxide
UHV	Ultra-high vacuum
UV	Ultraviolet

1. Introduction

The methods of Analytical chemistry are needed when compounds have to be quantified, qualified or separated. Analytical chemistry is used in e.g. environmental analysis and medical analysis. When a new quantitative analysis method is developed, it is important to know the detection limit and the linear range needed for a specific analysis. The trend is nowadays towards lower and lower detection limits, but of course the detection limit depends on the analysis and the lowest possible detection limit is not necessary in every application.

Portability of the measurement equipment is beneficial, because then the analysis can be made near the sampling place and the extra steps of sample transportation and storage can be avoided. The fastness and easiness of the analysis are also important issues especially in medical analyses, when e.g. blood sugar is monitored in order to decide the need of extra insulin. If this kind of analysis system can be miniaturised, it can be used as a point-of-care measurement system.

The detection methods can be based on various chemical or physical properties of the compound to be analysed. The analysis method used in this thesis is hot electron-induced electrochemiluminescence (HECL), which is one subclass of luminescence. In luminescence, an atom or a molecule absorbs energy and results in its excited state. When the excited atom or molecule returns back to its ground state it emits light. Luminescence is divided into different categories depending on the source of the absorbed energy. In photoluminescence (PL), luminescence is induced by photons. In chemiluminescence (CL), luminescence is produced by a chemical reaction. In electrochemiluminescence (ECL), at least one of the intermediates is produced electrochemically. The classification of the luminescent methods is described in Figure 1.

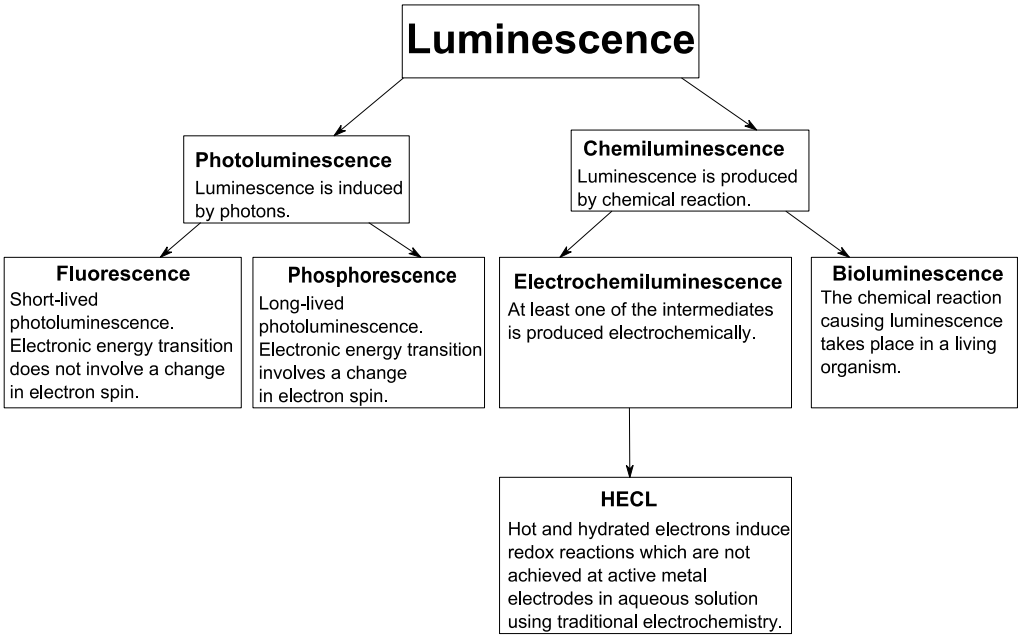

Figure 1. Classification of the luminescent methods.

Electrochemiluminescence is a relatively new phenomenon which was used for the first time in scientific experiments in the middle of the 1960s[1,2]. The basics of the phenomenon were, however, known already at the late 1920s[3,4].

ECL studies are carried out e.g. either at a single working electrode whose potential is varied to generate the reduced and oxidised species that react in the diffusion layer near the electrode, or by producing the oxidised and reduced species at separate electrodes and rapidly flowing them together[5]. The set-up usually consists of working, counter and reference electrodes. The working and counter electrodes are usually made of noble metals or carbon. Several luminophores can show ECL[6-10], but the most commonly used ECL luminophores are ruthenium(II)tris-(2,2´-bipyridine) ($Ru(bpy)_3^{2+}$) chelate and its derivatives.

One subclass of electrochemiluminescence is hot electron-induced electrochemiluminescence (HECL), where hot and hydrated electrons can induce redox reactions which are not achieved at active metal electrodes in aqueous solution using traditional electrochemistry[11-17]. Many organic luminophores, such as fluorescein

(Publication I) and rhodamine B[18], can be excited at aqueous media in HECL process, because highly reducing and highly oxidising radicals are present simultaneously[18]. These luminophores cannot be cathodically excited at active metal electrodes in fully aqueous solution. In HECL, the electrode set-up consists typically only of working and counter electrodes, while in traditional ECL method also a reference electrode is normally needed.

HECL is a selective and sensitive method which can be used to determine luminophores even in picomolar concentrations[19]. Also some oxidants, such as hydrogen peroxodisulfate and peroxodiphosphate, can be indirectly determined using HECL[20]. In the typical application, however, HECL luminophores are used as labels[21-25]. Because HECL method easily provides both time and wavelength discrimination, different luminescent molecules and chelates, even ones with different optical and redox properties, can be excited simultaneously. This enables, for example, multiparametric bioaffinity assays where several biological analytes are determined during the same measurement. HECL is also a low-cost method and its instrumentation is relatively simple and easy to miniaturise: only a suitable pulse generator, a sample cell, a detector (usually photomultiplier tube), and a photon counter are needed.

The aim of this thesis was to research the suitability of different cathode materials and electrode geometries for HECL measurements. A wider selection of conductor/insulator pairs usable in HECL measurements is beneficial when e.g. the energetics, optical properties or antibody binding abilities of the surface are important for certain applications. Also the convenience and costs of the electrode production can vary a lot depending on the selection of substrate and conductor material as well as on the process used to produce the thin insulator film (Publications III and IV).

An important difference between the research in this thesis and the earlier HECL research is the usage of integrated electrodes (Publication V). In the present devices, both the working electrode and the counter electrode are combined on a single microfabricated chip. In some of these devices, the sample confinement is also integrated on the chip. Different electrode geometries and sample confinement structures were designed and investigated for HECL purposes. The integrated electrode chips enable the miniaturisation of the whole measurement system. Even with the traditional equipment they make the analysis faster and more convenient for the user. In addition, they decrease the volume of

the reagents needed. The difference between the integrated electrode chip and the traditional system which necessitates using a discrete Pt counter electrode is illustrated in Figure 2.

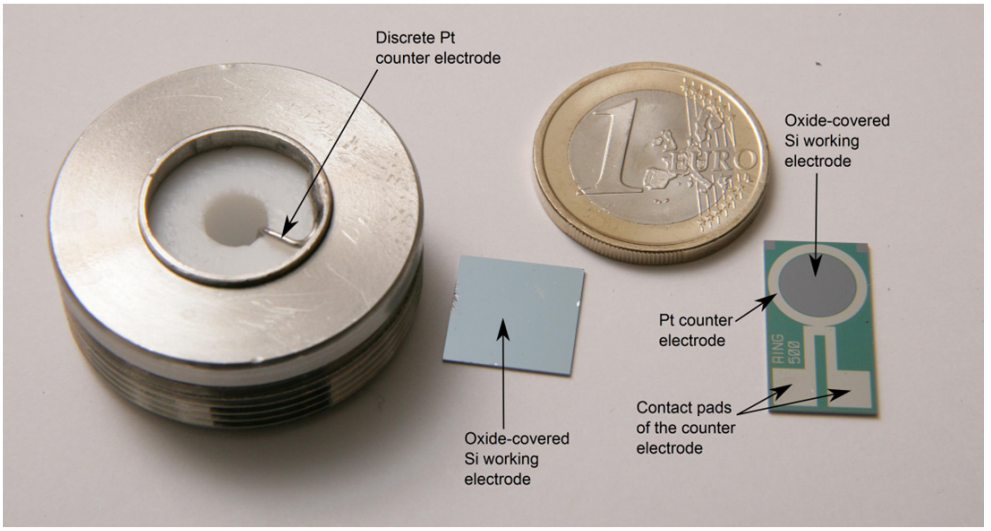

Figure 2. A SiO_2-coated silicon working electrode (12 mm×12 mm) which necessitates using of a discrete Pt counter electrode (on the left) and an integrated electrode chip (10 mm×19 mm) with SiO_2-coated silicon working electrode and Pt counter electrode (on the right).

Two HECL luminophores were studied to find out their most probable reaction pathways and to investigate their usability in bioaffinity assays (Publications I and II). Research of new luminophores is important for e.g. multiparametric bioaffinity assays because these assays would need labels emitting at different wavelength ranges and/or time domains.

One application of HECL, bioaffinity assay of C-reactive protein (CRP), is also described in the Research chapter. CRP was determined both with discrete working and counter electrodes (Publication VI) and by using integrated electrode chip with hydrophobically defined sample confinement (Publication VII). These methods have a great potential for a real point-of-care application.

2. Principles of hot electron-induced electrochemiluminescence

HECL measurement starts by cathodic pulse polarisation of conductor/insulator/electrolyte (C/I/E) tunnel junction electrodes. These electrodes are capable of transferring considerably more energetic electrons into aqueous electrolyte than active metal electrodes or typical semiconductor electrodes[11,13]. This is based on the capability of the C/I/E electrodes to reach cathodic potentials which are more negative than that of the conduction band edge of water before they start to tunnel emit electrons through the insulator film. For example, n-silicon behind the insulating oxide film can reach more negative potentials than the conduction band edge of water (–3.1 V vs. standard hydrogen electrode (SHE) or –1.3 eV on vacuum scale)[26] before the onset of the electric field of tunnel emission[14]. These high-energy electrons are called hot electrons. Hot electrons can be defined as electrons with thermal energies greater than the thermal energy of a phase or as electrons at energy level far above the Fermi energy of a phase[27]. In addition to injection from an electrode, hot electrons can be produced by high energy radiation or by photoionisation methods[27].

During the pulse polarisation, hot electrons are tunnel emitted through the insulator film. If the energy of these electrons is above the conduction band edge of water, they may enter the conduction band of water and are likely to become hydrated electrons after thermalisation and solvation[11,13-15]. This process is described in Figure 3. The time needed for hot electrons to thermalise depends on the nature of the liquid and it can vary from nanoseconds (liquid Xe and Kr) to the picosecond regime (molecular liquids)[27]. In these conditions, redox reactions which cannot be achieved at active metals in aqueous solution using traditional electrochemistry can take place, because both extremely strong oxidants and reductants are simultaneously created in the vicinity of the electrode surface[11,13-17].

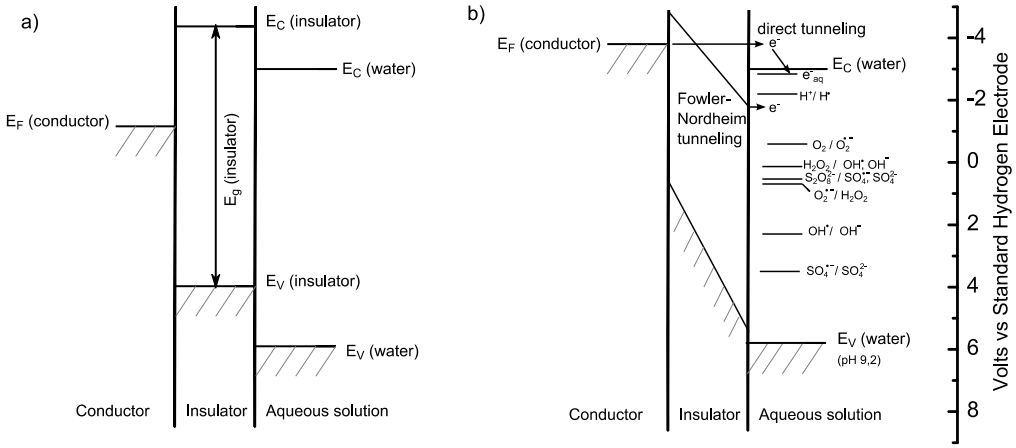

Figure 3. Energy diagram at the surface of a thin insulator film-coated HECL working electrode at a theoretical flat band potential (a) and during cathodic polarisation (b)[13,28,29]. E_C, E_F, E_g and E_V are energy of the conduction band edge, Fermi energy, forbidden energy gap, and energy of the valence band edge, respectively.

The insulating film thickness of the C/I/E electrodes is a critical value in HECL measurements. It must be sufficiently thin to allow field-assisted direct tunnelling of hot electrons[14,30]. If the film is too thick, electrons are transferred via Fowler–Nordheim tunnelling. These electrons are less energetic when entering the solution and they are not able to induce HECL[14,30]. The differences in these two tunnelling mechanisms can be seen in Figure 3.

HECL luminophores are excited by the cathodically generated species at the oxide film/electrolyte interface by successive one-electron transfer steps and they usually react either by oxidation-initiated reductive (ox-red) or reduction-initiated oxidative (red-ox) excitation pathways[11,13-17]. Normally, the luminophore results in its original oxidation state but in singlet or triplet excited state[11,13-17]. However, the HECL mechanism can also be based on the decomposition of the luminophore[17].

An interesting feature in HECL is that the onset pulse potential for HECL reaction can be about the same for different luminophores having considerable differences in their redox and luminescence properties. For example, both $Ru(bpy)_3^{2+}$ chelate and different Tb(III) chelates have been shown to have an onset pulse potential of about –3 V vs. standard hydrogen electrode (SHE)[13]. This result indicates that the reaction mechanism of all of these chelates is based on the same primary process.

2.1. Reaction mechanisms

Hydrated electrons are known to have Rehm–Weller like behaviour rather than to follow Marcus electron transfer theory[31]. According to Marcus theory, the rate constant should increase with decreasing Gibbs free energy change (ΔG), when ΔG is relatively high. Respectively, the rate constant should decrease with decreasing ΔG, when ΔG is low. In this aspect, "low ΔG" means negative ΔG with high absolute value. In other words, the dependence of the rate constant on ΔG is bell-shaped. The region where the rate constant decreases with decreasing ΔG is called the inverted region. This kind of behaviour is typical for charge transfer reactions ($A^- + B \rightarrow A + B^-$) and charge recombination reactions ($A^+ + B^- \rightarrow A + B$). However, Rehm and Weller have observed that charge separation reactions ($A + B \rightarrow A^+ + B^-$) do not usually have the inverted region. This means that the plot of the rate constant versus free energy first rises rapidly and then reaches the diffusion limit and stays there no matter how exergonic the process becomes[32,33]. The Marcus equation gives the first-order rate constant for a donor-acceptor pair at a fixed separation, while the Rehm–Weller behaviour is concerned with a second-order rate constant. The Rehm–Weller equation (1)[32] can be used to evaluate the possibility of an electron transfer process and the formation of an excited state.

$$\Delta G = E\frac{\mathrm{D}}{\mathrm{D}^{\bullet+}} - E\frac{\mathrm{A}}{\mathrm{A}^{\bullet-}} - \frac{e^2}{\epsilon a} - E_{00} \qquad (1)$$

where ΔG is the free energy for the electron transfer, E(D/D$^{\bullet+}$) is the oxidation potential of the donor, E(A/A$^{\bullet-}$) is the reduction potential of the acceptor, E_{00} is the energy of the excited state formed and $e^2/\varepsilon a$ is the Coulombic term for the solvent.

In case of HECL, the Rehm–Weller type behaviour means that hydrated electrons are capable of, for example, completing ox-red excitation pathways by an extremely rapid reduction step, although the Gibbs free energy change for these reactions would be highly negative.

In addition to inducing reduction steps of the luminophore, hot and hydrated electrons can efficiently produce strongly oxidising species from dissolved oxygen or from added

coreactants, such as peroxodisulphate and peroxodiphosphate ions or hydrogen peroxide[17]. Also possible F^+-centres (anionic vacancies in the insulating film) can act as strong one-electron oxidants, because they are able to trap one electron[12]. In case of HECL, F^+-centres can be regenerated by an anodic current peak after each cathodic pulse or by purposely added anodic pulses.

Dissolved oxygen, added coreactants, and F^+-centres are behaving as free radical scavengers. The most important free radical scavengers for the present work are hydrated electron scavengers and hydroxyl radical scavengers.

2.1.1. Hydrated electron scavengers

Peroxodisulphate, peroxodiphosphate and hydrogen peroxide are hydrated electron scavengers which can scavenge hydrated electron and produce rapidly highly oxidising radicals, according to equations 2–4. The concentration of hydrogen peroxide needs to approximately exceed the concentration of dissolved oxygen in the solution ($2 \cdot 10^{-4}$ mol L^{-1})[34] to get the enhancing effect.

$$e^-_{aq} + S_2O_8^{2-} \rightarrow SO_4^{\bullet -} + SO_4^{2-} \qquad (2)$$

$$e^-_{aq} + P_2O_8^{4-} \rightarrow PO_4^{\bullet 2-} + PO_4^{3-} \qquad (3)$$

$$e^-_{aq} + H_2O_2 \rightarrow OH^{\bullet} + OH^- \qquad (4)$$

The second-order reaction rate constants for the reactions 2–4 are $k = 1.2 \cdot 10^{10}$ L mol^{-1} s^{-1} (2), $k = 1.8 \cdot 10^8$ L mol^{-1} s^{-1} (3) and $k = 1.2 \cdot 10^{10}$ L mol^{-1} s^{-1} (4)[31].

A possible excitation route in HECL is one where hot or hydrated electrons are the primary reducing species and hydroxyl radical is the primary oxidising species inducing the HECL intensity.

There are two routes for the hydroxyl radical to be generated in the HECL system. In the first route, hydroxyl radicals are generated from dissolved oxygen (equations 5a–5c).

$$O_2 + e^-_{aq} \rightarrow O_2^{\bullet -} \quad (5a)$$

$$O_2^{\bullet -} + 2H^+ + e^-_{aq} \rightarrow H_2O_2 \quad (5b)$$

$$H_2O_2 + e^-_{aq} \rightarrow OH^\bullet + OH^- \quad (5c)$$

The second-order reaction rate constants for these reactions are $k = 1.9 \cdot 10^{10}$ L mol^{-1} s^{-1} (5a), $k = 1.3 \cdot 10^{10}$ L mol^{-1} s^{-1} (5b), and $k = 1.2 \cdot 10^{10}$ L mol^{-1} s^{-1} (5c)[34].

In the second route, F^+-centres act as strongly oxidising species which can oxidise hydroxyl ions or surface hydroxyl groups to hydroxyl radicals in aqueous solution (equation 6).

$$F^+\text{-centre} + OH^- \rightarrow \text{F-centre} + OH^\bullet \quad (6)$$

2.1.2. Hydroxyl radical scavengers

Azide ion is an example of hydroxyl radical scavengers. When an azide ion reacts with a hydroxyl radical, an azide radical is produced (equation 7).

$$OH^\bullet + N_3^- \rightarrow OH^- + N_3^\bullet \quad (7)$$

The second-order rate constant for the reaction (7) is $1.2 \cdot 10^{10}$ L mol^{-1} s^{-1} [31].

Halide or pseudo-halide ions can be one-electron oxidised by hydroxyl radical and a series of oxidising secondary radicals are produced as follows (equations 8a–8d):

$$OH^{\bullet} + X^{-} \rightarrow OH^{-} + X^{\bullet} \quad (8a)$$

$$X^{\bullet} + X^{-} \rightarrow X_2^{\bullet -} \quad (8b)$$

$$X^{\bullet} + X^{\bullet} \rightarrow X_2 \quad (8c)$$

$$X_2 + X^{-} \rightarrow X_3^{-} \quad (8d)$$

There are several coreactants which can either enhance or decrease the HECL signal. When the effect of these coreactants on a HECL luminophore is tested, it is often possible to deduce the most probable excitation pathway of the luminophore. This kind of approach is described in detail in the Results chapter where two luminophores were tested for their applicability in HECL measurements (Publications I and II).

2.2. Suitable luminophores for HECL studies

The luminophores used in HECL studies have usually been rare earth metal chelates[11,12,15,16,21-23,29,35-41], like Tb[11,12,15,21-23,28,35,37], Eu[38] or Ru[11,13,16,17,35,39,42] chelates or organic dyes[11,17-19,25,35,42-44], like eosin[35], luminol[17,19], and lucigenin[42]. Also (9-fluorenyl)methanol (FMOC-OH)[13] and toluene[14] have been shown to produce HECL. However, toluene needs cathodically generated sulphate radicals for HECL reactions. In addition, solutions of silver nanoclusters can exhibit HECL and it is proposed that they could be used as HECL labels in the same manner as molecular labels[45].

In this research, Tb(III) chelates were used as luminophores in the studies where different electrodes were tested (Publications III–V). They were also used as labels in immunoassays (Publications VI and VII). Tb(III) chelates were chosen because of their long luminescence lifetime and high emission intensity which provide low detection limits[38].

HECL of aromatic Tb(III) chelates in aqueous solution is based on either the ligand reduction initiated oxidative excitation pathway (red-ox pathway) or on the ligand oxidation initiated reductive excitation pathway (ox-red pathway)[11,12,21,22,28,46]. These

reaction pathways involve one-electron reduction or oxidation of the ligand to a radical species followed by one-electron oxidation or reduction of the ligand radical. If the oxidant or reductant of the second step is strong enough, the excited state of the ligand is formed. The ligand can then transfer its excitation energy intramolecularly to the central ion by photophysical processes, similar to those in photoluminescence[47,48]. Finally, the central ion emits light by $^5D_4 \rightarrow {}^7F_{6,5,4,3,2,1,0}$ transitions[28].

The whole process requires that (i) the triplet state of the ligand must be somewhat higher in energy than the resonance level of the central ion, (ii) the triplet state of the ligand does not react with the central ion by a rapid redox reaction, and (iii) the emitting central ion does not react with the ligand[47-49]. Tb(III) ion often meets these requirements[38].

2.3. HECL electrode materials

The simplest way to have a suitable working electrode with a thin insulator film for HECL purposes is to use an aluminium band or sheet which is just cut with normal scissors and flattened. Aluminium has a native oxide layer of approximately 2–3 nm[17] and this aluminium oxide thickness is nearly optimal for HECL studies. Aluminium oxide is known to have a wide band gap. In addition, it provides a high barrier height from the Fermi level of aluminium to the conduction band edge of the oxide and it efficiently blocks the charge transfer via quantum mechanical tunnelling in the absence of an externally induced electric field[36].

Although low-cost aluminium bands and sheets are very easy to use, their quality can vary substantially between batches and these variations affect also HECL results, especially the background luminescence. To improve the performance of the low purity Al band, a thin film (around 100 nm) of pure aluminium can be vacuum evaporated on the surface of impure Al/Al_2O_3. With this kind of electrode, the light reaching the detector comes only from the outer Al/Al_2O_3 layer. The double barrier $Al/Al_2O_3/Al/Al_2O_3$ electrode seems to work very well for the HECL purposes[50].

Another previously used electrode material is thermally oxidised silicon wafer[21,39]. Silicon is commonly used in microfabrication and semiconductor processes and silicon wafers are readily available with high doping levels. Thermal silicon oxide is a chemically robust material which works reliably and reproducibly in HECL measurements. Usually the thermal oxidation is produced under clean room conditions, but relatively good results have also been obtained using thermal oxidation under normal laboratory conditions[39]. SiO_2 is chemically more resistant than Al_2O_3 and therefore, Si/SiO_2 electrodes can be used in a wider pH range than Al/Al_2O_3 electrodes[51].

In addition, chemically oxidised Mg working electrodes have been successfully applied as working electrodes[15]. Promising results have also been obtained with optically transparent *n*-ZnO:Al/MgO composite electrodes where MgO is deposited by atomic layer deposition (ALD) on Al^{3+} doped ZnO-coated glass electrodes (*n*-ZnO:Al glass)[15]. Although the surface topography of *n*-ZnO:Al glass with the tested deposition method was not sufficiently smooth for highly efficient tunnel emission electrode, the results revealed that it would be possible to make electrodes with general construction *n*-ZnO:Al/insulating oxide/aqueous electrolyte/indium tin oxide (ITO). It would also be possible to make an optically transparent electrode by adding an optically transparent layer (such as polydimethyl siloxane (PDMS)) between the *n*-ZnO:Al and ITO glass. This kind of device would provide both parallel and perpendicular time-resolved spectrophotometric observation of the rise and decay of different radicals produced in the cell by a cathodic pulse[15].

Ta_2O_5-coated Ta electrode[27], AuSb alloy electrode with a thin antimony oxide film[52], thin oxide-covered glassy carbon (C/C_xO_{1-x}) electrodes[53,54], and screen printed carbon electrodes[55] have also been proven to be suitable for HECL purposes. The advantage of AuSb alloy and C/C_xO_{1-x} electrodes is their biocompatibility. Self-assembled thiol monolayers can be formed on the AuSb alloy surface due to the presence of Au, which makes AuSb an attractive candidate in fabricating biosensors. Self-assembled monolayer (SAM) of thiolacetic acid, for example, can bind streptavidin to which biotinylated antibody can then bind effectively[52]. C/C_xO_{1-x} electrodes, on the other hand, have surface carbonyl group that can covalently interact with antibodies. These electrodes have been used, for example, as reagentless DNA biosensors utilising the efficient quenching effect

of ferrosene on intrinsic cathodic ECL intensity[54]. In screen printed carbon electrodes, the thin insulating film is formed from the components of the printing inks. These electrodes are low-cost, easy to modify, and very suitable for mass production[55,56].

However, the problem with most of the mentioned electrodes is that they are dependent on the conductive substrate material. The research part of this thesis describes different conductor/insulator pairs that can be deposited on even non-conductive substrates (Publications III and IV). The good performance of e.g. Al_2O_3 was exploited in the research part of this thesis by testing Al_2O_3 layers made by atomic layer deposition (ALD) on different conductor materials (Publication IV).

2.4. Application of HECL: immunoassay

HECL can be used in bioaffinity assays, such as DNA hybridisation[25] and immunoassays[21-23]. Because immunoassay of C-reactive protein was carried out in this research, immunoassay is discussed in more detail in this chapter.

Immunoassays are based on a very specific reaction between an antigen and the corresponding antibody. Because one antibody is capable of binding very strongly to its own antigen, immunoassay is a very selective method. Antibodies are Y-shaped molecules, which are produced in animal body during immune response reactions.

The tested HECL immunoassay methods consist of labelling of either the antibody or the antigen. A potential HECL label must be able to participate in the HECL reaction sequence and to attach to the biological compound to be labelled. The label has to retain its high quantum yield and the necessary kinetics after binding. In addition, the labelling process should not change physical or chemical properties or, even more importantly, biological activity of the compound to be labelled.

A Y-shaped antibody consists of two Fab parts (the “horns” of the letter Y) containing the antigen binding sites, and of one Fc region (the “tail” of the letter Y) which in a living body is responsible for binding to certain cells[57]. Antibodies can be immobilised on solid

surface using different methods. The optimal position of an antibody for immunoassay purposes is when its Fc part is bound to the surface and the Fab parts are pointing towards the solution.

Physical adsorption is the easiest and simplest immobilisation method. However, the position of the antibody cannot be controlled in this procedure. Because of that, the Y-shaped antibodies can, in addition to the wanted orientation, be lying or between standing up and lying and even at a position where the Fab parts are bound to the surface. Covalent binding usually gives better results than physical adsorption. However, the antibodies can go to coincidental positions also when covalent binding is used, if they have multiple binding sites[58,59].

There are many immobilisation methods which enable more specific control of the immobilisation position of an antibody. One of these methods utilises the high specific binding (association constant is about 10^{15} M^{-1}) between avidin and biotin[60,61]. The avidin–biotin binding is even stronger than that of antigen–antibody interactions. The antibody can be biotinylated without changing its biological activity and after biotinylation, the antibody binds to avidin-coated surface to an optimal position for immunoassay. There are also proteins, like protein A (*i.e.* a protein in the cell wall of Staphylococcus aureus)[58] and protein G (*i.e.* a protein in the cell wall of most Streptococci)[62], which are specific receptors for Fc parts. When this kind of proteins are immobilised on the substrate surface, the antibodies bind to them to the optimal position.

It is also possible to split antibodies to fragments consisting only of the antigen binding sites. These fragments can be immobilised directly to Au surface using chemisorption. The thiol group in the antibody forms a thiolate bond with Au surface. The thiol groups are on the different side of the fragment than the antibody binding sites.[63,64]

Immunoassays utilising antibodies and labels can be divided to non-competitive and competitive assays (Figure 4). In non-competitive immunoassay, the antigen is first bound to the primary antibody, which is usually immobilised on a solid surface, and then the labelled secondary antibody is bound to the antigen. During the measurement, the signal coming from the labels of the secondary antibody is directly proportional to the amount of the antigen. This method is also called immunometric or sandwich assay. In competitive

immunoassay, the unlabelled antigens in the sample compete with the labelled antigens to bind to the antibody: a labelled antigen cannot bind to an antibody already occupied by an unlabelled sample antigen. In this method, the measured signal is inversely related to the amount of the antigen in the sample.[65]

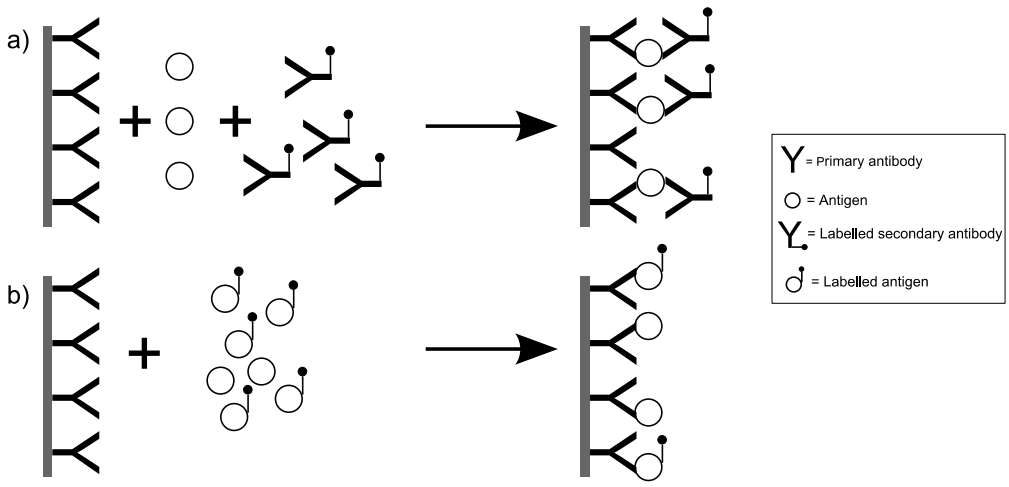

Figure 4. Non-competitive (a) and competitive (b) immunoassay[65]. In non-competitive immunoassay, the immobilised antigen is first bound to the primary antibody and then the labelled secondary antibody is bound to the antigen. During the measurement, the signal coming from the labels of the secondary antibody is directly proportional to the amount of the antigen. In competitive immunoassay, the unlabelled antigens in the sample compete with the labelled antigens to bind to the antibody: a labelled antigen cannot bind to an antibody already occupied by an unlabelled sample antigen. The measured signal is inversely related to the amount of the antigen in the sample. In both cases, the immobilised antibodies are drawn to the ideal position having the Fab parts (the "horns" of the letter Y) pointing up from the substrate surface.

Both non-competitive and competitive immunoassays can be carried out using homogeneous or heterogeneous method. If the method includes a separation of the complex consisting of labelled antibody and antigen (or antibody and labelled antigen), it is called heterogeneous. If no separation is required, it is called homogeneous or separation free. Although the sensitivity of the homogeneous immunoassay seems to be lower[66], it is a more popular method, because it needs less time when the separation step is not included. In addition, a separation step has a potential risk of sample loss, which is avoided by using homogeneous immunoassay.

It has been earlier demonstrated that isothiocyanate derivatives of several Tb(III) chelates can be used as efficient electrochemiluminescent labels in bioaffinity assays[24].

Electrochemiluminescent Tb(III) labels can be used both in non-competitive immunoassays and in competitive immunoassays[23].

An interesting feature in HECL immunoassays is that the immunoassay itself can be carried out using a discrete solid support, such as latex particles, while the electrode with a thin insulator film is used merely as an excitation source for labels[12]. This is due to the ability of hot and hydrated electrons to mediate cathodic reactions up to a distance of about 200 nm from the surface of the electrode[51]. However, the more common method where also the immunoassay is executed on the thin insulating film-covered electrode gives considerably lower detection limits[12].

3. Surface modification and microfabrication techniques

Miniaturisation is very popular in modern analytical chemistry, because it has many benefits, including portability, parallelisation, increased reaction rates, capability of processing a large number of samples in a short period of time, and significant decrease in the amount of sample, reagents and waste[67,68]. With microfabrication techniques it is possible to integrate parts of the measurement systems and even a whole measurement system on a single chip[69].

It is quite difficult to miniaturise electrochemical applications without using integrated electrodes, because the sensitivity and reproducibility of the analysis suffers significantly if discrete electrodes are miniaturised[68]. Integrated electrodes are already used in e.g. capillary electrophoresis[70] and impedimetric immunosensors[68].

Many microfabrication processes are originally developed for semiconductor industry and for production of microelectronics. Production of micrometre-sized structures requires extremely clean environment, because otherwise structures are easily destroyed by particles. Therefore, microfabrication is processed in cleanrooms. Cleanrooms are usually classified according to their particle concentration, but also other variables, such as temperature, humidity, and air quality, have to be strictly controlled[71]. Laminar airflow in the whole room or at least above the process equipment is used to sweep any particles away. The main source of contamination in the cleanroom is the persons working there. Therefore, strict protocol has to be followed before entering the cleanroom and people have to wear protective garment. Also all materials, like new tools or chemical containers, have to undergo cleaning procedure before they can be taken to the cleanroom.

The wafers or substrates must be properly cleaned before any microfabrication process. The most common cleaning process is RCA-cleaning (invented in Radio Corporation of America) which consists of three steps: removal of organic contaminants, removal of native oxide layer, and removal of ionic contaminants. These steps are carried out with dipping the wafers or substrates in a hot bath consisting of (i) SC-1 (NH_4OH/H_2O_2 solution

at 80 ^{0}C), (ii) dilute HF, and (iii) SC-2 (HCl/H_2O_2 solution at 80 ^{0}C). The abbreviation SC stands for standard cleaning.

This chapter introduces the basics of the thin film deposition methods and microfabrication techniques used to produce the HECL electrodes described in the Results chapter.

3.1. Thin film deposition

In this research, thin film deposition methods were used to produce metal thin films on Si or glass substrate and to produce thin insulating layer on the cathode material (Publications III–V). Thin metal films were produced by sputtering, thin Al_2O_3 layers by atomic layer deposition (ALD), thin SiO_2 films by thermal oxidation, plasma enhanced chemical vapour deposition (PECVD) or liquid phase deposition (LPD), and thin Si_3N_4 films by PECVD and low pressure chemical vapour deposition (LPCVD).

3.1.1. Thermal oxidation

Silicon is widely used in semiconductor industry. One reason for its popularity is the stable and easily formed insulating oxide which has an excellent interface with silicon. Thermal oxidation is used in metal-oxide-semiconductor (MOS) applications, because the film is pinhole-free and a good quality film can be produced even in nanometre scale.[72-74]

Silicon can be thermally oxidised by wet oxidation or by dry oxidation. In wet oxidation, water steam is used as oxidant and in dry oxidation, the oxidant is gaseous oxygen. Wet oxidation is faster than dry oxidation, but both processes are pretty slow. The time needed for oxidation depends on orientation of the silicon crystal, degree of doping, and oxygen pressure[71]. According to Deal–Grove model[75], the film thickness increases linearly with time for thin films, but for prolonged processes the thickness varies as the square root of time[76]. However, this model is not fully valid for very thin oxide layers where oxide thickness is less than 15–20 nm[73].

Before thermal oxidation, silicon must be cleaned from native oxide and from possible contaminants in order to get good control of oxide thickness and defect levels. Thermal oxidation is typically made in a furnace at temperatures between 800 and 1200 ^{0}C[71].

3.1.2. Physical vapour deposition (PVD)

The term physical vapour deposition (PVD) covers a variety of methods used to deposit thin films by the condensation of the vaporised form of the film material on the substrate surface. PVD processes consist of creation of the vapour phase species, transportation of the vapour species from the source to the substrate, and deposition of the film on the substrate surface[77].

PVD is the dominant method for metal thin film deposition[71]. PVD techniques are widely used for thin-film deposition in many photovoltaics, microelectronics and optics[78]. PVD processes are typically line-of-sight depositions having poor step coverage on sidewalls and bottoms of trenches and therefore, substrate with complex topography cannot be conformally coated[71,78]. PVD is usually carried out in room temperature which makes it suitable for several substrate materials[71].

One of the PVD techniques is evaporation. In evaporation, heated metals having high vapour pressure are transported and condensed to the substrate surface. The process takes places in either high vacuum (HV) or ultra-high vacuum (UHV) which means pressures 10^{-6}–10^{-8} Torr ($1.3\cdot10^{-4}$–$1.3\cdot10^{-6}$ Pa) and $<10^{-9}$ Torr ($< 1.3\cdot10^{-7}$ Pa), respectively. Due to the high vacuum, the atoms can travel directly to the substrate without experiencing collisions.[71,77]

Sputtering is the most important PVD technique[71]. In sputtering, a glow discharge plasma is first created and the argon ions of the plasma are accelerated towards a negatively biased target material. When these ions collide to the target material, they are capable of ejecting atoms (or molecules or clusters of atoms) from the surface of the target material. The ejected target atoms will then be transported to the substrate surface in vacuum and the substrate surface will be coated by a thin film of the target material. The sputtered atoms will experience many collisions before reaching the substrate, because sputtering pressures, 1–10 mTorr (0.13–1.3 Pa), are three to five orders of magnitude higher than evaporation pressures.[71,79]

3.1.3. Chemical vapour deposition (CVD)

In chemical vapour deposition (CVD), the gas phase precursors are decomposed on a heated substrate to form a film. The process consists of (i) input of the precursor gases into the chamber by pressurized gas lines, (ii) diffusion of reactants through the boundary layer (*i.e.* a layer between the bulk gas velocity and the chamber wall having zero velocity), (iii) adsorption of reactants on the substrate, (iv) chemical reactions on the substrate surface, (v) diffusion of the atoms on the surface to growth sites, (vi) desorption of reaction by-products, and finally (vii) diffusion of reaction by-products through boundary layer to the main gas flow region[79,80]. A wide variety of materials, like semiconductors, metals and insulators, can be grown by CVD. SiO_2, for example, can be grown as follows (equation 9):

$$SiH_4\ (gas) + 2N_2O\ (gas) \rightarrow SiO_2\ (solid) + 2H_2\ (gas) + 2N_2\ (gas) \quad (9)$$

The advantages of CVD are its relatively simple instrumentation and fairly free selection of the substrate material[79]. CVD also provides good step coverage. The main problem in CVD is high temperatures (400–900 ^{0}C) needed for deposition processes. The quality of CVD oxide is not as good as the quality of thermal oxide[81]. In addition, CVD precursors and the reaction by-products are often hazardous or toxic and extra steps are needed to handle them[79,80].

There are several sub-classes of chemical vapour deposition such as plasma enhanced chemical vapour deposition (PECVD) and low pressure chemical vapour deposition (LPCVD). In PECVD method, plasma is used to enhance the chemical reactions between the precursors. The energetic electrons in the plasma collide with gaseous precursor molecules resulting in excited or ionised precursor molecules which have lower activation energies for chemical reactions and usually also higher sticking coefficients to the surface than the parent precursor molecules have. This makes it possible to apply lower deposition temperatures (usually 250–350 ^{0}C) than in an equivalent CVD process[77,79]. However, the quality of the thin film produced at lower temperatures is poorer compared to the films produced at higher temperatures[82].

In low pressure chemical vapour deposition (LPCVD) method, sub-atmospheric pressure prevents or at least reduces the unwanted reactions in the gas phase and also makes the film more uniform and conformal[82].

3.1.4. Liquid phase deposition (LPD)

Liquid phase deposition (LPD) is a technique, which can form a metal oxide thin film by dipping the substrate in aqueous solutions. The metal oxide formation is based on a ligand-exchange equilibrium reaction between a metal–fluoro complex ions and metal oxide in aqueous solution. During the deposition process, the metal oxide is forced to precipitate on the substrate surface either directly by adding water or by destabilising the complex by adding H_3BO_3 or aluminium metal[83-85].

The simplest LPD method for the growth of SiO_2 films on silicon is to use a fluorosilicic acid solution supersaturated with silicon oxide and to catalyse the reaction with water[86] (equation 10):

$$H_2SiF_6 + 2H_2O \leftrightarrow SiO_2(\text{solid}) + 6HF \qquad (10)$$

LPD is a simple and inexpensive method which does not require high temperatures, vacuum conditions or complicated instrumentation[87-90]. In addition, it can be applied to different substrates and it is possible to deposit complex shaped substrates[87-90]. However, control over composition, microstructure and growth rate of the resulting film is poorer than in vapour-phase methods[79].

3.1.5. Atomic layer deposition (ALD)

Atomic layer deposition (ALD) has some similarities with CVD. However, the biggest difference between those two methods is that in ALD the precursor materials are kept separated during the reaction. This means removing of any excess precursors and reaction by-products, which can be either in the gas phase or physisorbed on the surface, by an inert gas purge (e.g. N_2) before introducing the next precursor. Additionally, each precursor is introduced into the chamber in a sufficient amount to produce a saturated monolayer on the substrate surface. The thickness of the film can be precisely controlled by the number of the deposition cycles, because each deposition cycle produces one monolayer of the compound on the substrate.[91-93] The basic principle of producing Al_2O_3 films by ALD can be seen in Figure 5.

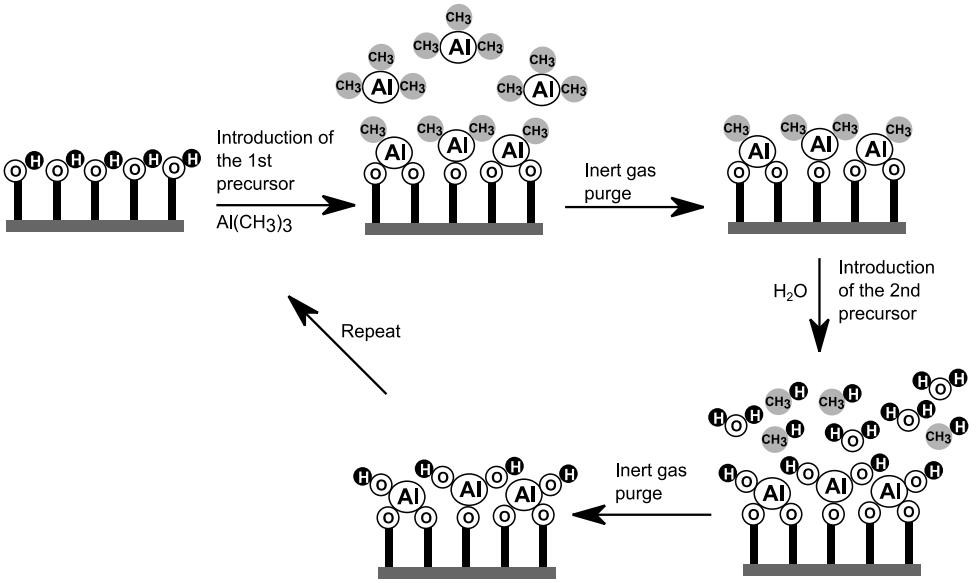

Figure 5. The principle of Al_2O_3 deposition by ALD using trimethylaluminium (TMA) and water as precursors.

ALD method provides excellent thickness control even at atomic level. The produced films are highly uniform and they have low roughness. Furthermore, ALD can be used for conformal and dense film deposition onto very complex substrate surfaces[94-97]. The temperature in ALD process is usually 100–250 ^{0}C[78].

Ideally, ALD process with fixed deposition time should produce the same film thickness regardless of the substrate material. However, with some of the substrate materials tested in this research (Publication IV), the film thickness measured by ellipsometer was higher than expected and with some substrate materials it was lower than expected. This kind of behaviour is caused either by the presence of native oxide or by delayed deposition, respectively.

3.2. Basic microfabrication methods

In this research, basic microfabrication techniques were used to produce the integrated electrode chips (Publication V). The cathode area of the electrode chips was defined by patterning by optical lithography and by using wet etching. Lift-off was used to pattern Pt films acting as the counter electrode. Polydimethyl siloxane (PDMS) casting was used to produce integrated PDMS sample chambers.

3.2.1. Optical lithography

Optical lithography is used to transfer images on wafer. The wafer is first covered by a photosensitive film, *i.e.* photoresist. Basically, photoresist is a polymer doped with a light-sensitive compound.[71]

Photoresist is applied on a wafer by spin coating. In this method, a droplet of the resist is dispensed on the wafer placed on a spinner. When the spinner is accelerated to about 5 000 rpm, the resist is spread on the wafer surface.[71]

During the next step, a photomask is aligned to the wafer and exposed to suitable radiation, usually UV radiation. The exposed areas of the photoresist become more soluble (positive resists) or more insoluble (negative resists) in the developer which enables selective removal of the resist during development process. Depending on the photoresist, the image on the wafer will be either the same (positive resists) or opposite (negative resists) compared to the image on the mask.[71] The basic principle of optical lithography can be seen in Figure 6.

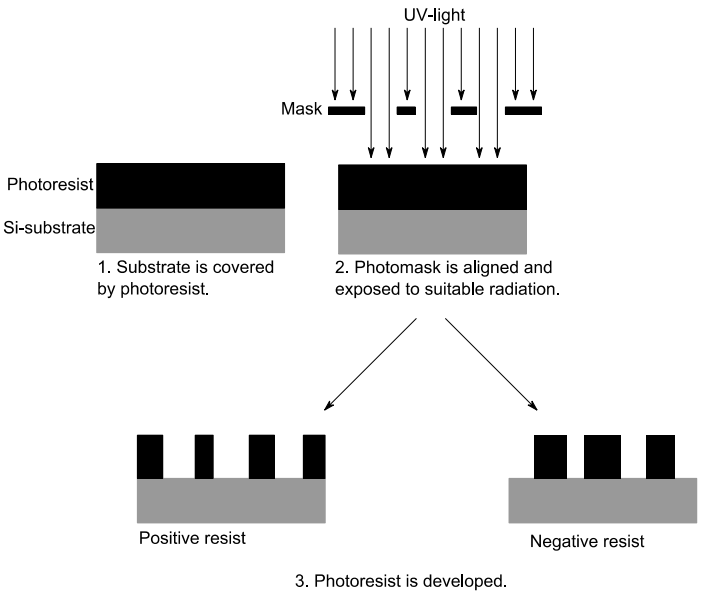

Figure 6. The basic principle of optical lithography.

It is possible to continue processing after lithography and to use photoresist as a protective layer in these processes. However, the resist meets some special requirements depending on the process. Typical processes after lithography are wet etching, plasma etching, ion implantation, lift-off, and electroplating[71]. The principle of etching is discussed in chapter 3.2.2. and the principle of lift-off is discussed in this chapter, because those processes were used in making integrated HECL electrode chips.

Lift-off is a technology which can provide fine metallisation patterns. After lithography, metal is deposited on the substrate both in the areas defined by the photoresist and on the photoresist itself. After dissolution of the resist and metal lift-off, all the metal that is not in contact with the substrate is removed. Evaporation, for example, is a good deposition method for lift-off, because it is a line-of-site method which has poor step coverage.[71,82] The principle of lift-off is shown in Figure 7.

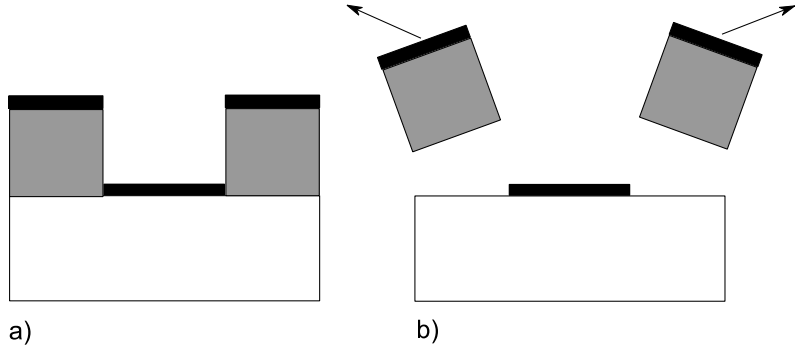

Figure 7. The basic principle of lift-off[71]. First, the desired metal is deposited on the resist and on the free substrate surface (a). After dissolution of the resist and metal lift-off, all the metal that is not in contact with the substrate is removed (b). White areas describe the substrate, grey areas the resist and black areas the deposited metal.

Many kinds of substrates can be patterned by lift-off and it is especially suitable for materials which are hard to etch. On the other hand, lift-off cannot be applied to substrates with complex topography due to its poor step coverage.[71]

3.2.2. Etching

The purpose of etching is to remove material selectively and with high resolution. A mask is provided to cover the sites that should not be etched. The minimum requirement for a mask is that it does not dissolve or at least it is etched much slower than the material to be patterned.[76]

The etching methods are usually divided into wet etching and plasma etching. However, the term “dry etching” is sometimes used contrary to wet etching and as a synonym for plasma etching, even if there are also dry etching methods other than plasma. In wet etching, solid substrate reacts with liquid etchant producing soluble products and in plasma etching, solid substrate reacts with gaseous etchant producing volatile products. Typical etch rates are 100–1 000 nm/min for both processes.[71,82] Reactions 11 and 12 are examples of wet and plasma etching.

Wet etching:

$$Si(s) + 2OH^- + 2H_2O \rightarrow Si(OH)_2(O^-)_2(aq) + 2H_2(g) \quad (11)$$

Plasma etching:

$$SiO_2(s) + CF_4(g) \rightarrow SiF_4(g) + CO_2(g) \quad (12)$$

Etching processes can also be divided into isotropic and anisotropic, depending on the etching profile. The differences in the etching profiles can be seen in Figure 8. In isotropic etching process, the substrate is etched at the same rate into all directions and it is etched also under the etch mask (*i.e.* undercutting). Undercutting can be desirable or undesirable depending on the case. It is impossible to make closely spaced lines when undercutting occurs but, on the other hand, undercutting is needed in making free-standing structures, like cantilevers or released resonating bridges. Silicon isotropic etchants are HF:HNO_3-based.[71,82]

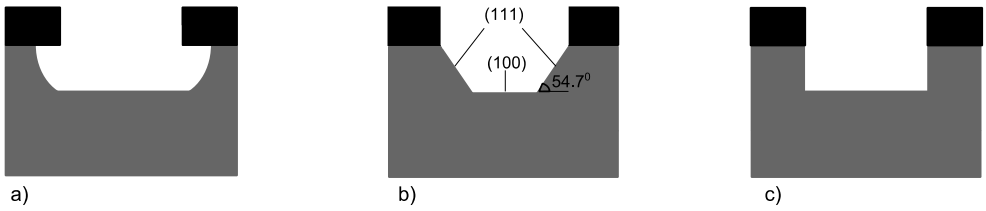

Figure 8. Different etching profiles when isotropic etching (a), anisotropic wet etching (b) and anisotropic plasma etching (c) are used. In isotropic etching, the substrate is etched at the same rate from all directions and also undercutting occurs (a). In anisotropic plasma etching, the etching angle is 54.7^0 between (100) and (111) planes. (100) planes are etched faster than (111) planes and the etching process ends when (111) planes meet (b). In anisotropic plasma etching, the etching profile has vertical or nearly vertical side walls (c).[71]

Anisotropic etching is divided into anisotropic wet etching and anisotropic plasma etching. Silicon is commonly anisotropic wet etched by potassium hydroxide (KOH) or tetramethyl ammonium hydroxide (TMAH). When (100) silicon wafer is anisotropically wet etched, the etching angle is 54.7^0 between (100) and (111) planes. (100) planes are etched faster than (111) planes and the etching process ends when (111) planes meet. In anisotropic plasma etching, the substrate is bombarded by ions from plasma reactor. This etching profile has vertical or near vertical side walls.[71,82]

3.2.3 Polydimethyl siloxane (PMDS) casting

PDMS casting is used to fabricate microfluidic channels in PDMS[98]. PDMS has attractive optical and chemical properties for the fabrication of microfluidic systems with an integrated optical detection system. It is transparent from 235 nm to the near-infrared allowing optical detection over the entire visible spectrum[98]. In addition, the autofluorescence of PDMS is lower than that for many other polymers such as polystyrene [99].

The PDMS casting process starts with creating a master mould. The mould can be produced on silicon wafer by standard photolithography techniques. The mould is re-usable providing low-cost technology suitable for batch production. When the master mould is ready to use, a mixture of PDMS pre-polymer and curing agent is mixed, placed to a vacuum chamber to remove air bubbles, and poured to the master mould. After that it is cured in oven. The cured PDMS is peeled off the master mould and it can be bonded to the desired chip.[98,100,101]

4. Experimental

This chapter briefly describes the instrumentation, measurement methods, and manufacturing procedures used in the research. More detailed information of the experiments is given in Publications I–VII.

4.1. HECL instrumentation

In HECL measurements, the cathodic pulse polarisation of the electrode was created by an in-house built coulostatic pulse generator[22]. A potentiostat (Pine Instrument RD4) was used in some of the measurements in Publication I. The voltage, rate, and electrical charge of the pulses used in each measurement are described in detail in Publications I–VII. In most cases, the measurements were carried out using time-resolved technique. This means that a certain delay was applied after every pulse before starting data acquisition period. The delay depends on the luminophore displaying long-lived luminescence. Light detection was performed with a photomultiplier tube (PerkinElmer MH1993, 1364-H-064) through a suitable interference filter. A separate photon counter (SR400 two channel gated photon counter, Stanford Research System) with an amplifier (Model SR445, DC-300 MHz amplifier, Stanford Research System) was connected to the photomultiplier module. Photoluminescence (PL) measurements, HECL spectra, and fluorescence spectra were obtained by Perkin-Elmer LS5 luminescence spectrometer.

Four different sample holders were used: (i) a 5.6 mm diameter polytetrafluoroethylene (PTFE) cell (volume 250 µl) with a platinum wire counter electrode mechanically sealed in a sample holder providing contact from backside of the electrode (Publications I, III and IV), (ii) a 7.6 mm diameter PTFE cell (volume 500 µl) with an o-ring mechanically sealed in the sample holder providing two contacts from both front and backside of the electrode (Publication V), (iii) a sample holder without any discrete cell providing two contacts from both front and backside of the electrode (Publications V and VII), and (iv) a sample track with 12 separate Pt wires and a microtiter strip with 12 sample cups (Publication VI).

In the research modelling the miniaturisation of the electrode, the photomultiplier tube was PerkinElmer MP1993, 1363-P-064. The optical fibers used in this part of the research were Ocean Optics QP-1000-2-UV-BX and Ocean Optics QP-100-2-UV-BX.

The immunoassays in Publication VI were carried out with a semiautomatic electrochemiluminometer modified from a PerkinElmer Wallac Fluorometer[23].

The model luminophore used in Publications III–V was Tb(III) chelated by 2,6-bis[N,N-bis(carboxymethyl)aminomethyl]-4-benzoylphenol.

4.2. Experimental procedures in thin film deposition

Table 1 presents the metal thin films sputtered on a silicon substrate and the thin film thicknesses.

The tested conductor materials and insulating films, deposition methods used to produce the insulating films and the tested film thicknesses are described in Table 2. The silicon used as a working electrode substrate was highly conductive n-type silicon wafer of 0.005–0.018 Ω cm resistivity and (111) orientation.

Table 1. The metal thin films sputtered on a silicon substrate and the thin metal film thicknesses.

Metal thin film	Thickness / nm
Al	120
Cr	50
Cu	200
Pt	50
Ti	40
W	60

Table 2. The tested conductor materials and insulating films, deposition methods used to produce the insulating films, and the tested film thicknesses. The ALD process was carried out by using TMA/H_2O or TMA/O_3 as precursors. In case of TMA/O_3, Ti and Pt were excluded, because they were not available during the tests.

Conductor material	Insulating film	Deposition method	Tested film thickness / nm
Al, Cr, Cu, Pt, Ti, Si and W	Al_2O_3	ALD (TMA/H_2O)	3–100
Al, Cr, Cu, Si and W	Al_2O_3	ALD (TMA/O_3)	3–100
Al, Cr, Cu, Pt, Ti, Si and W	SiO_2	PECVD	3–40
Si	SiO_2	LPD	2–5
Si	Si_3N_4	LPCVD	3–8
Si	Si_3N_4	PECVD	3–7
Si	SiO_2	Thermal oxidation	2–7

Thermal SiO_2 was grown in a Centrotherm oxidation furnace at 850 °C in an atmosphere containing 10 % oxygen and 90 % nitrogen. Si_3N_4 was deposited in a Centrotherm LPCVD furnace using a standard recipe of 40 standard cubic centimetres per minute (sccm) dichlorosilane and 200 sccm ammonia at 250 mTorr (33 Pa) pressure and 770 °C deposition temperature. PECVD of SiO_2 and Si_3N_4 were carried out in an Oxford Plasmalab 80 Plus single-wafer reactor using standard recipes with reduced RF power and silane flow. The films were deposited at 300 °C and at 1 000 mTorr (130 Pa) pressure with RF power of 5 W. The reactant gas flows were 2.0 sccm SiH_4, 710 sccm N_2O, and 161.5 sccm N_2 for silicon dioxide and 20 sccm SiH_4, 30 sccm NH_3, and 380 sccm N_2 for Si_3N_4. Aluminium oxide was grown by atomic layer deposition in a Beneq TFS-500 reactor at 220 °C temperature and at approximately 5 mbar (500 Pa) pressure, using trimethyl aluminium (TMA) and ozone or TMA and water as precursors. Liquid phase deposition of silicon dioxide was carried out from SiO_2-saturated hexafluorosilicic acid (H_2SiF_6) solution by addition of water and boric acid (H_3BO_3) at 35 °C temperature.

Dielectric thickness was monitored with a Philips SD 2300 ellipsometer. The measurements were made by using the bulk refractive index of the deposited film. This

approach is not fully satisfactory for determination of the absolute value of the thickness. However, it works for testing the reproducibility.

The cleaning, other pre-treatment processes and the deposition processes are described in detail in Publications III and IV.

4.3. Fabrication of integrated electrodes

The electrode chips were made on silicon and on glass wafers. The electrode chips with oxide-covered silicon working electrodes were fabricated from n-type silicon wafers having resistivity of 0.005–0.018 Ω cm and (111) orientation. The wafers were initially RCA-cleaned and then wet oxidised to yield a 380 nm field oxide, which passivates and protects the semiconductor surface outside the active device area. The working electrode area was defined by patterning the field oxide by optical lithography and by using HF wet etching. RCA-cleaning was used to remove any native oxide, and ca. 4 nm thick tunnelling oxide was grown on the working electrode by dry oxidation. After lithography, a 50 nm thick Pt layer, acting as the counter electrode, was deposited by sputtering and patterned by lift-off. Though not always necessary, the backside contact could be improved by wet etching the wafer backside free of oxide, and sputtering onto it an approximately 100 nm thick aluminium layer. The size of the chip is 10 mm×19 mm. The chip is shown in Figure 9.

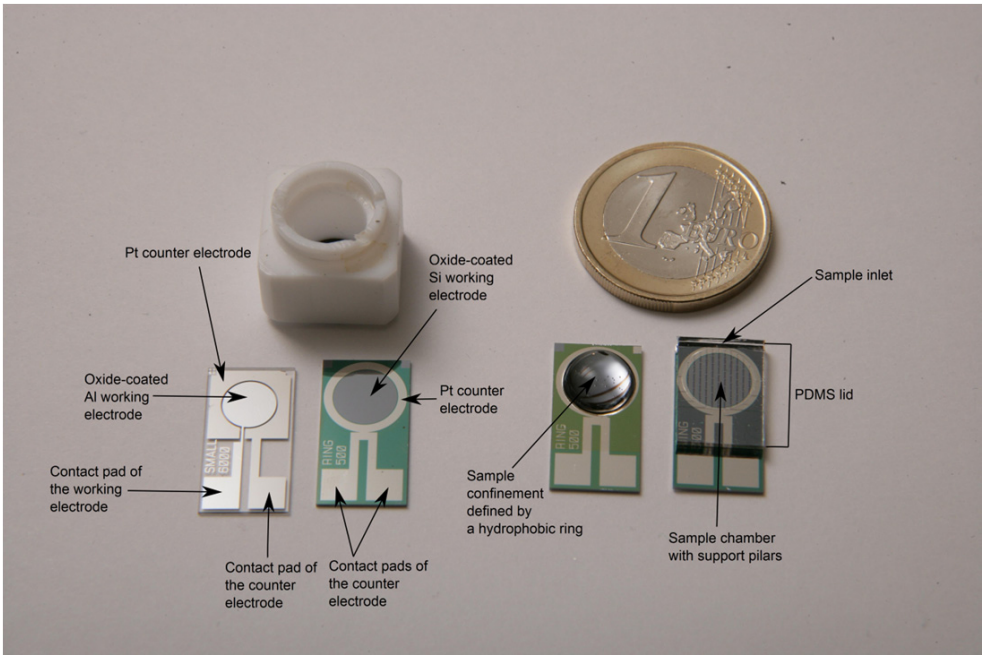

Figure 9. The integrated electrode chips are from left to right: (i) glass device with Al/Al_2O_3 working electrode and Pt counter electrode, (ii) silicon device with Si/SiO_2 working electrode and Pt counter electrode, (iii) silicon device with an integrated sample confinement defined by a hydrophobic ring, and (iv) silicon device with an integrated PDMS sample chamber. The chips (i) and (ii) need a discrete sample cell which is above them. The chips (iii) and (iv) have an integrated sample confinement which can be filled by dispensing the sample on the sample confinement or by capillary forces from a droplet of a sample, respectively.

Pyrex glass wafers were initially cleaned with SC-1 and 400 nm of aluminium was sputtered to form the working electrodes. Aluminium also acted as a sacrificial layer in the patterning of platinum. First, the counter electrode areas were defined by standard optical lithography and aluminium was removed from those areas by wet etching. The aluminium film was intentionally overetched by 100 % to form an undercut in the photoresist, which was not removed at this stage. Platinum was then sputtered and patterned by lift-off, facilitated by the overhanging resist. After that, the aluminium working electrode was defined by lithography and wet etching. About 4 nm thick aluminium oxide layer was deposited by ALD. This layer was removed from the platinum counter electrode and from contact pads by photolithography and etching. Finally, the photoresist was removed. The chip is shown in Figure 9.

Hydrophobic sample confinement was made on the silicon chip by depositing a hydrophobic fluoropolymer film around the electrode area by a plasma deposition process

and by patterning by lift-off. Because the electrodes and contact pads were masked by photoresist during the fluoropolymer deposition process, they were left hydrophilic, although the surrounding areas became strongly hydrophobic. When the sample is then dispensed on the cathode, it remains as a droplet on the area defined by the hydrophobic ring. The volume of the sample confinement is 100 µl. The chip with a hydrophobic sample confinement is shown in Figure 9.

The PDMS sample chamber was produced by PDMS casting. The master mould was made on a silicon wafer by processing SU-8 epoxy-based negative photoresist structures on its surface by standard photolithographic techniques. Once complete, the master was coated with antisticking Teflon-like fluoropolymer by reactive ion etching system. This facilitates easier peeling of the cured PDMS from the master, and prolongs the master's lifetime, without affecting the bonding properties of the PDMS. In the casting process, Sylgard 184 silicone elastomer and curing agent were mixed in a 10:1 ratio onto the master mould in a Petri dish. The wet PDMS was then outgassed in vacuum and cured. The cured PDMS was peeled off the master, cut into individual chips, and bonded to the glass chip with integrated electrodes. Bonding was improved by exposing both the PDMS fluidic chip and the electrode chip to oxygen plasma. In addition, the plasma treatment makes the PDMS surface hydrophilic, which enables filling of the sample chamber by capillary force. The volume of the sample chamber is 15 µl. The chip with a PDMS sample chamber is shown in Figure 9.

The fabrication of the integrated electrode chips is described in more detail in Publication V.

4.4. Immunoassay procedures

The immunoassays in both Publications VI and VII were carried out using sandwich method.

In Publication VI, SiO_2-coated Si electrodes (boron doped p-type (100) having resistivity of 10.0–20.0 mΩ cm) were coated with monoclonal anti-human C-reactive protein (anti-hCRP) primary antibodies by immersing them in microtiter strips containing 250 µL of coating solution. The reaction was incubated overnight at room temperature in a humid plastic container. After that, the coated Si electrodes were moved to the other microtiter strips containing 350 µL of the saturation solution and allowed to stand overnight in a humid plastic container. The immunoassay was carried out by adding a mixture of hCRP calibration standards (100.0 µL) and the labelled secondary antibody (100.0 µL, the final concentration of the labelled secondary antibody was 82 µg L^{-1}) diluted in assay buffer in the microtiter strips. The labelled secondary antibody was an isothiocyanate derivative of Tb(III) chelate (Tb(III)-1-NCS, where 1 is 2,6-bis[N,N-bis(carboxymethyl)aminomethyl]-4-benzoylphenol). Different incubation times were tested and typically incubation times used were between 2 and 15 min. After the incubation, the Si electrodes were washed three times in microtiter wells with 300 µL of washing solution and measured. The detailed composition of each reagent is described in Publication VI.

In Publication VII, integrated Si chips were coated with hCRP primary antibodies by physical adsorption by dispensing 57 µL coating solution on the cathode area of the chip. The reaction was incubated for 1 h in a 100 % humidity chamber. After incubation, excess coating solution was removed by suction and the coated cathode was washed by letting 1 mL of washing solution flow over the electrode four times. After that, the electrodes were saturated by dispensing 90 µL of saturation solution on the coated cathode area. The chips were kept in a 100 % humidity chamber for 1 h. Excess saturation solution was removed by suction. After saturation, the chips were dried at room temperature for 3 h in a box with silica beads. The box with the chips was kept in a refrigerator overnight. The immunoassay was carried out by two different dispensing procedures. In the first one, 3.5 µL of desired standard solution was dispensed on the cathode area of the chip and directly after that, 1 µL of label solution was dispensed on the cathode area. In the second

one, 5 µL of the solution containing both the antigen and labelled antibodies was dispensed on the cathode area. The label was an isothiocyanate derivative of Tb(III) chelate (Tb(III) chelated by N^1-(4-isothiocyanatobenzyl)diethylenetriamine-N^1,N^2,N^3,N^3-tetraacetate). The same mass of the antigen and the labelled antibody was used in both procedures. After 5 min incubation in the humidity chamber, each chip was washed by letting 1 mL borate–azide buffer flow over the electrode four times. Before the measurement, 100 µL of the borate–azide measuring buffer was dispensed on the cell area of the chip. The detailed composition of each reagent is described in Publication VII.

5. Results and discussion

This chapter summarises the main results of the research described in Publications I–VII.

5.1. New HECL luminophores

Fluorescein was chosen as a luminophore for testing (Publication I), because the fluorescence quantum yield of fluorescein (2-(6-hydroxy-3-oxo-xanthen-9-yl)benzoic acid) is relatively good (about 0.91 in alkaline solution)[102] and it is known to show radiochemiluminescence induced by hydrated electrons and hydroxyl radicals[103,104], which are also suggested to be the primary reactive species in the HECL system. In addition, fluorescein derivatives have been used as a label in bioaffinity assays by photoluminescent methods[102].

When cathodic pulses are applied to oxide-covered aluminium electrodes fluorescein peak appears at about 515 nm and its HECL emission spectrum is similar to its fluorescence emission spectrum[105]. The luminescence lifetime of fluorescein in the tested conditions is much longer than that of coumarins, for example. Its decay is multiexponential and the decay curve can be fitted with two exponential functions giving luminescence lifetime of 17 μs and 60 μs, respectively. The decay curves of coumarin and fluorescein are described in Figure 10.

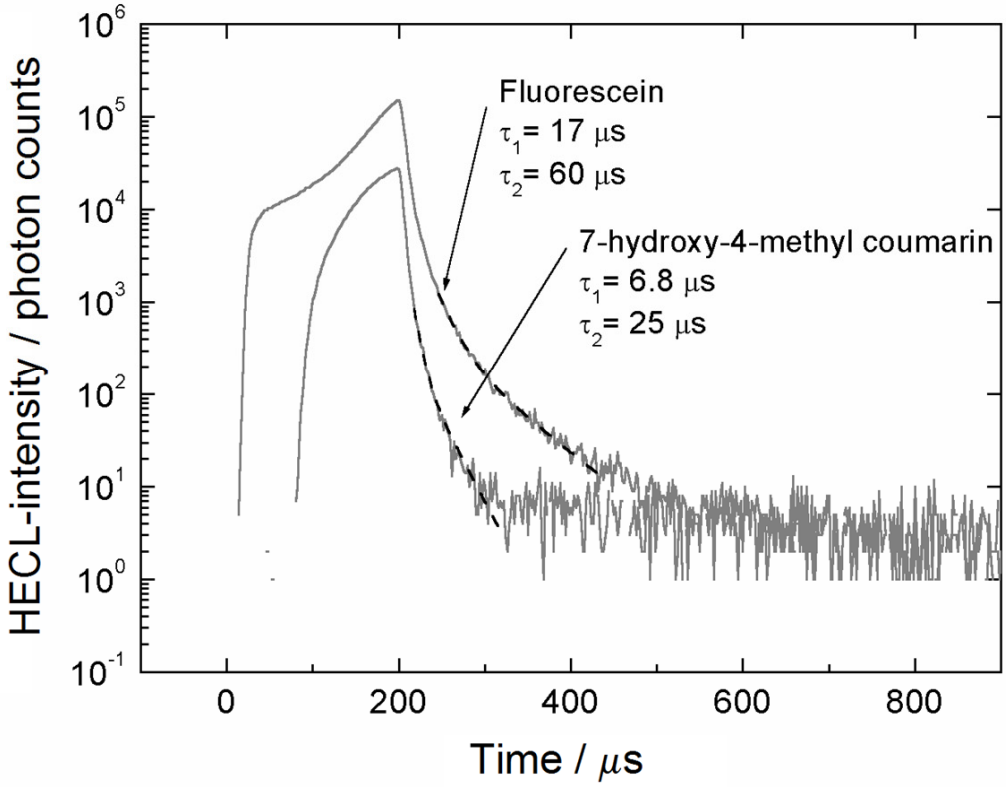

Figure 10. The rise and decay of the cathodic HECL pulse of fluorescein and 7-hydroxyl-4-methyl coumarin. Conditions: $1 \cdot 10^{-6}$ M fluorescein or coumarin in 0.05 M $Na_2B_4O_7$ buffer at pH 9.2 containing 0.1 M Na_2SO_4, Pine Instrument RD4 potentiostat, pulse voltage 10 V, pulse frequency 50 Hz.

The slow decay is probably based on the excitation reactions still going on after the cathodic pulse. The reason for faster rise time and smaller lag time of fluorescein compared to 7-hydroxy-4-methyl coumarin might be that coumarin has slower reaction rates with the primary radicals of excitation system. The HECL intensity of fluorescein is relatively constant within pH range 4–11 and fluorescein is efficiently excited over the whole pH range where Al_2O_3 film is stable. Because the pK_a values of fluorescein are 2.2, 4.4, and 6, fluorescein exists as a dianion (Flu^{2-}) in alkaline solutions and it is tested to be excited best below pH 10 when aluminium electrodes with a 4 nm thick Al_2O_3 film are used. According to the earlier research, a wider usable pH range would be obtained at silicon oxide-covered silicon electrodes[21,106].

The effect of several hydrated electron and hydroxyl radical scavengers on HECL with fluorescein was tested. The results are shown in Figure 11.

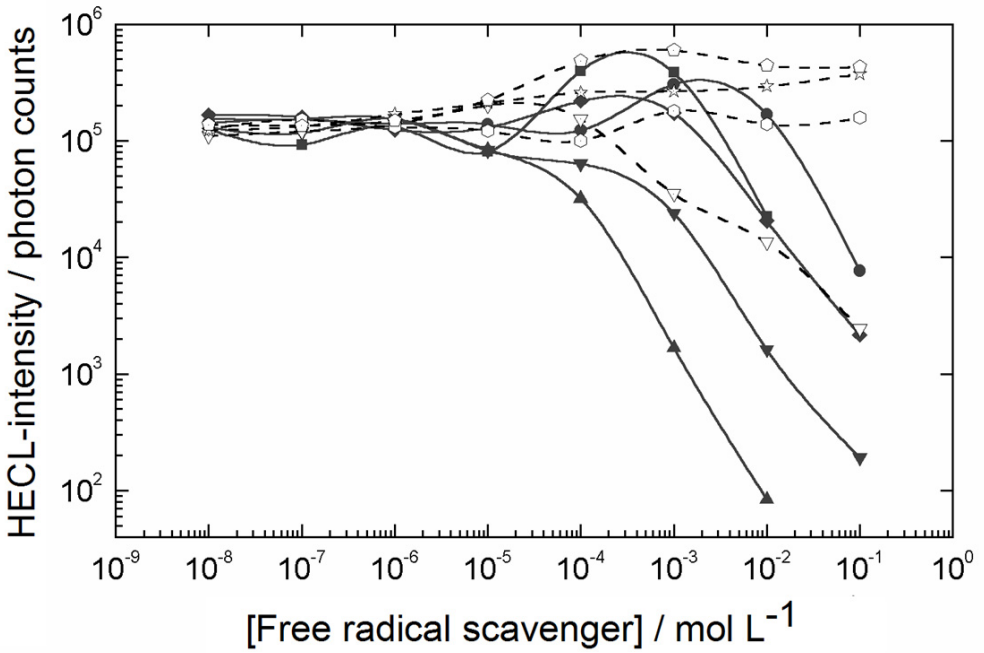

Figure 11. Effect of several free radical scavengers on the HECL intensity of fluorescein. Hydrated electron scavengers: $K_2S_2O_8$ (black squares), H_2O_2 (black diamonds), $K_4P_2O_8$ (black circles), $NaNO_3$ (black triangles, apex down), Benzophenon-4-carboxylate (black triangles, apex up). Hydroxyl radical scavengers: NaCl (open hexagons), NaBr (open stars), NaI (open triangles), NaN_3 (open pentagons). Conditions: $1{\cdot}10^{-6}$ M fluorescein in 0.05 M $Na_2B_4O_7$ buffer at pH 9.2 containing 0.1 M Na_2SO_4, Pine Instrument RD4 potentiostat, 515 nm interference filter, pulse voltage 10 V, pulse frequency 50 Hz, measurement window 2.00 ms, and delay time 5.0 µs. The intensities were integrated over 1 000 excitation pulses.

From the tested hydroxyl radical scavengers both azide (($E^0(N_3^{\bullet}/N_3^-)$ = 1.33 V vs. SHE)[107] and bromide (($E^0(Br^{\bullet}/Br^-)$ = 1.92 V vs. SHE)[107] enhance the HECL intensity at high concentrations. Azide also improves the signal-to-blank ratio, because it does not enhance the background intensity, like peroxodiphosphate and peroxodisulphate do. The enhancing effect of azide and bromide indicates that Br^- and $N_3^{\bullet}$ can participate in light generating pathways more efficiently than hydroxyl radicals. When the concentration of bromide is increased, $Br_2^{-\bullet}$(($E^0(Br_2^{-\bullet}/Br_2)$ = 1.62 V vs. SHE)[107] is formed and it is also a sufficiently strong oxidant in the HECL system.

Chloride (($E^0(Cl^{\bullet}/Cl^-)$ = 2.41 V vs. SHE)[107] does not have any effect on the HECL intensity, because at the present pH (pH 9.2) it cannot be oxidised by hydroxyl radical, which has the formal reduction potential 2.3 V (at pH 7), 2.1 V (at pH 9), and 2.0 V vs. SHE (at pH 12)[108].

The reaction of iodide with hydroxyl radical produces weakly oxidising agents, such as, $I^{\bullet}$ ($E^0(I^{\bullet}/I^-)$ = 1.33 V vs. SHE)[107] and at high concentrations also $I_2^{\bullet-}$ ($E^0(I_2/I_2^{\bullet-})$ = 0.21 V vs. SHE)[107]. Strong decrease in the HECL-intensity can be observed when the concentration of iodide ion increases. Same kind of behaviour can be seen with thiocyanate ion, because $(SCN)_2^{\bullet-}$ is a very weak oxidising agent ($E^0((SCN)_2^{\bullet-}/(SCN)_2^{2-})$ = 0.21 V vs. SHE)[107]. In addition, the rate constants of thiocyanate reactions (8b) and (8c) are very high[109].

At high concentrations, the above mentioned scavengers start to decrease HECL-intensity, because they spoil the balance of the reducing and oxidising equivalents at the close vicinity of the electrode surface. Some hydrated electron scavengers have stronger HECL-decreasing effect than the others and the HECL-decreasing effect is related to the second-order reaction rate of the scavenger reacting with hydrated electron. One exception is nitrite ion: even if its second-order reaction rate constant with hydrated electron ($4.1 \cdot 10^9$ L mol^{-1} s^{-1})[31] is lower than the corresponding reaction rate constant of nitrate ion ($9.7 \cdot 10^9$ L mol^{-1} s^{-1})[31], its HECL-decreasing capability is stronger than that of nitrate ion[105]. The explanation is that nitrite reacts rapidly also with hydroxyl radical ($k(OH^{\bullet} + NO_2^-)$ = $1.0 \cdot 10^{10}$ L mol^{-1} s^{-1})[31] and thereby consumes hydrated electrons and hydroxyl radicals from the excitation pathways.

The strong HECL-decreasing effect of ethanol is based on its reaction with hydroxyl radicals which produces strongly reducing secondary radicals by hydrogen abstraction[31] (*i.e.* a free radical removes a hydrogen atom from a molecule turning the molecule into a free radical). In other words, ethanol consumes strongly oxidising species which are needed in excitation processes. The intensity-decreasing efficiency of the tested hydroxyl radical scavengers is ethanol > iodide ions > thiocyanate ions. In general, the high intensity-decreasing efficiency of hydroxyl radical scavengers is caused by low redox potential of the oxidising secondary radicals and high reaction rate constant of the scavenger.

To conclude, these results with different scavengers support the assumption that cathodic pulse polarisation generates hydrated electrons and oxidising species similar to hydroxyl radical and that these redox species play important role in the excitation pathway of HECL luminophores when working electrodes with thin oxide film are used. Because azide was a

better oxidant than hydroxyl radical, it can be concluded that 1.3 V vs. SHE is a sufficient oxidising power for the oxidant in the described HECL system.

The most probable excitation pathway of fluorescein during the HECL process was deduced using the results of the scavenger tests and earlier studies of the reactions of fluorescein.

Fluorescein dianion is known to be reduced by a hydrated electron at the rate near the diffusion controlled rate ($k = 1.4 \cdot 10^{10}$ L mol^{-1} s^{-1}, pH 9.2)[110], and this excitation pathway would continue by a reaction with $Ox^{\bullet}$ to get the emitting form Flu^{2-*}. $Ox^{\bullet}$ stands for a hydroxyl radical, some other secondary radical formed in reaction with hydroxyl radical or a sulfate or a phosphate radical produced by reduction. This excitation pathway (equations 13a and 13b) is the red-ox pathway.

$$Flu^{2-} + e_{aq}^{-} \rightarrow Flu^{3\bullet-} \qquad (13a)$$

$$Flu^{3\bullet-} + Ox^{\bullet} \rightarrow Flu^{2-*} + Ox^{-} \qquad (13b)$$

Also hydroxyl radical reacts with fluorescein dianion almost at the same rate as the hydrated electron ($k = 1.2 \cdot 10^{10}$ L mol^{-1} s^{-1}, pH = 10) (equation 14 a). This oxidation reaction would continue with reduction by hydrated electron to obtain the emitting form (equation 14b).

$$Flu^{2-} + OH^{\bullet} \rightarrow Flu^{\bullet-} + OH^{-} \qquad (14a)$$

$$Flu^{\bullet-} + e_{aq}^{-} \rightarrow Flu^{2-*} \qquad (14b)$$

However, hydroxyl radical can also form an adduct radical with fluorescein[111] (equation 15a), and after that, the adduct radical would be reduced by a hydrated electron to result in the emitting species (equation 15b).

$$Flu^{2-} + OH^{\bullet} \rightarrow OH - Flu^{2-\bullet} \qquad (15a)$$

$$OH - Flu^{2-\bullet} + e_{aq}^{-} \rightarrow Flu^{2-*} + OH^{-} \qquad (15b)$$

In the present case, azide seems to enhance HECL intensity of fluorescein. Azide radical does not have a tendency to make adducts with aromatic rings but it almost exclusively acts as a one-electron oxidant[109]. This means that the excitation pathway cannot be the

adduct formation, because azide blocks the adduct radical formation reaction (equation 15a) and thereby enhances HECL intensity. In addition, azide radical is not a sufficiently strong oxidant to complete the red-ox pathway. Therefore, the increased intensity cannot be due to red-ox pathway. The predominant excitation mechanism seems to be ox-red pathway (equations 14a and 14b) as it is also in the case of radiochemiluminescence (RCL)[103].

The calibration curve of fluorescein was linear over 5 decades without azide ions and over 6 decades when 0.1 M NaN_3 solution was used. When 1 mM $K_4P_2O_8$ is used to enhance the HECL intensity, intensities even higher than those with azide ions are achieved. However, the calibration curve is not anymore linear at low concentrations. The calibration curves can be seen in Figure 12. In these measurements, time-resolved detection was used and in this case it means that the data acquisition was started after a 5 μs delay after every excitation pulse. It was possible to use time-resolved method, because of the earlier mentioned relatively long life-time of fluorescein HECL emission. Time-resolved measurement further enhances sensitivity because the long-lived luminescence is efficiently separated from the background luminescence.

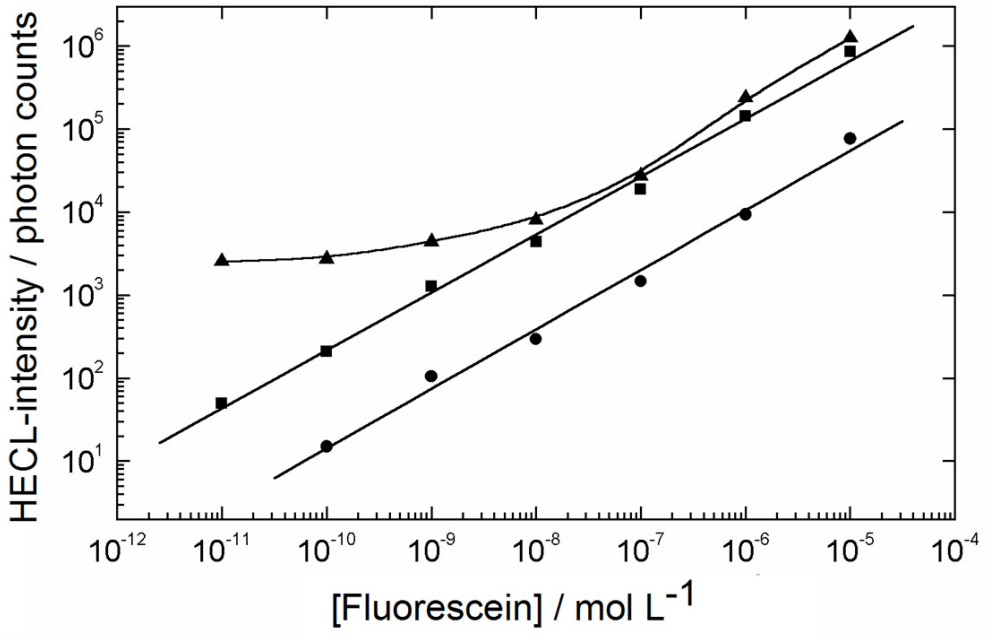

Figure 12. Calibration curves of fluorescein using native Al_2O_3-covered aluminium electrodes. HECL was measured without any coreactant (circles), in the presence 0.1 M NaN_3 solution (squares), and in the presence of 1 mM $K_4P_2O_8$ (triangles). Conditions: Fluorescein in 0.05 M $Na_2B_4O_7$ buffer at pH 9.2 containing 0.1 M Na_2SO_4, Pine Instrument RD4 potentiostat, 515 nm interference filter, pulse voltage 10 V, pulse frequency 50 Hz, measurement window 2.00 ms, and delay time 5.0 µs. The intensities were integrated over 1 000 excitation pulses.

According to these results (Publication I), it is proposed that fluorescein derivatives containing suitable linking groups should be suitable for the purposes of bioaffinity assays.

Other tested luminophores were [4-ethoxycarbonyl-4'-carboxy-2,2'-bipyridine]bis(2,2' bipyridine)ruthenium(II) hexafluorophosphate ($Ru(bpy)_2L_a^{2+}$) and [4,4'-diethoxycarbonyl-2,2'-bipyridine]bis(2,2'-bipyridine) ruthenium(II) hexafluorophosphate ($Ru(bpy)_2L_b^{2+}$) which are carboxylic acid derivatives of ruthenium(II)tris-(2,2'-bipyridine) chelate ($Ru(bpy)_3^{2+}$) (Publication II). Also the synthesis of these derivatives is described in Publication II. These luminophores were chosen, because $Ru(bpy)_3^{2+}$ has earlier been shown to work well as a luminophore in HECL measurements[16]. $Ru(bpy)_3^{2+}$ cannot, however, be easily linked with biologically interesting compounds. The carboxylic acid derivative of $Ru(bpy)_3^{2+}$ can instead be used as a label in bioaffinity assays, for example. The carboxyl functional group can be linked with primary amino groups of e.g. antibodies

and oligonucleotides and with the N-hydroxysuccinimide ester of proteins, peptides and DNA. This linking capability enables labelling of large variation of biological compounds. Unsubstituted $Ru(bpy)_3^{2+}$can also be detected by other chemiluminescence methods[6,106,112,113]. One-electron reduction of the tested derivatives takes place a bit easier than one-electron reduction of the unsubstituted $Ru(bpy)_3^{2+}$. In addition, one-electron oxidation of the tested derivatives is only slightly more difficult than that of the unsubstituted version. Therefore, the traditional anodic ECL at noble metal electrodes[6,112] would also be a usable excitation method for these complexes. In addition, these derivatives can be excited using photoluminescence (Publication II).

$Ru(bpy)_2L_a^{2+}$ has a single exponential decay at SiO_2-coated n-silicon electrode with a luminescence lifetime of 40.0 μs as can be seen in Figure 13. Therefore, also time-resolved measurement is possible. However, the decay at Al_2O_3-covered aluminium electrode does not seem to be a single exponential process. This might be related to the features of the electrode material itself[29]. Time-resolved measurements are still possible using Al_2O_3-covered aluminium electrodes.

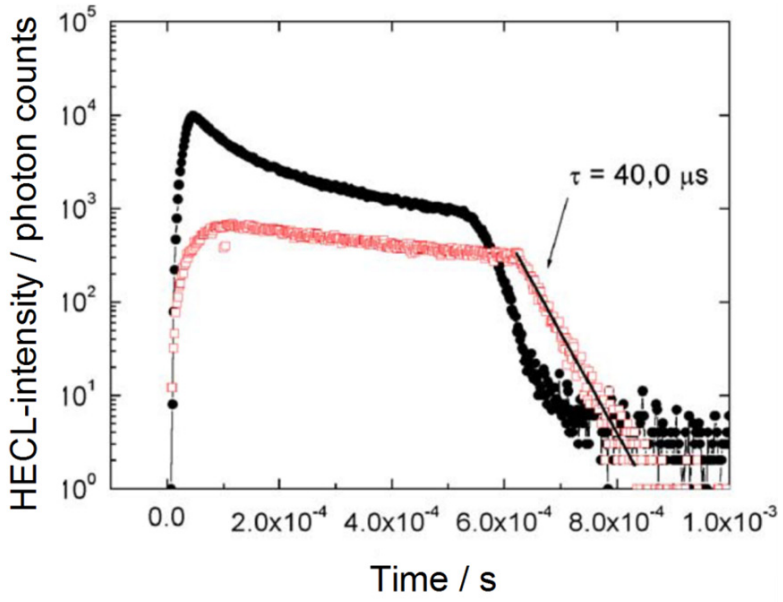

Figure 13. Rise and decay of HECL pulse measured with $1 \cdot 10^{-5}$ M $Ru(bpy)_2L_a^{2+}$ using native Al_2O_3-covered aluminium electrodes (black circles) and thermally oxidised Si electrodes (open squares). Conditions: $1 \cdot 10^{-5}$ M $Ru(bpy)_2L_a^{2+}$ in 0.05 M $Na_2B_4O_7$ buffer at pH 9.2 containing 1.0 mmol L^{-1} $K_2S_2O_8$, 620 nm interference filter, pulse charge 120 µC, pulse voltage 45 V, and pulse frequency 20 Hz.

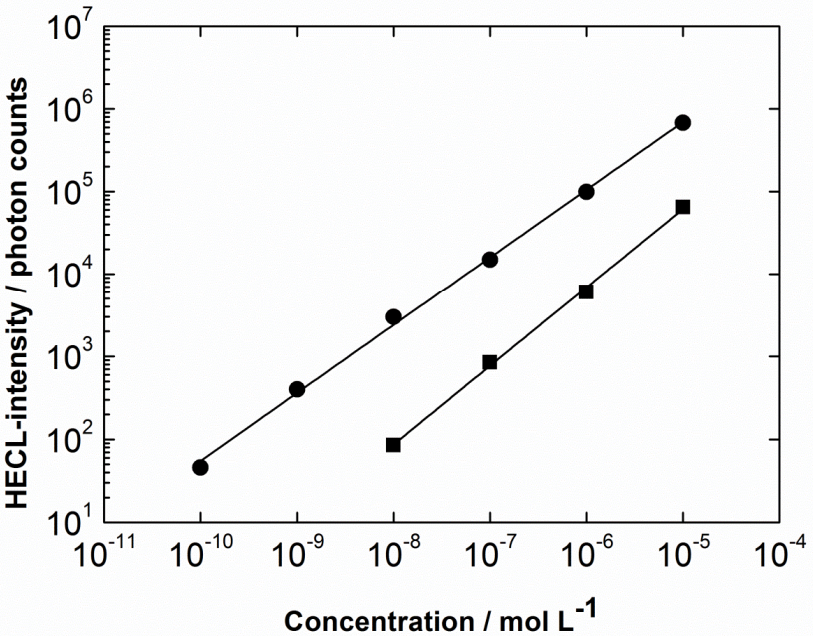

Figure 14. Calibration curves of $Ru(bpy)_2L_a^{2+}$ (circles) and $Ru(bpy)_2L_b^{2+}$ (squares) using native Al_2O_3-covered aluminium electrode. Conditions: $Ru(bpy)_2L_a^{2+}$ or $Ru(bpy)_2L_b^{2+}$ in 0.05 M $Na_2B_4O_7$ buffer at pH 9.2 containing 1.0 mmol L^{-1} $K_2S_2O_8$, 620 nm interference filter, pulse charge 120 µC, pulse voltage 45 V, and pulse frequency 20 Hz. The intensities were integrated over 500 excitation cycles.

As can be seen in Figure 14, the calibration curve of both $Ru(bpy)_2L_a^{2+}$ and $Ru(bpy)_2L_b^{2+}$ is linear over several decades of concentration. According to the results, at least $Ru(bpy)_2L_a^{2+}$ should be applicable as an electrochemiluminescent label. Because $Ru(bpy)_2L_b^{2+}$ has strong red shift in its emission spectrum, the results with $Ru(bpy)_2L_b^{2+}$ could have been much better if a red sensitive detector, such as an avalanche photodiode or electron multiplying charge-coupled device (CCD), and an appropriate optical filter would have been available. Also $Ru(bpy)_2L_a^{2+}$ has a red shift in its emission spectrum and coupling with a biomolecule might even induce an additional red shift. Therefore, a red sensitive detector might be reasonable also in the case of real bioaffinity applications with $Ru(bpy)_2L_a^{2+}$.

5.2 Deposited dielectrics on silicon and metal thin films

Different dielectric films made by different techniques and conductor materials were tested (Publications III and IV). Figures 15–18 show the dependence of the HECL intensity on the dielectric film thickness. Only those conductor/insulator pairs giving a significant HECL signal are included. The luminophore used in these studies was Tb(III) chelated by 2,6-bis[N,N-bis(carboxymethyl)aminomethyl]-4-benzoylphenol.

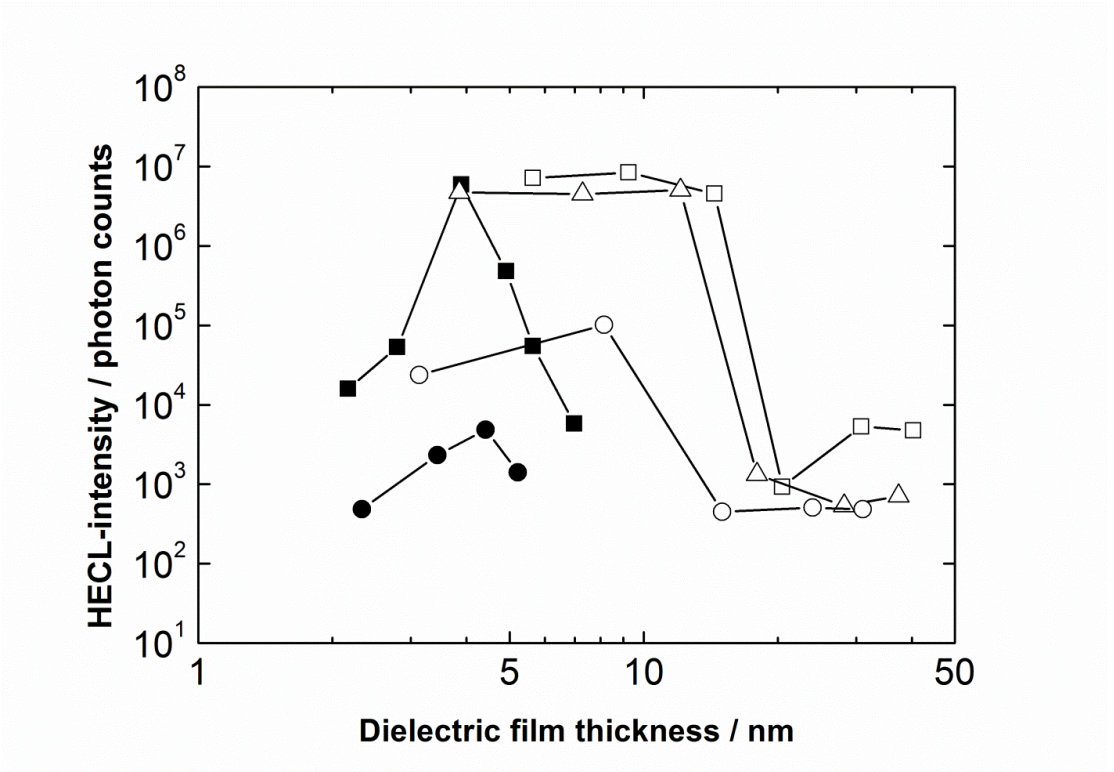

Figure 15. Effect of the silicon oxide thickness on HECL intensity. SiO_2 was made by thermal oxidation, LPD and PECVD on silicon or on metal thin films. Thermal Si/SiO_2 (black squares), LPD Si/SiO_2 (black circles), PECVD Al/SiO_2 (open squares), PECVD Si/SiO_2 (open triangles), and PECVD Pt/SiO_2 (open circles). Conditions: 10^{-6} M Tb(III) chelate in 0.05 M $Na_2B_4O_7$ buffer at pH 9.2, 550 nm interference filter with 40 nm bandwidth, pulse charge 12.6 µC, pulse voltage 25 V, pulse frequency 20 Hz, measurement window 6 ms, and 50 µs delay. The intensities were integrated over 1 000 excitation pulses.

When thermally oxidised silicon is used (Figure 15), the highest HECL intensity is measured using a cathode where SiO_2 thickness is 4 nm. There is a significant peak at 4 nm and the HECL intensity decreases fast when the oxide thickness is under or above 4 nm. About the same kind of behaviour can be observed with LPD SiO_2 (Figure 15), although the film thickness vs. HECL intensity curve is not as sharp as with thermal SiO_2. The intensities are, however, much lower than when using thermally oxidised silicon.

When PECVD SiO_2 is used as the insulating film (Figure 15), the highest intensities are measured when the film thickness is around 4–10 nm. After that thickness range, the HECL intensity decreases substantially. When PECVD SiO_2 is used on Si or Al, the highest HECL intensities are at the same level as they are when thermally oxidised Si is used. Cu, Cr, Ti or W with PECVD SiO_2 did not give any significant HECL signal.

SiO_2 or Si_3N_4 films deposited by PECVD and SiO_2 deposited by LPD differ from high-quality films. They contain dangling bonds, such as lone pairs and vacant orbitals, and various reaction products from the deposition process. These factors are due to the low deposition temperatures. The dangling bonds are unwanted especially in semiconductor industry, because they create mid-gap states between the valence and conduction bands preventing the desired band gap of the semiconductor[114]. The low film quality expresses itself as very high etch rate compared to the etch rate of thermal oxide (Publication III). Therefore, the good results with PECVD SiO_2 were quite surprising. A potential explanation might be oxynitride formation caused by high ratio of N_2 and N_2O to SiH_4 during deposition. Plasma deposited oxynitrides have been used as tunnelling dielectrics in non-volatile memory applications[115,116], and oxynitride formation has also improved the performance of CVD gate dielectrics in MOS devices[117,118].

Both PECVD and LPCVD Si_3N_4 layers on Si substrate (Figure 16) also gave a significant HECL intensity, even though it was slightly smaller than the intensity with thermally oxidised Si. The highest HECL intensity was measured when the Si_3N_4 thickness was about 4 nm. With PECVD Si_3N_4 the highest intensity can be clearly seen as a peak, but with LPCVD Si_3N_4 the range is somewhat wider.

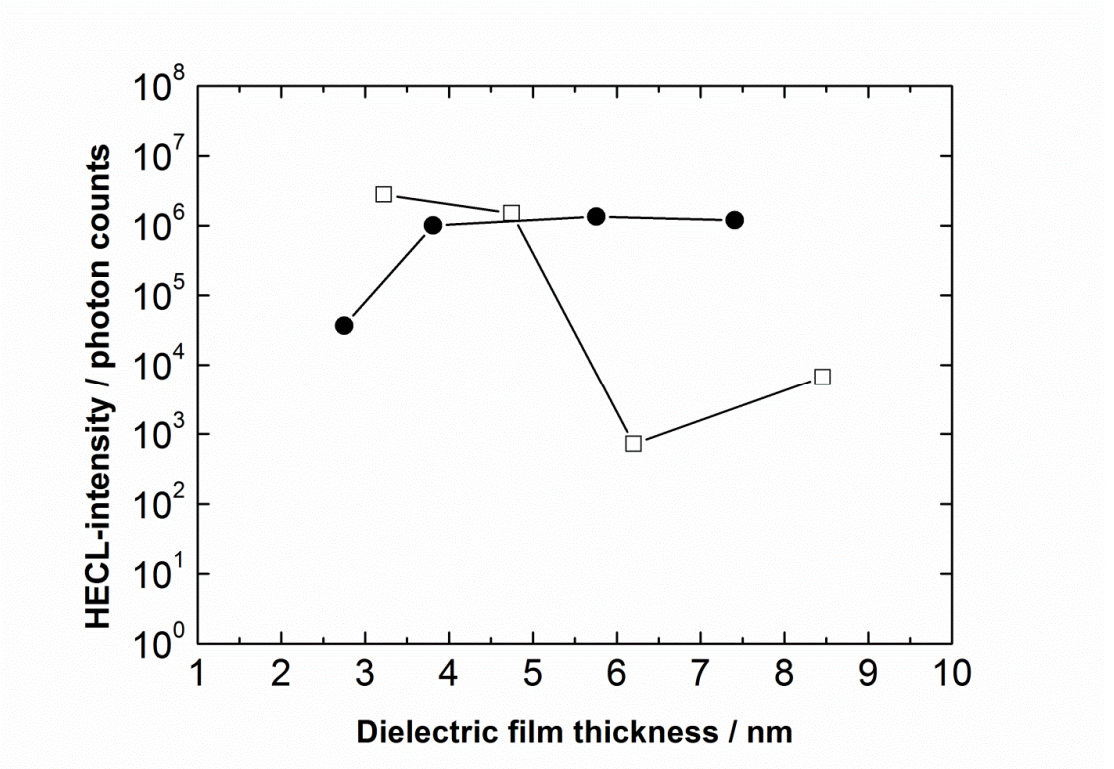

Figure 16. Effect of Si_3N_4 thickness on HECL intensity. Si_3N_4 was made by LPCVD (open squares), and PECVD (black circles) on silicon substrates. Conditions: 10^{-6} M Tb(III) chelate in 0.05 M $Na_2B_4O_7$ buffer at pH 9.2, 550 nm interference filter with 40 nm bandwidth, pulse charge 12.6 µC, pulse voltage 25 V, pulse frequency 20 Hz, measurement window 6 ms, and 50 µs delay. The intensities were integrated over 1 000 excitation pulses.

LPCVD Si_3N_4 was uniform across the wafer, although the standard deviation was higher for both thickness uniformity in one wafer and thickness variation between wafers with short deposition time than with long deposition time. The film thickness increased almost linearly with the deposition time (Publication III). The Si_3N_4 film was tested to be pinhole free by comparing the etch rates of LPCVD SiO_2 and Si_3N_4 to that of thermal oxide. According to the etching tests, Si_3N_4 films seemed to have an approximately 2 nm thick unwanted native oxide layer at the interface. This oxide layer was probably formed during the loading, pumping, and temperature ramping phases of the deposition process and it might effect on the results of the film thickness measurements.

When ALD of Al_2O_3 was used as a dielectric (Figures 17 and 18), Al and Si gave the best signals, while Cr, Cu or Ti did not give any significant intensity (Publication IV). The highest intensities were at the same level or even slightly higher than in the case of thermally oxidised Si. Also Pt (only TMA/H_2O growing process was tested) and W gave a

significant signal, although it was lower than in case of Al and Si. When W electrode was used, a clear intensity peak could be seen at the Al_2O_3 thickness of about 4 nm.

The highest intensities were obtained with Al and Si electrodes in the Al_2O_3 thickness range 4–10 nm, which was the same range as in the case of PECVD SiO_2. The effect of the film thickness was more critical in the ozone process than in the water process. Especially with Si electrode, the optimal film thickness range was much larger in the water process than in the ozone process, but similar behaviour could also be seen with Al electrode. This is due to the fact that ozone is more aggressive oxidant than water[119] and therefore, it is likely to produce denser Al_2O_3 films. In addition, the ozone process leaves less residual carbon in the bulk of the film, and produces less aluminium sub-oxides near the substrate interface[120]. In this research, OH radical and carbon contamination seemed to have a significant effect, because the difference between the ozone and the water process could be seen with both Al and Si electrodes. However, the stronger effect on Si electrodes might be due to aluminium cluster formation at the Si/Al_2O_3 interface during TMA/O_3 process when bare hydrogen-terminated n^+ silicon surface is used[121].

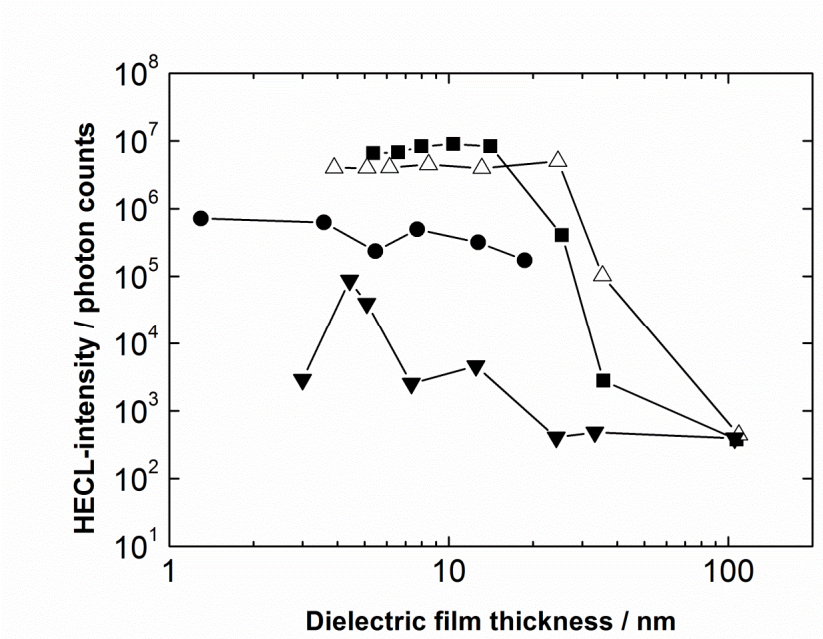

Figure 17. Effect of ALD (TMA/H_2O) Al_2O_3 thickness on HECL intensity. Al_2O_3 layers were deposited on Si (open triangles) and on metal thin films of Al (black squares), Pt (black circles), and W (black triangles). Conditions: 10^{-6} M Tb(III) chelate in 0.05 M $Na_2B_4O_7$ buffer at pH 9.2, 550 nm interference filter with 40 nm bandwidth, pulse charge 12.6 µC, pulse voltage 25 V, pulse frequency 20 Hz, measurement window 6 ms, and 50 µs delay. The intensities were integrated over 1 000 excitation pulses.

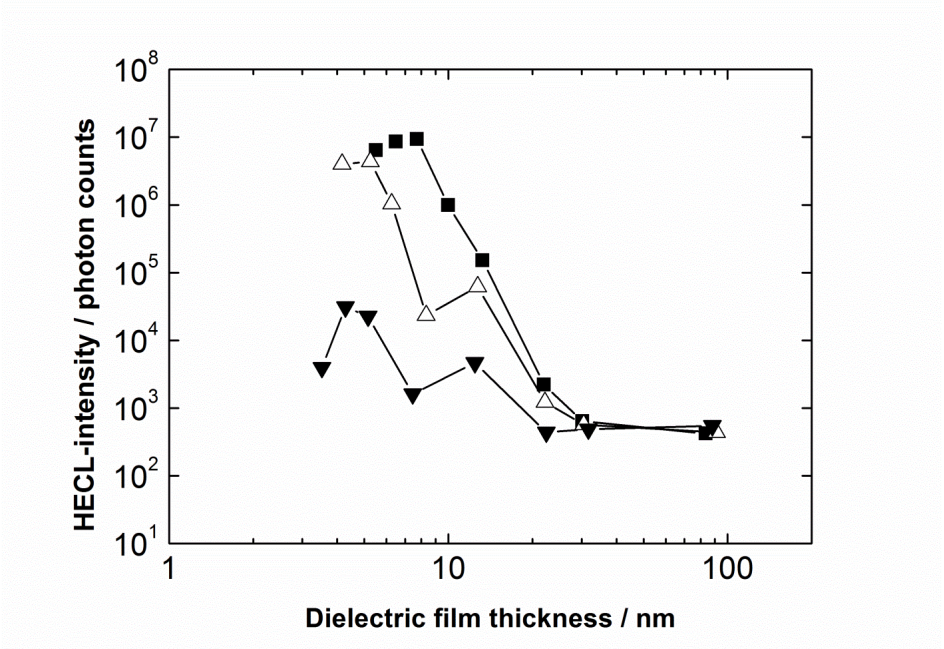

Figure 18. Effect of ALD (TMA/O_3) Al_2O_3 thickness on HECL intensity. Al_2O_3 layers were deposited on Si (open triangles) and on metal thin films of Al (black squares) and W (black triangles). Conditions: 10^{-6} M Tb(III) chelate in 0.05 M $Na_2B_4O_7$ buffer at pH 9.2, 550 nm interference filter with 40 nm bandwidth, pulse charge 12.6 µC, pulse voltage 25 V, pulse frequency 20 Hz, measurement window 6 ms, and 50 µs delay. The intensities were integrated over 1 000 excitation pulses.

Cr, Cu and Ti did not work as an electrode with either ALD or PECVD methods. Pt worked moderately in both processes and W worked only in ALD process. The poor performance of Cr, Ti and Pt correlates strongly with negative thickness offset (*i.e.* negative thickness value when the thickness data is extrapolated to zero deposition time or zero deposition cycles). Especially with Pt and Cr, the measured film thickness was consistently lower than expected due to delayed deposition (Publication IV). After the onset of the deposition, the deposition rate was nevertheless identical with other samples. However, some of the samples with negative thickness offset did not get deposited at all during the shortest deposition processes.

Because of the poor growth initiation, the quality of the deposited film may be worse close to the metal/dielectric interface. This would lead to breakdown of the dielectric when voltage is applied. In case of delayed deposition, the growth might be initiated as individual disconnected islands, leading to non-uniform film thickness. When the film has then become continuous and sufficiently thick in the delayed areas, the film thickness can be already too thick for HECL purposes from other areas of the surface. However, an island structure or increase in surface roughness could not be seen in atomic force microscopy (AFM) images of Cr or Pt samples (Publication IV). Instead, surface grains were smoothening and broadening and the vertical range of the images remained constant. The AFM results are in line with the fact that even in case of delayed deposition the growth rate remained constant after the onset of the deposition.

On the basis of the thickness offset, it could be expected that W electrodes had worked better. However, the growth rates of W samples in ALD process were slightly higher compared to the other samples (Publication IV). This refers to unwanted oxidation at the metal/dielectric surface during the deposition process. Therefore, the resulting dielectric structure is non-uniform and it might contain, in addition to the wanted Al_2O_3 or SiO_2 layer, also oxides of tungsten. Cu samples became strongly discoloured during the deposition process and a reasonable dielectric thickness could not be measured. In this case, it is probable that the surface has been oxidised and no deposition of Al_2O_3 or SiO_2 has occurred at all.

Figures 19–21 describe the performance of the dielectric films as a function of excitation pulses. In each case, the tested film thickness is optimal for the HECL measurements.

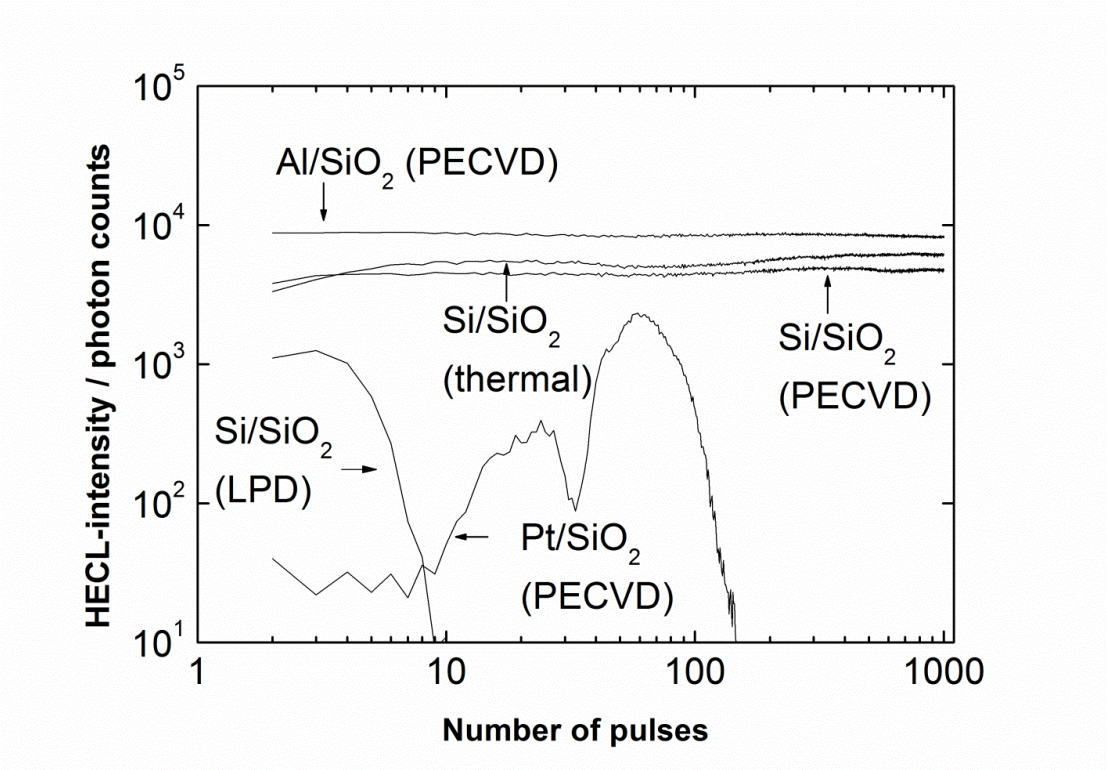

Figure 19. Stability of HECL intensity as a function of excitation pulses in case of thermal, LPD, and PECVD SiO_2. Conditions: 10^{-6} M Tb(III) chelate in 0.05 M $Na_2B_4O_7$ buffer at pH 9.2, 550 nm interference filter with 40 nm bandwidth, pulse charge 12.6 µC, pulse voltage 25 V, pulse frequency 20 Hz, measurement window 6 ms, and 50 µs delay.

Both thermally oxidised Si and PECVD SiO_2 give very stable HECL intensity, as can be seen in Figure 19. PECVD SiO_2 was tested to last up to 4 000 excitation pulses before a significant decrease in the HECL intensity. Al thin film with an optimal PECVD SiO_2 layer gave a stable signal during 40 000 pulses. The intensity was, however, decreased gradually by 25 % from the beginning of the measurement. Pt electrodes with an optimal PECVD SiO_2 layer did not give a stable signal, but there were several increases and decreases in the HECL intensity during the measurement. With LPD Si/SiO_2, a significant HECL signal is observed only during about the first 10 pulses of the measurement. This together with quite low intensities makes LPD SiO_2 practically unusable for HECL measurements.

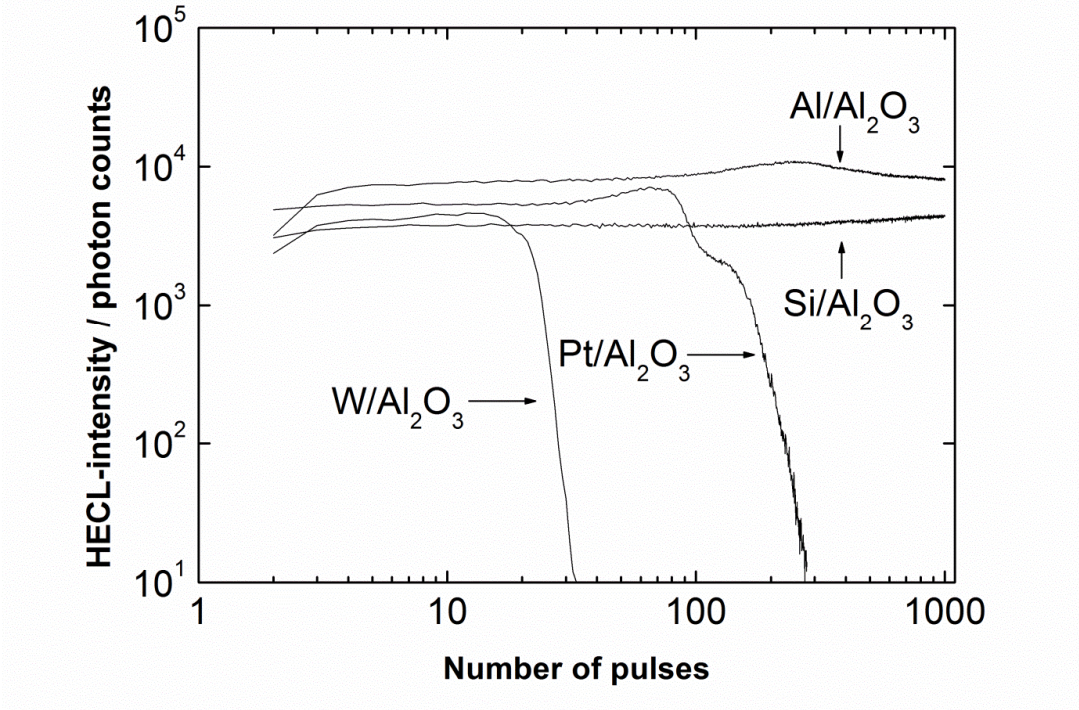

Figure 20. Stability of HECL intensity as a function of excitation pulses in case of ALD Al_2O_3 (TMA/H_2O). Conditions: 10^{-6} M Tb(III) chelate in 0.05 M $Na_2B_4O_7$ buffer at pH 9.2, 550 nm interference filter with 40 nm bandwidth, pulse charge 12.6 μC, pulse voltage 25 V, pulse frequency 20 Hz, measurement window 6 ms, and 50 μs delay.

ALD Al_2O_3 layers on Si and Al were extremely stable during the measurement. ALD Al_2O_3 layer on Al (both TMA/H_2O and TMA/O_3) was measured to last at least for 40 000 excitation pulses with a gradual decrease in the intensity. ALD Al_2O_3 layer (TMA/O_3) on Si performed well over 10 000 excitation pulses before breakdown. On the other hand, electrodes with ALD Al_2O_3 on W or Pt lasted only for 20 and 100 excitation pulses, respectively (Figure 20). The exceptionally good stability of ALD Al_2O_3 on Al might be due to self-healing of the defects formed during operation. Bare aluminium surfaces are known to oxidate rapidly in either water or air and the thickness of this native oxide has been tested to be close to optimal for HECL measurements.[17]

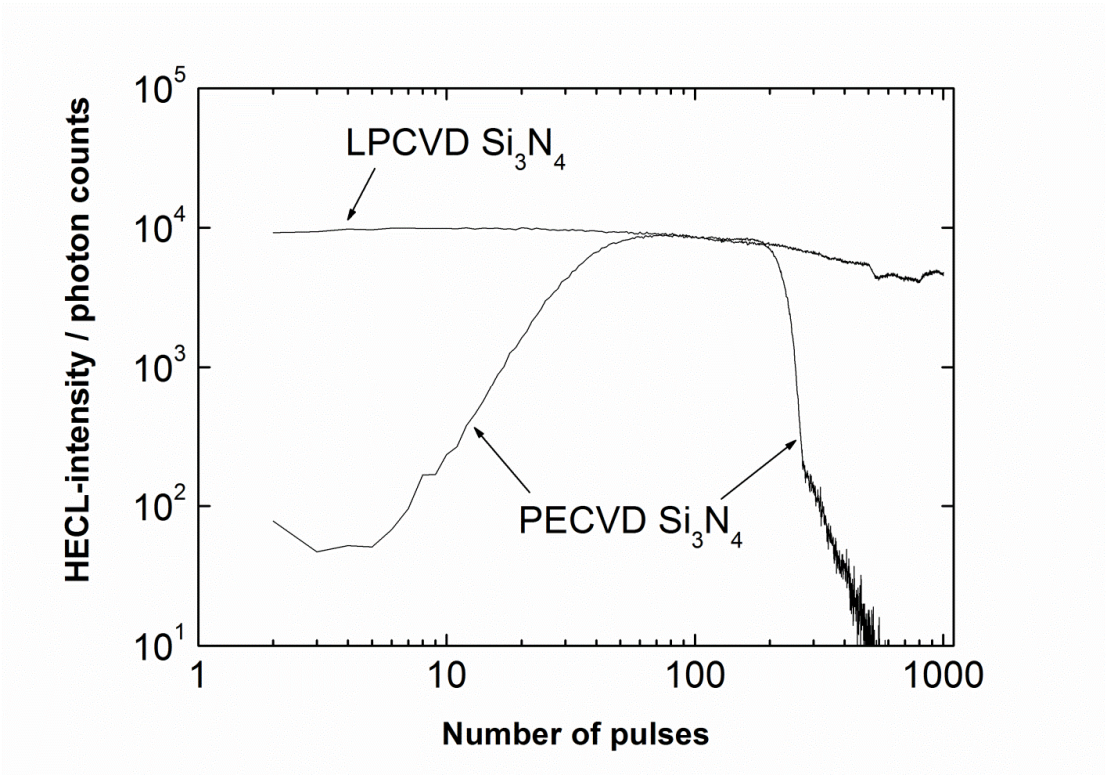

Figure 21. Stability of HECL intensity as a function of excitation pulses in case of Si_3N_4. Si_3N_4 layers were made by LPCVD and PECVD on silicon substrate. Conditions: 10^{-6} M Tb(III) chelate in 0.05 M $Na_2B_4O_7$ buffer at pH 9.2, 550 nm interference filter with 40 nm bandwidth, pulse charge 12.6 µC, pulse voltage 25 V, pulse frequency 20 Hz, measurement window 6 ms, and 50 µs delay.

With LPCVD Si_3N_4 layer on Si, the signal is stable during the measurement, but with Si electrodes with a PECVD Si_3N_4 layer, the signal first rises, then it is stable and then it starts to decrease (Figure 21). Same kind of intensity profile was always measured with these samples. The signal-to-noise ratio of this kind of working electrodes could be improved by integrating the data over pulses from 50 to 200, where the signal is stable.

To conclude, the highest intensities from all of the tested conductor/insulator pairs were measured with thermally oxidised Si, ALD Al_2O_3-covered Al or Si, PECVD SiO_2-covered Al or Si, and LPCVD or PECVD Si_3N_4-covered Si. The HECL intensity integrated over 1 000 measurement pulses was in order of magnitude 10^6 with all of these electrodes, even if the difference between the highest intensity ($9.4 \cdot 10^6$ with ALD Al_2O_3-covered Al) and the lowest intensity ($1.3 \cdot 10^6$ with PECVD Si_3N_4-covered Si) is almost one decade. Except PECVD Si_3N_4, these electrodes also gave a stable signal during the measurement, some of them even much longer. Electrodes with TMA/H_2O or TMA/O_3 ALD Al_2O_3 worked equally well in the HECL measurements. These two processes differed only in the film

thickness required for the highest HECL intensity and in the thickness offset which was consistently more positive in the TMA/O_3 process (Publication IV).

According to these results, various insulating layers can work as well as thermally oxidised silicon. Therefore, it can be assumed that a wide variety of dielectrics work well in HECL measurements. This means that an appropriate dielectric could be chosen for specific application, depending on its optical or electrical properties or antibody binding abilities. However, the deposition method, the resulting overall film quality, and selection of the electrode metal are critical.

One major advantage of the tested working electrodes is their good shelf life. The electrodes could be stored in normal laboratory air without any degradation in their performance even after 10 months storage (Publication IV).

When deposited metal thin films are used as conductors, the substrate material can be also a non-conductive material. In addition, ALD and PECVD are relatively low temperature processes. This enables the usage of cheap glass or even plastic substrates and allows integration of other sensors or electronics on the same chip. The results of Publications III and IV were utilised in designing integrated electrode chips for HECL measurements (Publication V).

5.3. Integrated HECL chips

This chapter presents microfabricated HECL chips with integrated electrodes having different electrode geometries and sample confinement systems studied in Publication V.

Before making chips with integrated electrodes, the effects of the miniaturising of the cathode were modelled by collecting the HECL data through optical fibres, placed before the PMT, with diameters 1 000 nm and 100 nm. In these experiments, the traditional measurement system with separate working and counter electrodes was used. The areas where the photons were collected in these experiments were 28 mm^2, 0.8 mm^2, and

0.008 mm^2. According to the results of these preliminary tests, it was assumed that the area of the working electrode will set the ultimate detection limit for the system. Results of the preliminary test are described in Figure 22.

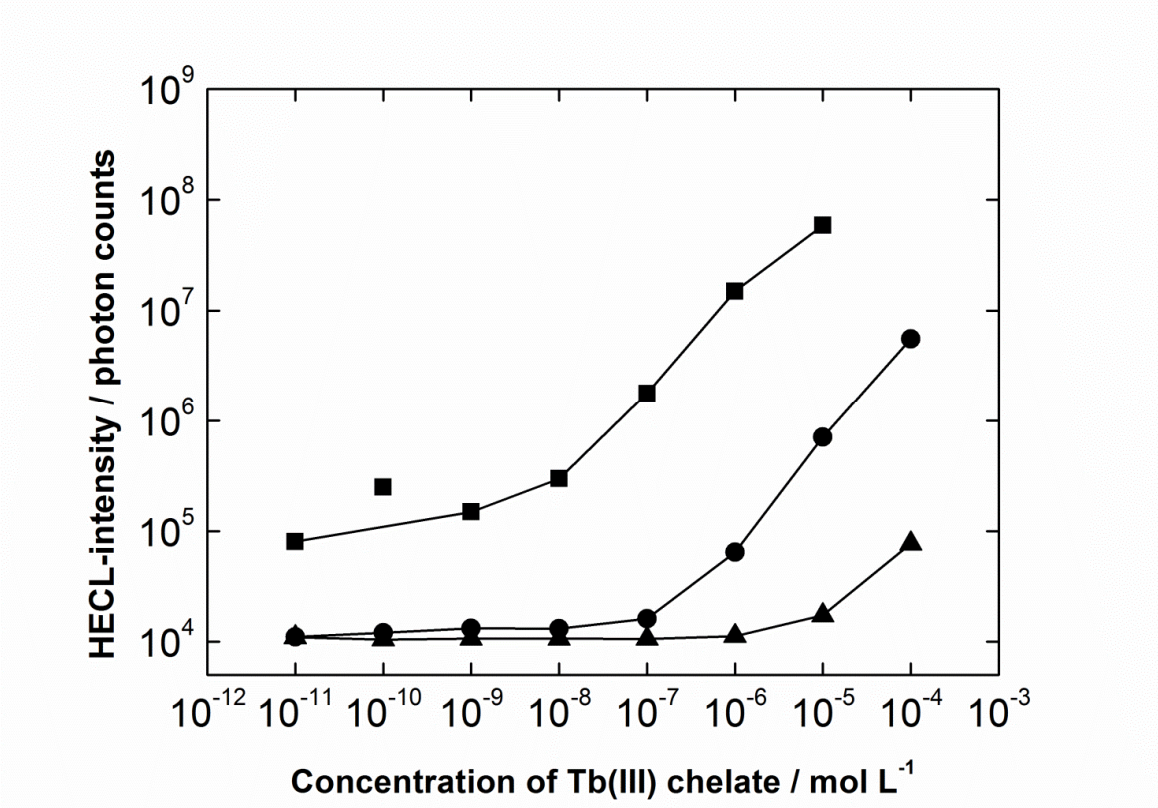

Figure 22. Effect of the cathode area on HECL intensity. The area where the data was collected was 28 mm^2 (squares), 0.8 mm^2 (circles) and 0.008 mm^2 (triangles). Conditions: Tb(III) chelate in 0.05 M $Na_2B_4O_7$ buffer at pH 9.2, native Al_2O_3-covered Al electrode, pulse charge 12.6 µC, pulse voltage 25 V, pulse frequency 10 Hz, 5 ms measurement window, and 100 µs delay. The intensities were integrated over 1 000 excitation pulses.

Two basic structures for integrated electrode chips were tested: silicon chips having dry oxidised silicon as the working electrode and pyrex glass chips having sputtered aluminium thin film covered by ALD Al_2O_3 as the working electrode. Platinum thin film was used as a counter electrode in both devices. With the silicon chips, electrical contact to the platinum counter electrode was made through contact pads on the front of the wafer, while the silicon working electrode was contacted through the backside of the wafer. With the glass chips, electrical contact was made to both the working and counter electrodes through their respective contact pads on the front of the wafer. The chips are illustrated in Figure 9.

The fabrication process of the integrated silicon-based electrode chips would have been simpler, if the conductor material of both working and counter electrode had been Pt. However, this kind of design might slightly degrade the performance of the device. In the glass device fabrication, on the other hand, the insulating layer might as well have been PECVD SiO_2, but ALD was chosen because of its excellent repeatability in producing ultra-thin films.

The chips were used either with a separate polytetrafluoroethylene (PTFE) sample cell which was mechanically sealed on the chip or with an integrated sample confinement. The integrated sample confinement was either a hydrophobic ring around the electrode area or a PDMS chamber. The sample confinements could be filled by dispensing the sample directly on the surface of the electrode or by capillary forces, respectively. The differences between the sample holder with a discrete Pt counter electrode (Publications I–IV), the sample holder for the integrated electrode chip (Publication V), and the sample holder for the integrated electrode chip with an integrated sample confinement (Publications V and VII) are shown in Figure 23.

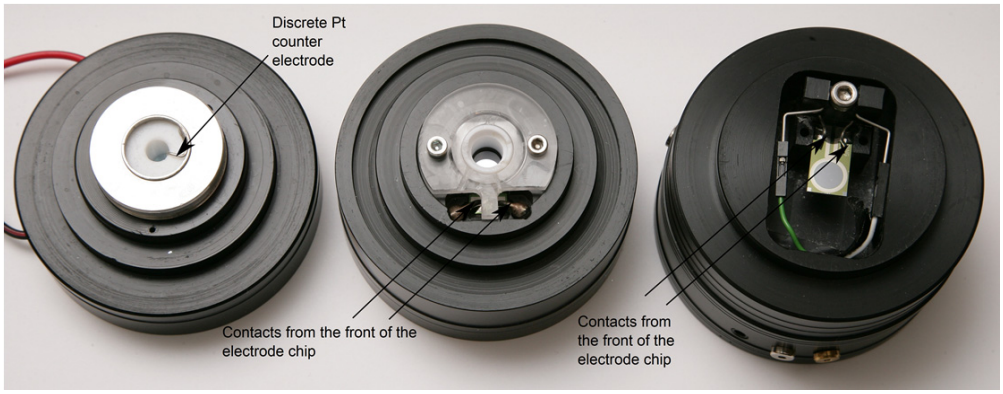

Figure 23. The sample holder with a discrete Pt counter electrode (on the left), the sample holder for the integrated electrode chip (in the middle), and the sample holder for the integrated electrode chip with an integrated sample confinement (on the right). The holder on the left provides a contact from the backside of the working electrode and the discrete Pt counter electrode is in contact with the sample solution. The sample is dispensed on the hole on the white PTFE cell. The holder in the middle provides one contact from the backside of the electrode chip and two contacts from the front of the electrode chip. The sample is dispensed on the hole on the white PTFE cell. The holder on the right provides two contacts from both front and backside of the integrated electrode chip. When the integrated electrode chip illustrated in the figure is used, the sample can be dispensed straight on the surface of the electrode.

An inlet channel at one end of the chip having a PDMS sample chamber is used to fill the chamber by dipping the chip's edge in sample solution. The multiple channels allow air to escape during filling. Small pillars support the chamber's PDMS ceiling. In the design described here, the pillars are evenly distributed throughout the fluidic chamber and not optimised according to the working or counter electrode geometry. The PDMS lid covers only the electrode area of the chip, leaving the electrical contact pads exposed. The differences between the integrated electrode chips with and without an integrated sample confinement are illustrated in Figure 9.

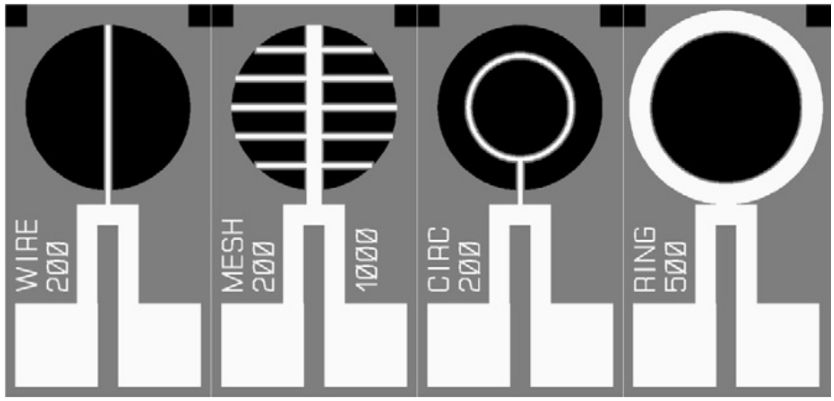

Figure 24. The basic geometries of the tested integrated electrodes. Black and white areas represent the working and counter electrodes, respectively. Grey areas are insulation. All geometries were tested with several different ratios between the working electrode and counter electrode area.

Several different working and counter electrode geometries were tested, and some of these geometries are described in Figure 24. Electrode designs include simple wires running across the working electrode (WIRE), meshes of wires spread across the working electrode (MESH), circular counter electrodes within the working electrode area (CIRC), and ring-shaped counter electrodes fully enclosing the round working electrode (RING).

Both the linewidth of the counter electrode in all designs and the density of the lines in the MESH designs were varied. Also the area of the working electrode was varied. The first figure in the MESH names tells the width of the counter electrode lines and the second number tells the line spacing. For example, MESH 200/1000 has 200 µm wide counter electrode lines at 1 000 µm line spacing.

The tests with different electrode geometries revealed that the area of the working electrode was naturally one of the most important factors affecting the HECL intensity. However, there has to be some kind of optimum in the ratio between the area of the working electrode and the area of the counter electrode. Best results were got with the chips where this ratio was between 5:1 and 20:1 (Publication V). This trend could be observed with both glass and silicon devices.

The electrode geometry *per se* seemed to have little or no effect on device performance, when mechanically sealed PTFE sample confinement was used. However, the electrode geometry became more critical in case of small volume integrated sample confinement.

For example, RING-type electrodes gave the highest HECL-intensities of the tested geometries with discrete PTFE sample cell, but the chips with RING electrode geometry gave hardly any signal at all with an integrated PDMS sample chamber. The performance of chips with RING electrode geometry was reduced also when hydrophobically defined sample confinement was employed. The explanation might be the increased electrical resistance within the sample solution itself. When discrete PTFE sample cell is employed, the sample volume is 500 µl and thereby a relatively thick liquid layer is formed on the electrode surface. In PDMS sample chamber, instead, only a 350 µm thick liquid layer is formed and this leads to higher resistance within the solution compared to the resistance in the PTFE sample cell. The increased lengths of the electric pulses during the measurement with the chips with a PDMS sample chamber confirm this explanation.

The best electrode geometry also varies depending on the application where it is supposed to be used. If the integrated electrodes are used e.g. in immunoassay, it is preferable to use electrodes with large cathode area, because then the antibodies have larger area to be bound. In this kind of applications, compromise has to be done between the best possible performance of the device and the best possible electrode geometry.

The uniformity of electrochemiluminescence was tested by taking long-exposure photographs from devices in normal operation (Publication V). In PTFE sample cell, the luminescence of RING- and WIRE-type of electrodes seems to be very uniform. When PDMS sample chamber is employed to the WIRE-electrode, the luminescence is concentrated around the counter electrode area. Same kind of behaviour can be seen with hydrophobically confined version of RING-type electrode. An explanation to this is a voltage drop which originates from the electrical resistance of the sample solution. The voltage drop increases, and thereby the electron tunnelling decreases, as the distance from the counter electrode increases. Therefore, the luminescence is confined near the counter electrode's edge. Also the support pillars of the PDMS lid can cause some non-uniformity. This was, however, observed only in the case of a strong sideways voltage gradient, like with WIRE-electrode, which causes increased resistive voltage drops in the solution. The support pillars do not bond hermetically to the surface of the electrode chip and the sample solution is able to penetrate underneath them. Therefore, luminescence occurs uniformly from the MESH 200/1000-type electrode with PDMS fluidistics. However, with WIRE 800 electrode luminescence is decreased in the thin sample film under the pillars.

This is caused by a strong sideways voltage gradient which increases resistive voltage drop in the solution.

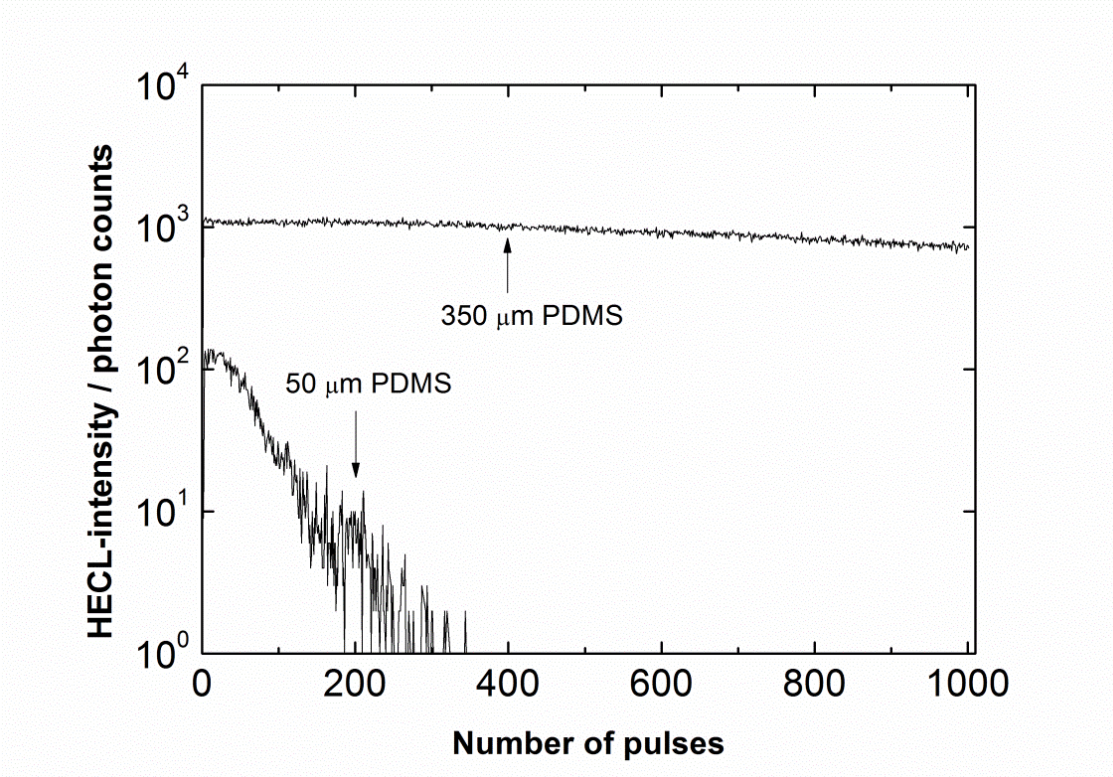

Figure 25. HECL intensity as a function of excitation pulses when MESH 200/1000 type of integrated electrode with PDMS sample chamber is used. Two heights of the PDMS chamber were tested: 50 μm and 350 μm. Conditions: 10^{-6} M Tb(III) chelate in 0.05 M $Na_2B_4O_7$ buffer at pH 9.2, 550 nm interference filter with 40 nm bandwidth, pulse charge 12.6 μC, pulse voltage 25 V, pulse frequency 20 Hz, measurement window 3 ms, and 50 μs delay.

Because MESH 200/1000-type electrode gave a sufficiently high signal both with PDMS sample chamber and hydrophobically defined sample confinement, this geometry was chosen for the more detailed research. Two heights of PDMS fluidistics were tested: 50 μm and 350 μm. As can be seen in Figure 25, a significant HECL-intensity could be observed with a 50 μm chip at the beginning of the measurement, but the intensity was one order of magnitude smaller than with a 350 μm chip. However, the signal started to decrease immediately and after 100 measurement pulses it had already decreased by an order of magnitude. The PDMS device with a pillar height of 350 μm, on the other hand, maintained nearly constant signal throughout the whole measurement. The primary reason

for the poorer performance of a 50 µm PDMS device is that gas bubbles are formed at the electrodes. Because of the gas bubbles, the 50 µm chamber was empty after the measurement. Gas bubbles caused minor problems with other PDMS fluidistic chips, because larger sample volumes of these devices compensated the sample loss. In addition, the thinner sample film in 50 µm high device aggravates the effects of resistive voltage drop and thereby decreases electron tunnelling and luminescence.

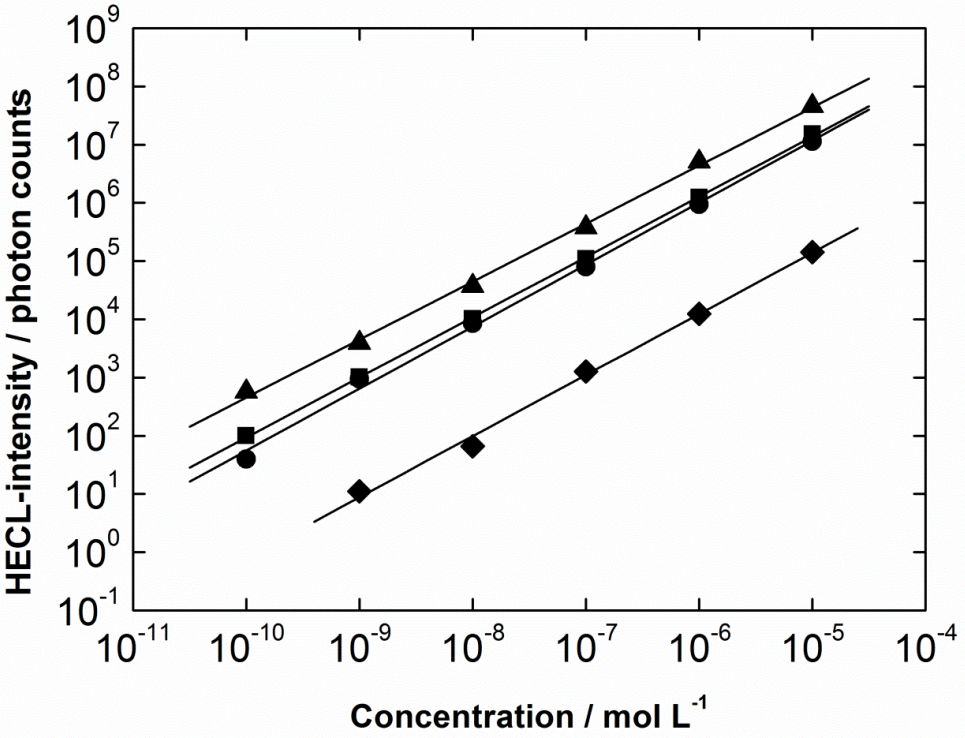

Figure 26. Calibration curve of Tb(III) chelate using integrated electrodes. The tested electrodes were RING 500 with a separate sample cell (triangles), MESH 200/1000 with a sample confinement defined by a hydrophobic ring (squares), MESH 200/1000 with a PDMS sample cell (circles), and a glass device of RING 500 geometry with a separate sample cell (diamonds). Conditions: Tb(III) chelate in 0.05 M $Na_2B_4O_7$ buffer at pH 9.2, 550 nm interference filter with 40 nm bandwidth, pulse charge 12.6 µC, pulse voltage 25 V, pulse frequency 20 Hz, measurement window 3 ms, and 50 µs delay.

Figure 26 describes calibration curves of Tb(III) chelate measured by a RING 500 devices operated in the PTFE sample cell, a MESH 200/1000 device with hydrophobic sample confinement, a MESH 200/1000 device with 350 µm high PDMS fluidics, and a glass device similar to the RING 500 design, also operated in the PTFE sample cell. All devices offered excellent linearity over 4–5 orders of magnitude and the detection limits were in

subnanomolar range. The upper limit of the linear range of the calibration curve is determined by the saturation of the photomultiplier tube, not by the HECL method itself. RING 500 operated in the PTFE cell provides the highest intensity. However, the difference between its performance and the performance of the devices with integrated sample confinements is small. The devices with integrated sample confinement provide less assembly and thus shorter analysis time compared to the PTFE system. In addition, the sample volumes are small: the volume of the hydrophobic sample confinement is 100 µl and the volume of the PDMS capillary-filling device (with 350 µm high fluidistics) is only 15 µl. The devices with integrated sample confinement are also free from cross-contamination between samples, because the device itself is disposable and the individual sample is in connection only to the device, not to any other part of the measurement setup. The glass device gives lower intensities and it has higher detection limits than the silicon devices. Nevertheless, it provides excellent linearity and nanomolar detection limit.

5.4. Immunoassay of C-reactive protein by HECL

In this research, C-reactive protein (CRP) has been used as a model analyte. The analysis has been carried out by two different measurement systems: by a semiautomatic electrochemiluminometer modified from a PerkinElmer Wallac fluorometer (Publication VI) and with the earlier mentioned measurement system using integrated electrode chip with a hydrophobically defined sample confinement (Publication VII). The aim of this part of the research was to test the analytical applicability of the HECL chip and to investigate the applicability of HECL to point-of-care measurements of CRP.

There are already some point-of care CRP tests commercially available[122], but these tests are usually for measuring CRP concentrations between 5–200 mg L^{-1} [123,124]. These high CRP concentrations are used to differentiate between bacterial and viral diseases and thus to help doctors to choose whether the antibiotics prescription is needed[123,125,126]. The tests are especially useful in differentiating between pneumonia and acute bronchitis[123].

Low concentrations of CRP can act both as an early diagnostic marker for cardiovascular diseases in apparently healthy people and as a method to monitor pharmacological interventions used to prevent and treat cardiovascular disease[127]. American Heart Association and Centers for Disease Control and Prevention (CDC) have endorsed guidelines for CRP concentrations: <1, 1–3, and >3 mg L^{-1}, where the concentrations suggest lower, moderate and high relative risk of incident vascular disease, respectively[127]. In addition, it is suggested to be a useful surrogate marker for detection of inflammation associated with multiple sclerosis relapses[128].

Both immunoassay methods of this research were carried out by sandwich method which is described in Figure 27. First, the cathode was coated by primary antibody using physical adsorption. After that, non-specific adsorption of the secondary antibody labelled by an isothiocyanate derivative of Tb(III) chelate was prevented by filling the free areas of the electrode surface by bovine serum albumin (saturation). Antigen was then bound to the primary antibody and the labelled secondary antibody was bound to the antigen. Excess labelled secondary antibody was washed away before the measurement to guarantee that the HECL-signal is coming only from those labelled secondary antibodies which are bound to the antigen. The immunoassay procedure is described in detail in Publications VI and VII.

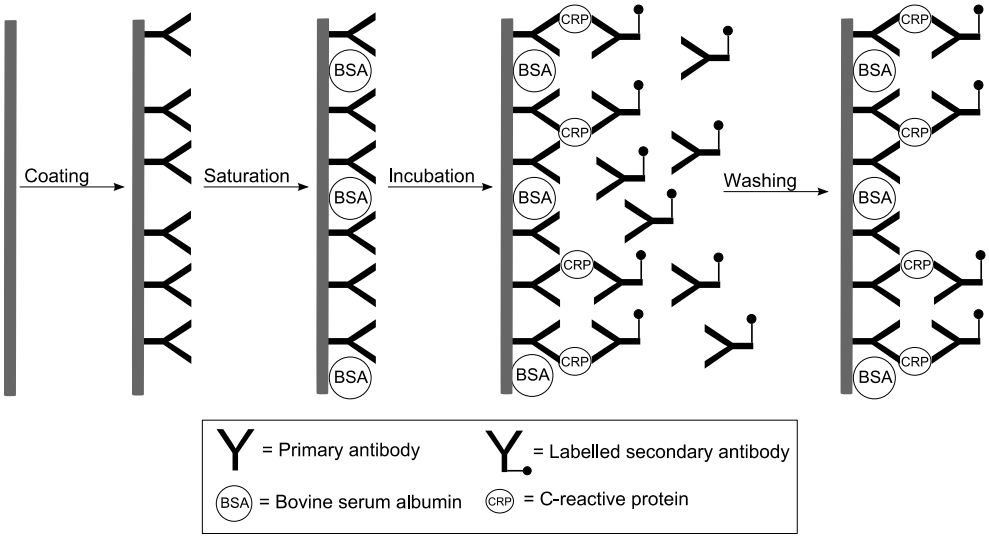

Figure 27. The CRP-immunoassay procedure using sandwich method. The substrate surface is first coated with primary antibodies. The immobilised antibodies are drawn to the ideal position having the Fab parts (the "horns" of the letter Y) pointing up from the substrate surface. During saturation, BSA molecules are used to fill the empty areas on the substrate surface to prevent non-specific adsorption. During incubation, CRP-antigens are bound to primary antibodies and labelled secondary antibodies are bound to antigen. The purpose of washing is to remove excess labelled secondary antibody.

The antibodies were immobilised using physical adsorption. This method was selected, because the whole immunoassay procedure was wanted to keep as simple and easy to handle as possible. Regardless of the defects of physical adsorption, it seemed to be a sufficiently good immobilisation method for this purpose.

In the immunoassay applying integrated chips, a RING-type chip with a hydrophobically defined sample confinement was chosen, even if the MESH geometry gave better results with the hydrophobically defined sample confinement. This choice was made, because with RING geometry there is more cathode area available for antibodies to bind. In the immunoassay by electrochemiluminometer, the working electrode was a 20×4.0 mm oxide-covered Si electrode and the counter electrode was a Pt wire.

In the measurement with the semiautomatic electrochemiluminometer, CRP could be detected in the concentration range 0.0003–1 mg L^{-1}, while the concentration range with the chips was 0.01–10 mg L^{-1}. The calibration curves of these measurements are shown in Figure 28. According to these results, both methods are suitable for high-sensitivity point-of-care CRP-measurements. With the semiautomatic electrochemiluminometer, the detection limit is lower. When real blood samples are measured, dilution is often included

in sample preparation and lower detection limit is therefore preferable. However, the electrochemiluminometer measurement meets its upper detection limit at 1 mg L^{-1}, when the measurement with the chip meets it at ca. 10 mg L^{-1}. In addition, the PMT used in the chip measurement is capable of detecting CRP-concentrations up to 1 000 mg L^{-1}. For such high concentrations, the amount of the labelled antibody must first be optimised, but after optimisation, this method should be applicable also to higher concentrations of CRP.

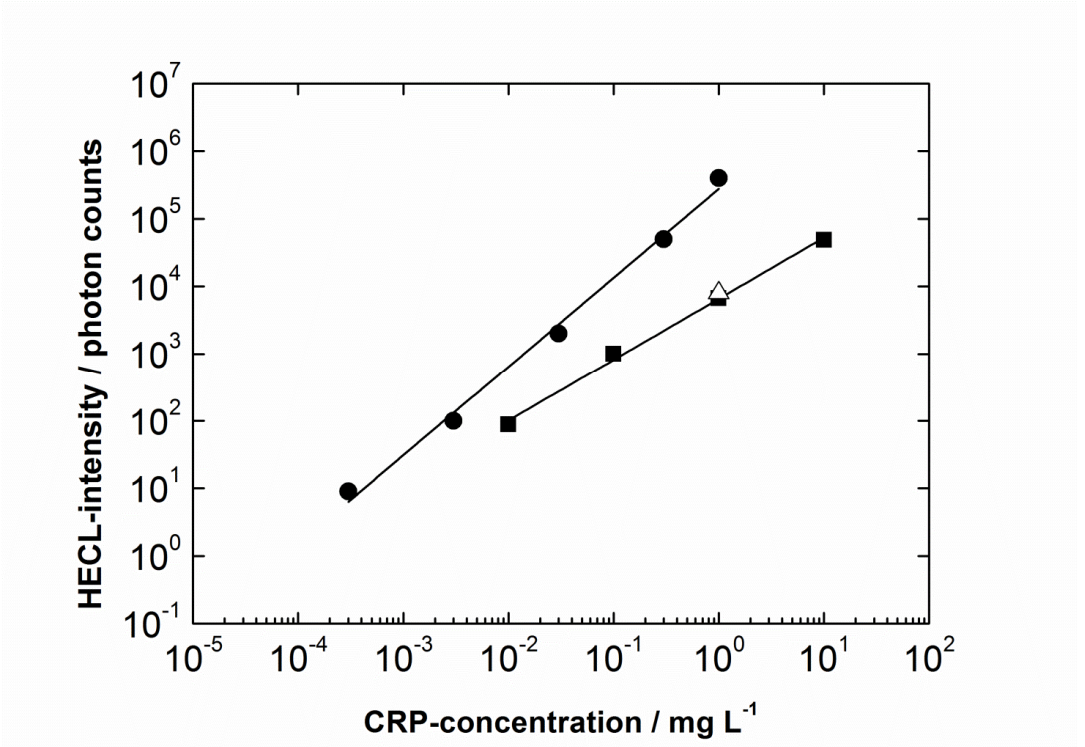

Figure 28. The calibration curves of CRP-immunoassay by a) SiO_2-coated Si electrodes using electrochemiluminometer (circles) and b) integrated electrodes with hydrophobic sample confinement (squares). The calibration curves are achieved by incubation procedures where the analyte and the labelled secondary antibody are mixed before the contact to the electrode. The triangle describes an alternative incubation method where the analyte and the labelled secondary antibody are dispensed separately on the electrode surface of the integrated electrode. The incubation time was 2 minutes (circles) or 5 minutes (squares and triangle). The immunoassay procedures and the instrumentation are described in detail in Publications VI and VII.

The benefit of the semiautomatic electrochemiluminometer compared to the traditional measurement system (Publications I–IV) or to the measurement with integrated chips is that 12 samples can be measured at the same time using a set of 12 Pt counter electrodes. However, when the chips with hydrophobically defined sample confinement are used, no micro titer strips or separate counter electrodes are needed as they are in the case of immunoassay by electrochemiluminometer. This decreases the volume of the reagents

needed. The volume of the mixture including the antigen and the labelled secondary antibody were 200 µl in the electrochemiluminometer method and only 5 µl when the integrated chips were used. The measurement with the chips could be performed also using a method where the analyte and the label were dispensed separately. In this method, the volumes of the antigen and the labelled secondary antibody were 3.5 µl and 1 µl, respectively. The usage of the chips also simplifies the procedure and quickens the set-up time significantly. In addition, no washing of any part of the measurement setup is needed between the measurements. With the integrated chips, the whole procedure from introducing the antigen to reading the result can be done in less than 10 min.

When the chip method was used, the intensity was integrated over 300 excitation cycles. This integration range was selected because the intensity decreases substantially after about 300 excitation pulses, as can be seen in Figure 29. There are several potential reasons for the intensity decrease. The most probable reason is that the protein radicals combine with the luminophore radicals and these new combinations are not luminescent. Another reason could be that the antibodies begin to break down during the excitation pulses. The HECL intensity decreases as the concentration of the breakdown products from the coating and from the labels increases in the solution and several side reactions are able to take place due to this increase. One of the effects of the increase of the breakdown products in the analyte solution is the severe quenching of the actual luminescing compounds. However, more investigation is needed for a definite conclusion on the cause of the intensity decrease.

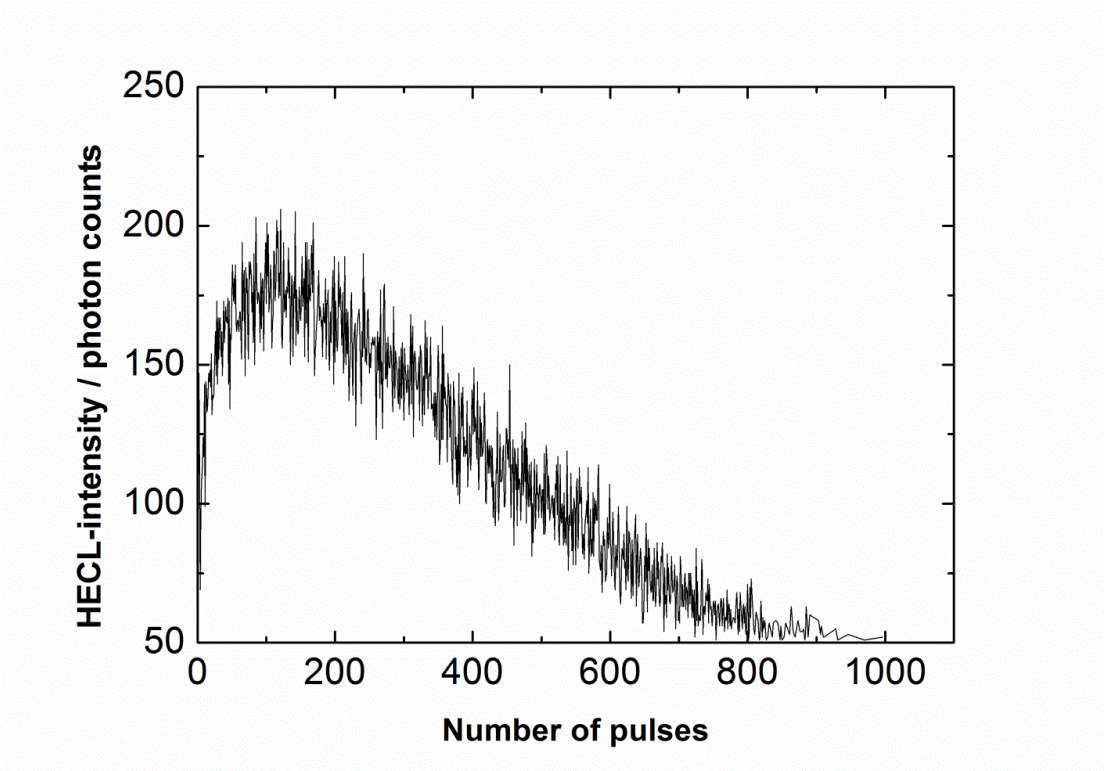

Figure 29. HECL intensity vs. the number of pulses. Conditions: Integrated electrode chip with a hydrophobically defined sample confinement, CRP-concentration 10 mg L^{-1}, 550 nm interference filter with 40 nm bandwidth, pulse charge 12.6 µC, pulse voltage 15 V, pulse frequency 20 Hz, measurement window 3 ms, and 50 µs delay.

The most time-consuming parts of the immunoassay are coating and saturation. However, it has been shown earlier that coated and saturated oxide-covered Al electrodes can be stored for up to one year in refrigerator and they are still usable[23]. Also coated and saturated oxide-covered Si electrodes remain usable at least for one year if they are dried at 30 ^{0}C and stored air-sealed at 2–4 ^{0}C. Therefore, electrodes could be coated and saturated already in advance and taken out from the storage just before use[49].

The HECL measurement system with integrated chips with hydrophobically defined sample confinement is a good candidate for point-of-care high-sensitivity CRP method. With the earlier mentioned optimisation, it might be applicable for point-of-care measurements of both low and high CRP-concentrations.

6. Conclusions

Hot electron-induced electrochemiluminescence provides low detection limit and large linear range for several rare earth metal chelates and organic dyes. It can be used in bioaffinity assays and due to its time and wavelength discrimination it provides an opportunity to determine several analytes simultaneously. Finding new luminophores emitting light at different time domains and/or different wavelength ranges are important for these analyses.

Traditionally, the HECL measurements have been made with discrete working and counter electrodes. In this research, also integrated electrode chips were designed and used. These chips make it easier for the HECL method to meet the requirements of modern analytical chemistry.

Different cathode materials and insulator films for HECL studies were tested. In addition to the tested SiO_2, Al_2O_3, and Si_3N_4 films, it is probable that also other dielectrics can be used. The thickness of the thin insulator film is, however, a critical value. The thin film deposition methods described in this thesis provide good or even excellent control over the film thickness. The methods are also repeatable. The substrate material of the electrode does not necessarily have to be a conductor, because also thin metal films deposited on a substrate can be used as the conductor of the working or counter electrode. The substrate material can be fairly freely chosen and it can be e.g. glass or plastic. Plastic is a promising material for electrode production because it can be low-cost and it provides many interesting options for the production of fluidic systems.

The integrated electrode chips make the HECL analysis faster and easier for the user. Their usage also reduces the volume of the reagents needed. When the chips with an integrated sample confinement are used, the washing step between the samples can be ignored and still cross-contamination between the samples is totally eliminated. The selection of the electrode geometry and sample confinement type depends on the application. In immunoassays, for example, a chip with large cathode area is preferable, because then the antibodies have larger area to be bound. Therefore, an absolutely best geometry of integrated electrode chip for HECL studies cannot be named. The production of integrated electrode chips would have been simpler, if platinum had been used as a conductor in both

the working and counter electrodes. However, this kind of device might have slightly poorer performance than the present devices.

In addition to being a useful device for the HECL studies with the present system, the chips with a PDMS sample chamber afford a proof-of-concept of the capability of integrating HECL detection into other microfluidic systems. The capillary-filling PDMS sample chamber is simple and PDMS fluidics can be easily fabricated in large production volumes. However, the bonding of the PDMS cover to the HECL chip is a major extra fabrication step. The production of hydrophobic sample confinement is more economical for mass production than the PDMS sample chamber, because hydrophobic surface modification is a simple wafer-scale deposition step.

The integrated HECL chips with a sample confinement defined by a hydrophobic ring were shown to work well in CRP-immunoassay. The method is a good candidate for point-of-care application, because the method is rapid, the chips are easy to use, and the instrumentation is simple and easy to miniaturise. In addition, the method provides a suitable detection range and a sufficiently low detection limit. The CRP used in this research was purified compound and therefore, it would be interesting to test also CRP analysis with real blood samples. Especially the alternative which needs only 1 µl of sample might be usable. However, analysing real blood samples might need some modification of the method and an extra pre-treatment step.

References

[1] Bard, A.J. editor, Electrogenerated Chemiluminescence, Marcel Dekker Inc., New York, 2004.

[2] Visco, R.E., Chandross, E.A., Electroluminescence in solutions of aromatic hydrocarbons, *J. Am. Chem. Soc.* **86** (1964) 5350–5351.

[3] Dufford, R.T., Nightingale, D., Gaddum, L.W., Luminescence of grignard compounds in electric and magnetic fields, and related electrical phenomena, *J. Am. Chem. Soc.* **49** (1927) 1858–1864.

[4] Harvey, N., Luminescence during Electrolysis, *J. Phys. Chem.* **33** (1928) 1456–1459.

[5] Maloy, J.T., Prater, K.B., Bard, A.J., Electrogenerated chemiluminescence. V. The rotating-ring-disk electrode. Digital simulation and experimental evaluation, *J. Am. Chem. Soc.* **93** (1971) 5959–5968.

[6] Richter, M., Electrochemiluminescence, *Chem. Rev.* **104** (2004) 3003–3036.

[7] Wilson, R., Akhavan-Tafti, H., DeSilva, R., Schaap, A.P., Comparison between acridan ester, luminol and ruthemium chelate electrochemiluminescence, *Electroanalysis* **13** (2001) 1083–1092.

[8] Marquette, C.A., Leca, B.D., Blum, L.J., Electrogenerated chemiluminescence of luminol for oxidase-based fibre-optic biosensors, *Luminescence* **16** (2001) 159–165.

[9] Kapturkiewicz, A., Electrogenerated chemiluminescence from the tris(4,7-diphenyl-1,10-phenanthroline)ruthenium(II) complex, *Chem. Phys. Lett.* **236** (1995) 389–394.

[10] Walworth, J., Brewer, K.J., Richter, M.M., Enhanced electrochemiluminescence from $Os(phen)_2(dppene)^{2+}$ (phen=1,10-phenanthroline and dppene=bis(diphenylphosphino)ethene) in the presence of Triton X-100 (polyethylene glycol tert-octylphenyl ether), *Anal. Chim. Acta* **503** (2004) 241–245.

[11] Ala-Kleme, T., Kulmala, S., Latva, M., Generation of free radicals and electrochemiluminescence at pulse-polarized oxide-covered silicon electrodes in aqueous solutions, *Acta Chem. Scand.* **51** (1997) 541–546.

[12] Kulmala, S., Kulmala, A., Ala-Kleme, T., Pihlaja, J., Primary cathodic steps of electrogenerated chemiluminescence of lanthanide(III) chelates at oxide-covered aluminum electrodes in aqueous solution, *Anal. Chim. Acta* **367** (1998) 17–31.

[13] Kulmala, S., Ala.Kleme, T., Heikkilä, L., Väre, L., Energetic electrochemiluminescence of (9-fluorenyl)methanol induced by injection of hot electrons into aqueous solution, *J. Chem. Soc., Faraday Trans.* **93** (1997) 3107–3113.

[14] Kulmala, S., Ala-Kleme, T., Joela, H., Kulmala, A., Hot electron injection into aqueous electrolyte solution from thin insulating film-coated electrodes, *J. Radioanal. Nucl. Chem.* **232** (1998) 91–95.

[15] Håkansson, M., Jiang, Q., Helin, M., Putkonen, M., Niskanen, A.J., Pahlberg, S., Ala-Kleme, T., Heikkilä, L., Suomi, J., Kulmala,S., Cathodic Tb(III) chelate electrochemiluminescence at oxide-covered magnesium and n-ZnO:Al/MgO composite electrodes, *Electrochim. Acta* **51** (2005) 289–296.

[16] Ala-Kleme, T., Kulmala, S., Väre, L., Juhala, P., Helin, M., Hot electron-induced electrogenerated chemiluminescence of $Ru(bpy)_3^{2+}$ chelate at oxide-covered aluminum electrodes, *Anal. Chem.* **71** (1999) 5538–5543.

[17] Kulmala, S., Ala.Kleme, T., Kulmala, A., Papkovsky, D., Loikas, K., Cathodic electrogenerated chemiluminescence of luminol at disposable oxide-covered aluminum electrodes, *Anal. Chem.* **70** (1998) 1112–1118.

[18] Jiang, Q., Spehar, A.-M., Håkansson, M., Suomi, J., Ala-Kleme, T., Kulmala, S., Hot electron-induced cathodic electrochemiluminescence of rhodamine B at disposable oxide-coated aluminum electrodes, *Electrochim. Acta* **51** (2006) 2706–2714.

[19] Suomi, J., Håkansson, M., Jiang, Q., Kotiranta, M., Helin, M., Niskanen, A.J., Kulmala, S., Time-resolved detection of electrochemiluminescence of luminol, *Anal. Chim. Acta* **541** (2005) 165–167.

[20] Håkansson, M., Jiang, Q., Spehar, A.-M., Suomi, J., Kotiranta, M., Kulmala, S., Direct current-induced electrogenerated chemiluminescence of hydrated and chelated Tb(III) at aluminum cathodes, *Anal. Chim. Acta* **541** (2005) 169–175.

[21] Helin, M., Väre, L., Håkansson, M., Canty, P., Hedman, H.-P., Heikkilä, L., Ala-Kleme, T., Kankare, J., Kulmala, S., Electrochemiluminoimmunoassay of hTSH at disposable oxide-coated n-silicon electrodes, *J. Electroanal. Chem.* **524–525** (2002) 176–183.

[22] Kulmala, S., Håkansson, M., Spehar, A.-M., Nyman, A., Kankare, J., Loikas, K., Ala-Kleme, T., Eskola, J., Heterogeneous and homogeneous electrochemiluminoimmunoassays of hTSH at disposable oxide-covered aluminum electrodes, *Anal. Chim. Acta* **458** (2002) 271–280.

[23] Eskola, J., Mäkinen, P., Oksa, L., Loikas, K., Nauma, M., Jiang, Q., Håkansson, M., Suomi, J., Kulmala, S., Competitive immunoassay by hot electron-induced electrochemiluminescence detection and using a semiautomatic electrochemiluminometer, *J. Lumin.* **118** (2006) 238–244.

[24] Kankare, J., Haapakka, K., Kulmala, S., Näntö, V., Eskola, J., Takalo, H., Immunoassay by time-resolved electrogenerated luminescence, *Anal. Chim. Acta* **266** (1992) 205–212.

[25] Spehar-Deleze, A.-M., Suomi, J., Jiang, Q., de Rooij, N., Koudelka-Hep, M., Kulmala, S., Heterogeneous oligonucleotide-hybridization assay based on hot electron-induced electrochemiluminescence of a rhodamine label at oxide-coated aluminum and silicon electrodes, *Electrochim. Acta* **51** (2006) 5438–5444.

[26] Bernas, A., Grand, D., Amoyal, E., Photoionization of solutes and conduction band edge of solvents. Indole in Water and Alcohols, *J. Phys. Chem.* **84** (1980) 1259–1262.

[27] Sung, Y.-E., Gaillard, F., Bard, A.J., Demonstration of electrocehmical generations of solution-phase hot electrons at oxide-covered tantalum electrodes by direct electrogenerated chemiluminescnece, *J. Phys. Chem.* **102** (1998) 9797–9805.

[28] Kulmala, S., Haapakka, K., Mechanism of electrogenerated luminescence of terbium(III)-"2,6-bis[N,N-bis(carboxymethyl)aminomethyl]-4-benzoylphenol" chelate at an oxide-covered aluminium electrode, *J. Alloys Compd.* **225** (1995) 502–506.

[29] Jiang,Q., Suomi, J, Håkansson, M, Niskanen, A, Kotiranta, M., Kulmala, S., Cathodic electrogenerated chemiluminescence of $Ru(bpy)_3^{2+}$ chelate at oxide-coated heavily doped silicon electrodes, *Anal. Chim. Acta* **541** (2005) 157–163.

[30] Kulmala, S., Ala.Kleme, T., Hakanen, A., Haapakka, K., F-centre luminescence from oxide-covered aluminium cathode induced by two-step reduction of peroxydisulfate anions, *J. Chem. Soc., Faraday Trans.* **93** (1997) 165–168.

[31] Buxton, G.V., Greestock, C. L., Helman, W. P., Ross, A. B., Critical review of rate constants for reactions of hydrated electrons. Chemical kinetic data base for combustion chemistry. Part 3: Propane, *J. Phys. Chem. Ref. Data* **17** (1988) 513–886.

[32] Arce, R., Carcia, C., Oyola, R., Pinero, L., Nieves, I., Cruz, N., Photophysical and photochemical properties of amitriptyline and nortriptyline hydrochloride: a 266 nm nanosecond laser flash and theoretical study, *J. Photochem. Photobiol., A* **154** (2003) 245–257.

[33] Tachiya, M., Murata, S., New explanation for the lack of the inverted region in charge separation reactions, *J. Phys. Chem.* **96** (1992) 8441–8444.

[34] Koppenol, W., Butler, J., Energetics of interconversion reactions of oxyradicals, *Adv. Free Radical Biol. Med.* **1** (1985) 91–131.

[35] Kulmala, S., Helin, M., Ala-Kleme, T., Väre, L., Papkovsky, D., Korpela, T., Kulmala, A., Electrochemiluminescent labels for applications in fully aqueous solutions at oxide-covered aluminium electrodes, *Anal. Chim. Acta* **386** (1999) 1–6.

[36] Kulmala, S., Ala-Kleme, T., Room temperature phosphorescence emission in fully aqueous medium induced by injection of hot electrons into an electrolyte solution, *Anal. Chim. Acta* ***355*** (1997) 1–5.

[37] Håkansson, M., Helin, M., Putkonen, M., Jiang, Q., Kotiranta, M., Suomi, J., Niskanen, A.J., Ala-Kleme, T., Kulmala, S., Electrochemiluminescence of Tb(III) chelates at optically transparent tunnel emission electrodes fabricated by atomic layer deposition, *Anal. Chim. Acta* **541** (2005) 135–139.

[38] Jiang, Q., Håkansson, M., Spehar, A.-M., Ahonen, J., Ala-Kleme, T., Kulmala, S., Hot electron-induced time-resolved electrogenerated chemiluminescence of a europium(III) label in fully aqueous solutions, *Anal. Chim. Acta* **558** (2006) 302–309.

[39] Jiang, Q., Ketamo, H., Niskanen, A.J., Suomi, J., Håkansson, M., Kulmala, S., Effects of thermal oxidation conditions of silicon electrodes on cathodic electrochemiluminescence of $Ru(bpy)_3^{2+}$ chelate, *Electrochim. Acta* **51** (2006) 3332–3337.

[40] Ala-Kleme, T., Haapakka, K., Latva, M., Near-infrared electrogenerated chemiluminescence of ytterbium(III) chelates in aqueous electrolytes, *Anal. Chim. Acta* **395** (1999) 205–211.

[41] Ala-Kleme, T., Haapakka, K., Latva, M., Y(III)-enhanced Dy(III) and Sm(III)-specific electrogenerated luminescence of heterodinuclear 1–Y(III)–Dy(III)–1 and 1–Y(III)–Sm(III)–1 chelates, *J. Alloys Compd.* **275–277** (1998) 911–914.

[42] Jiang, Q., Håkansson, M., Suomi, J., Ala-Kleme, T., Kulmala, S., Cathodic electrochemiluminescence of lucigenin at disposable oxide-coated aluminum electrodes, *J. Electroanal. Chem.* **591** (2006) 85–92.

[43] Helin, M., Jiang, Q., Ketamo, H., Håkansson, M., Spehar, A.-M., Kulmala, S., Ala-Kleme, T., Electrochemiluminescence of coumarin derivatives induced by injection of hot electrons into aqueous electrolyte solution, *Electrochim. Acta* **51** (2005) 725–730.

[44] Helin, M., Håkansson, M., Canty, P., Spehar, A.-M., Kulmala, S., Hot electron-induced electrogenerated chemiluminescence of 1-aminonaphthalene-4-sulphonate at oxide-covered aluminium electrodes in aqueous solution, *Anal. Chim. Acta* **454** (2002) 193–201.

[45] Diez, I., Pusa, M., Kulmala, S., Jiang, H., Walther, A., Goldmann, A. S., Muller, A.H.E., Ikkala, O., Ras, R.H.A., Color tunability and electrochemiluminescence of silver nanoclusters, *Angew. Chem., Int. Ed.* **48** (2009) 2122–2125.

[46] Kulmala, S., Ala-Kleme, T., Latva, M., Loikas, K., Takalo, H., Hot electron-induced electrogenerated chemiluminescence of rare earth(III) chelates at oxide-covered aluminum electrodes, *J. Fluoresc.* **8** (1998) 59–65.

[47] Soini, E., Lövgren, T., Time-resolved fluorescence of lanthanide probes and applications in biotechnology, *CRC Crit. Rev. Anal. Chem.* **18** (1987) 105–154.

[48] Hemmilä, I., Applications of fluorescence in immunoassays, John Wiley & Sons Ltd, New York, 1987.

[49] Kulmala, S., Kulmala, A., Latva, M., Haapakka, K., X-ray irradiated sodium chloride as an excitation source for the sensitized terbium(III)-specific chemiluminescence of aromatic Tb(III) chelates in aqueous solutions, *Anal. Chim. Acta* **347** (1997) 333–350.

[50] Håkansson, M., Jiang, Q., Suomi, J., Loikas, K., Nauma, M., Ala-Kleme, T., Kankare, J., Juhala, P., Eskola, J.U., Kulmala, S., Cathodic electrochemiluminescence at double barrier $Al/Al_2O_3/Al/Al_2O_3$ tunnel emission electrodes, *Anal. Chim. Acta* **556** (2006) 450–454.

[51] Suomi, J., Kulmala, S., Hot electron-induced electrogenerated chemiluminescence, *Rev. Fluoresc.* **6** (2011) 47–73.

[52] Wu, A.-H., Sun, J.-J., Fang, Y.-M., Su, X.-L., Chen, G.-N., Hot electron induced cathodic electrochemiluminescence at AuSb alloy electrode for fabricating immunosensor with self-assembled monolayers, *Talanta* **82** (2010) 1455–1461.

[53] Wu, A.-H., Sun, J.-J., Su, X.-L., Lin, Y.-W., Lin, Z.-B., Yang, H.-H., Chen, G.-N., Cathodic electrochemiluminescence at C/C_xO_{1-x} electrodes for the fabrication of label-free biosensor, *Analyst* **135** (2010) 2309–2315.

[54] Wu, A.-H., Sun, J.-J., Zheng, R.-J., Yang, H.-H., Chen, G.-N., A reagentless DNA biosensor based on cathodic electrochemiluminescence at a C/C_xC_{1-x} electrode, *Talanta* **81** (2010) 934–940.

[55] Wu, A.-H., Sun, J.-J., Fang,Y.-M., Zheng, R.-J., Chen, G.-N., Hot electron induced cathodic electrochemiluminescence at disposable screen printed carbon electrodes, *Electroanalysis* **22** (2010) 2702–2707.

[56] Kulmala, S., Niskanen, A., Kulmala, A., Loikas, K., Pusa, M., Low-cost electrode chip variants and methods for multi analyte analysis and referencing based on cathodic electroluminescence, PCT Int. Appl. (2011), WO 2011154591 A1 20111215.

[57] Buijs, J., Lichtenbelt, J., Norde, W., Lyklema, J., Adsorption of monoclonal IgGs and their F(ab′)$_2$ fragments onto polymeric surfaces, *Colloids Surf., B* **5** (1995) 11–23.

[58] Wang, H., Liu, Y., Yang,Y., Deng,T., Shen,G., Yu, R., A protein A-based orientation-controlled immobilization strategy for antibodies using nanometer-sized gold particles and plasma-polymerized film, *Anal. Biochem.* **324** (2004) 219–226.

[59] Toda, K., Masato, T., Sekiya, N., Ikeda M., Yoshioka, K-I., Electrochemical enzyme immunoassay using immobilized antibody on gold film with monitoring of surface plasmon resonance signal, *Anal. Chim. Acta* **463** (2002) 219–227.

[60] Nishi, H., Yamaguchi, T., Otsuji, E., Kotani, T., Taniguchi, K., Okamoto, K., Yata, Y., Tsuruta, H., Takahashi, T., Reduced blood accumulation of biotinylated monoclonal antibody A7 after the subsequent administration of avidin, *Cancer Lett.* **120** (1997) 127–134.

[61] Cui, X., Pei, R., Wang, Z., Yang, F., Ma, Y., Dong, S., Yang, X., Layer-by-layer assembly of multilayer films composed of avidin and biotin-labeled antibody for immunosensing, *Biosens. Bioelectron.* **18** (2003) 59–67.

[62] Neubert, H., Jacoby, E.S., Bansal, S.S., Iles, R.K., Cowan, D.A., Kicman, A.T., Enhanced affinity capture MALDI-TOF MS: Orientation of an immunoglobulin G using recombinant protein G, *Anal. Chem.* **74** (2002) 3677–3683.

[63] Brogan, K.L., Wolfe, K.N., Jones, P.A., Schoenfisch, M.H., Direct oriented immobilization of F(ab′) antibody fragments on gold, *Anal. Chim. Acta* **496** (2003) 73–80.

[64] O'Brien, J.C., Jones, V.W., Porter, M.D., Immunosensing platforms using spontaneously adsorbed antibody fragments on gold, *Anal. Chem.* **72** (2000) 703–710.

[65] Fähnrich, K.A., Pravda, M., Guilbault, G.G., Recent applications of electrogenerated chemiluminescence in chemical analysis, *Talanta* **54** (2001) 531–559.

[66] Hemmilä, I., Webb, S., Time-resolved fluorometry: an overview of the labels and core technologies for drug screening applications, *Drug Discovery Today* **2** (1997) 373–381.

[67] Kitamori, T., Miniaturization and chip technology in analytical chemistry, *Fresenius' J. Anal. Chem.* **371** (2001) 89–90.

[68] Huang, H.-H., Zhou, J., Huang, Y.P., Kong, J.-L., Impedimetric immunosensor with on-chip integrated electrodes for high-throughput screening of liver fibrosis markers, *J. Anal. Chem.* **63** (2008) 492–498.

[69] Nordman, N., Sikanen, T., Moilanen, M.-E., Aura, S., Kotiaho, T., Franssila, S., Kostiainen, R., Rapid and sensitive drug metabolism studies by SU-8 microchip capillary electrophoresis-electrospray ionization mass spectrometry, *J. Chromatogr., A* **1218** (2011) 739–745.

[70] Keynton, R.S., Roussel Jr.,T.J., Crain, M.M., Jackson, D.J., Franco, D.B., Naber, J.F., Walsh, K.M., Baldwin, R.P., Design and development of microfabricated capillary electrophoresis devices with electrochemical detection, *Anal. Chim. Acta* **507** (2004) 95–105.

[71] Franssila, S., Introduction to microfabrication, John Wiley & Sons Ltd, West Sussex, 2004.

[72] Hattori, T., Nohira, H., Takahashi, K., The initial growth steps of ultrathin gate oxides, *Microelectron. Eng.* **48** (1999) 17–24.

[73] Sofield, C.J., Stoneham, A.M., Oxidation of silicon: the VLSI gate dielectric, *Semicond. Sci. Technol.* **10** (1995) 215–244.

[74] Wu, E.Y., Suñé, J., Power-law voltage acceleration: A key element for ultra-thin gate oxide reliability, *Microelectron. Reliab.* **45** (2005) 1809–1834.

[75] Deal, B.E., Grove, A.S., General relationship for the thermal oxidation of Silicon, *J. Appl. Phys.* **36** (1965) 3770–3778.

[76] Lindroos, V., Tilli, M., Lehto, A., Motooka, T., Handbook of silicon based MEMS materials and technologies, Elsevier, Oxford 2010.

[77] Bunshah, R.F. editor, Handbook of deposition technologies for films and coatings, 2nd ed., Noyes Publications, New Jersey, 1994.

[78] Dameron, A., Christensen, S., Galante, M., Berry, J., Gillaspie, D., Perkins, J., Ginley, D., Gennet, T., Conductive conformal thin film coatings for textured PV: ALD versus sputtering, *Proc. SPIE* **8110** (2011) 81100M (6 pp.).

[79] Barron, A.R. editor, Chemistry of electronic materials, URL: http://cnx.org/content/col10719/1.9/, 2011.

[80] Pierson, H.O. editor, Handbook of chemical vapor deposition, Noyes Publications, New Jersey, 1992.

[81] Sinkkonen, J., Puolijohdeteknologian perusteet, Reports in Electron Physics, Otaniemi 1996.

[82] Schuegraf, K.K. editor, Handbook of thin-film deposition processes and techniques, Noyes Publication, New Jersey, 1988.

[83] Inoue, J., Ooya, T., Takeuchi, T., Protein imprinted TiO_2-coated quantum dots for fluorescent protein sensing prepared by liquid phase deposition, *Soft Matter* **7** (2011) 9681–9684.

[84] Gao, Y., Koumoto, K., Bioinspired ceramic thin film processing: Present status and future perspectives, *Cryst. Growth Des.* **5** (2005) 1983–2017.

[85] Fujita, R., Sakairi, M., Kikuchi, T., Nagata, S., Corrosion resistant TiO_2 film formed on magnesium by liquid phase deposition treatment, *Electrochim. Acta* **56** (2011) 7180–7188.

[86] Nagayama, H., Honda, H., Kawahara, H., A new process for silica coating, *J. Electrochem. Soc.* **135** (1988) 2013–2016.

[87] Lee, M.K., Ho, C.-L., Chen, P.-C., Light extraction efficiency enhancement of GaN blue LED by liquid-phase-deposited ZnO rods, *IEEE Photonics Technol. Lett.* **20** (2008) 252–254.

[88] Yongwei, C., Mingyan, L., Corrosion behavior of titania film coated by liquid-phase deposition on AISI304 stainless steel substrates, *AIChE J.* **58** (2012) 1907–1920.

[89] Wang, L.L., Liu, M.Y., Pool boiling fouling and corrosion properties on liquid-phase-deposition TiO_2 coatings with copper substrate, *AIChE J.* **57** (2011) 1710–1718.

[90] Lei, P.-H., Ding, M.-J., Lee, Y.-C., Chung, M.-J., Textured zinc oxide prepared by liquid phase deposition (LPD) method and its application in improvement of extraction efficiency for 650 nm resonant-cavity light-emitting diode (RCLED), *J. Alloys Compd.* **509** (2011) 6152–6157.

[91] Luka, G., Krajewski, T.A., Witkowski, B.S., Wisz, G., Virt, I.S., Guziewicz, E., Godlewski. M., Aluminum-doped zinc oxide films grown by atomic layer deposition for transparent electrode applications, *J. Mater. Sci.: Mater. Electron.* **22** (2011) 1810–1815.

[92] Szeghalm, A., Arnold, M., Berger, A., Schammelt, N., Fuechsel, K., Knez, M., Kley, E.B., Zahn, D.R.T., Tuennermann, A., Atomic layer deposition of iridium thin films and their application in gold Electrodeposition, *Proc. SPIE* **8168** (2011) 81680K (10 pp.).

[93] Knez, M., Nielsch, K., Niinistö, L., Synthesis and surface engineering of complex nanostructures by atomic layer deposition, *Adv. Mater.* **19** (2007) 3425–3438.

[94] Szeghalmi, A., Kley, E.B., Knez, M., Theoretical and experimental analysis of the sensitivity of guided mode resonance sensors, *J. Phys. Chem. C* **114** (2010) 21150–21157.

[95] Kemell, M., Ritala, M., Leskelä, M., Groenen, R., Lindfors, S., Coating of highly porous fiber matrices by atomic layer deposition, *Chem. Vap. Deposition* **14** (2008) 347–352.

[96] Comstock, D.J., Christensen, S.T., Elam, J.W., Pellin, M.J., Hersam, M.C., Synthesis of nanoporous activated iridium oxide films by anodized aluminum oxide templated atomic layer deposition, *Electrochem. Commun.* **12** (2010) 1543–1546.

[97] Fabreguette, F.H., Wind, R.A., George, S.M., Ultrahigh x-ray reflectivity from W/Al_2O_3 multilayers fabricated using atomic layer deposition, *Appl. Phys. Lett.* **88** (2006) 013116 (3 pp).

[98] Chabinyc, M.L., Chiu, D.T., McDonald, J.C., Stroock, A.D., Christian, J.F., Karger, A.M., Whitesides, G.M., An integrated fluorescence detection system in poly(dimethylsiloxane) for microfluidic applications, *Anal. Chem.* **73** (2001) 4491–4498.

[99] Wang, S.-C., Morris, M.D., Plastic microchip electrophoresis with analyte velocity modulation. Application to fluorescence background rejection, *Anal. Chem.* **72** (2000) 1448–1452.

[100] Chang, H.-I., Zhanh, F., Ding, J.-I., Chen, F.-I., Hong, S.-j., Kraft, M., Yuan, W.-z., A highly reliable integrated PDMS interconnector with a long cast flange for microfluidic systems, *Microsyst. Technol.* **18** (2012) 723–730.

[101] Dang, T.-D., Kim, Y.H., Choi, J.H., Kim, G.-M., A novel simple preparation method of a hydrogel mold for PDMS micro-fluidic device fabrication, *J. Micromech. Microeng.* **22** (2012) 010517 (8 pp.).

[102] Poole, J.S., Hadad, C.M., Platz, M.S., Fredin, Z. P., Pickard, L., Guerrero, E.L., Kessler, M., Chowdhury, G., Kotandeniya, D., Gates, K.S., Photochemical electron transfer Reactions of tirapazamine, *Photochem. Photobiol.* **75** (2002) 339–345.

[103] Pruetz, W., Land., K., Phosphorescence of aqueous dye solutions after irradiation with electron pulses, *Biophysik* **3** (1967) 349–360.

[104] Pruetz, W., Sommermeyer, K., Land, E., Light emission after pulse radiolysis of aqueous solution of dyes, *Nature* **212** (1966) 1043–1044.

[105] Suomi, J., Ylinen, T., Håkansson, M., Helin, M., Jiang, Q., Ala-Kleme, T., Kulmala, S., Hot electron-induced electrochemiluminescence of fluorescein in aqueous solution, *J. Electroanal. Chem.* **586** (2006) 49–55.

[106] Jiang, Q., Kotiranta, M., Langel, K., Suomi, J., Håkansson, M., Spehar, A.-M., Ala-Kleme, T., Eskola, J., Kulmala, S., Ruthenium(II) tris(2,2′-bipyridine) chelate as a chemiluminophore in extrinsic lyoluminescences of aluminium and magnesium in aqueous solution, *Anal. Chim. Acta* **541** (2005) 177–184.

[107] Stanbury, D., Reduction potentials involving inorganic free radicals in aqueous solution, *Adv. Inorg. Chem.* **33** (1987) 69–138.

[108] Koppenol, W., Thermodynamics of reactions involving oxyradicals and hydrogen peroxide, *Bioelectrochem. Bioenerg.* **18** (1987) 3–11.

[109] Neta, P., Application of radiation techniques to the study of organic radicals, *Adv. Phys. Org. Chem.* **12** (1976) 223–297.

[110] Cordier, P., Grossweiner, L.I., Pulse radiolysis of aqueous fluorescein, *J. Phys. Chem.* **72** (1968) 2018–2026.

[111] Pruetz, W.A., Land, E.J. ,Chemiluminescent reactions after pulse radiolysis of aqueous dye solutions. Absolute yields, *J. Phys. Chem.* **78** (1974) 1251–1253.

[112] Kulmala, S., Suomi, J., Current status of modern analytical luminescence methods, *Anal. Chim. Acta* **500** (2003) 21–69.

[113] Kulmala, S., Hakanen, A., Raerinne, P., Kulmala, A., Haapakka, K., Ruthenium(II) tris-(2,2'-bipyridine) -specific extrinsic lyoluminescences of x-ray irradiation colored and electrolytically colored alkali halides, *Anal. Chim. Acta* **309** (1995) 197–210.

[114] Kamiyama, E., Sueoka, K., Effect of dangling bonds of ultra-thin silicon film surface on electronic states of internal atoms, *Appl. Surf. Sci.* **258** (2012) 5265–5269.

[115] Jung, S., Kim, J., Son, H., Hwang, S., Jang, K., Lee, J., Lee, K., Park, H., Kim, K., Yi, J., Chung, H., Choi, B., Lee, K., Fabrication and characterization of metal-oxide-nitride-oxynitride-polysilicon nonvolatile semiconductor memory device with silicon oxynitride (SiO_xN_y) as tunneling layer on glass, *J. Appl. Phys.* **102** (2007) 094502 (4 pp.).

[116] Jung, S., Hwang, S., Kim, K., Dhungel, S.K., Chung, H.-K., Choi, B.-D., Lee, K.-Y., Yi, J., Electrical properties of ultra-thin oxynitrided layer using N_2O plasma in inductively coupled plasma chemical vapor deposition for non-volatile memory on glass, *Thin Solid Films* **515** (2007) 6615–6618.

[117] Ahn, J., Ting, W., Chu, T., Lin, S., Kwong, D.L., High quality thin gate oxide prepared by annealing low-pressure chemical vapor deposited SiO_2 in N_2O, *Appl. Phys. Lett.* **59** (1991) 283–285.

[118] Szekeres, A., Nikolova, T., Simeonov, S., Gushterov, A., Hamelmann, F., Heinzmann, U., Plasma-assisted chemical vapor deposited silicon oxynitride as an alternative material for gate dielectric in MOS devices, *Microelectron. J.* **37** (2006) 64–70.

[119] Grigoras, K., Franssila, S., Airaksinen, V.-M., Investigation of sub-nm ALD aluminum oxide films by plasma assisted etch-through, *Thin Solid Films* **516** (2008) 5551–5556.

[120] Jakschik, S., Schroeder, U., Hecht, T., Krueger, D., Dollinger, G., Bergmaier, A., Luhmann, C., Bartha, J.W., Physical characterization of thin ALD–Al_2O_3 films, *Appl. Surf. Sci.* **211** (2003) 352–359.

[121] Yang, W.S., Yeong, K.K., Yang, S.-Y., Choi J.H., Park, H.S., Lee, S. I., Yoo, V.-B., Effect of SiO_2 intermediate layer on $Al_2O_3/SiO_2/n^+$-poly Si interface deposited using atomic layer deposition (ALD) for deep submicron device applications, *Surf. Coat. Technol.* **131** (2000) 79–83.

[122] Monteny, M., ten Brinke, M.H., van Brakel, J., de Rijke, Y.B., Berger, M.Y., Point-of-care C-reactive protein testing in febrile children in general practice, *Clin. Chem. Lab. Med.* **44** (2006) 1428–1432.

[123] Cals, J.W.L., Hopstaken, R.M., Butler, C.C, Hood, K., Severens, J.L., Dinant, G.-J., Improving management of patients with acute cough by C-reactive protein point of care testing and communication training (IMPAC^{3}T): study protocol of a cluster randomised controlled trial, *BMC Fam. Pract.* **8:15** (2007) doi:10.1186/1471-2296-8-15 (11pp.).

[124] Cals, J.W.L., Butler, C.C., Dinant, G.-J., 'Experience talks': physician prioritisation of contrasting interventions to optimise management of acute cough in general practice, *Implementation Science* **4:57** (2009) doi:10.1186/1748-5908-4-57 (6 pp.).

[125] Cals, J.W.L., Chappin, F.H.F, Hopstaken, R.M., van Leeuwen, M.E., Hood, K., Butler, C.C., Dinant, G.-J., C-reactive protein point-of-care testing for lower respiratory tract infections: a qualitative evaluation of experiences by GPs, *Fam. Pract.* **27** (2010) 212–218.

[126] Cals, J.W.L., Schot, M.J.C., de Jong, S.A.M., Dinant, G.-J., Hopstaken, R.M., Point-of-care C-Reactive protein testing and antibiotic prescribing for respiratory tract infections: A randomized controlled trial, *Ann. Fam. Med.* **8** (2010) 124–133.

[127] Ridker, P.M., C-Reactive Protein: Eighty years from discovery to emergence as a major Risk marker for cardiovascular disease *Clin. Chem.* **55** (2009) 209–215.

[128] Soilu-Hänninen, M., Koskinen, J.O., Laaksonen, M., Hänninen, A., Lilius, E.-M., Waris, M., High sensitivity measurement of CRP and disease progression in multiple sclerosis, *Neurology* **65** (2005) 153–155.

Errata

In Publication I, in the caption of Figure 5, the delay time was 5.0 µs (not 50.0 µs). Equations (1) and (2) should be

$$e_{aq}^{-} + S_2O_8^{2-} \rightarrow SO_4^{\bullet -} + SO_4^{2-} \qquad (1)$$

$$e_{aq}^{-} + P_2O_8^{4-} \rightarrow PO_4^{\bullet 2-} + PO_4^{3-} \qquad (2)$$

In Publication III, at the end of section 2, measurements were performed in a 5.6 mm diameter sample cell (not 8 mm), and luminescence was measured after a 50 µs delay following the pulse (not 50 s).

In Publication VII, in the section 2.3.2., the coated cathode was washed by letting 4·1mL of Wallac Washing obtained from Wallac Oy Turku Finland flow over the electrode (not distilled water).

This doctoral thesis is mainly focused on different cathode materials and electrode geometries used in hot electron-induced electrochemiluminescence (HECL) measurements. The biggest difference between the research in this thesis and the earlier HECL research is the usage of integrated electrodes. In the present devices, the working electrode, the counter electrode and the sample confinement are combined on a single microfabricated chip. These chips enable the miniaturisation of the whole measurement system. They make the analysis faster and more convenient for the user. In addition, they decrease the volume of the reagents needed. This doctoral thesis presents also one application of HECL: bioaffinity assay of C-reactive protein (CRP). The method described here is applicable especially for determination of low CRP concentrations predicting future cardiovascular problems in apparently healthy people. The method has a great potential for a real point-of-care application.

Aalto-DD 150/2012

ISBN 978-952-60-4866-6
ISBN 978-952-60-4867-3 (pdf)
ISSN-L 1799-4934
ISSN 1799-4934
ISSN 1799-4942 (pdf)

Aalto University
School of Chemical Technology
Department of Chemistry
www.aalto.fi

BUSINESS + ECONOMY

ART + DESIGN + ARCHITECTURE

SCIENCE + TECHNOLOGY

CROSSOVER

DOCTORAL DISSERTATIONS